8-8-2018

Double Dissociation of Auditory Attention and Visual Scanning in Long Term Survivors of Childhood Cerebellar Tumor: A Deterministic Tractography and Volumetric Study of the Cerebellar-Frontal and the Superior Longitudinal Fasciculus Pathways

Alyssa S. Ailion
Georgia State University

DOUBLE DISSOCIATION OF AUDITORY ATTENTION AND VISUAL SCANNING IN LONG TERM SURVIVORS OF CHILDHOOD CEREBELLAR TUMOR: A DETERMINISTIC TRACTOGRAPHY AND VOLUMETRIC STUDY OF THE CEREBELLAR-FRONTAL AND THE SUPERIOR LONGITUDINAL FASCICULUS PATHWAYS

by

ALYSSA AILION

Under the Direction of Tricia Z. King, Ph.D.

ABSTRACT

Background. Right cerebellar-left frontal (RC-LF) white matter integrity (WMI) has been associated with working memory. Right Superior Longitudinal Fasciculus II (SLF II) WMI has been associated with visual attention. These relationships have held true for neurotypical controls and brain tumor survivors. The current study examined the relationships between RC-LF WMI and processing speed, attention, and working memory. SLF II WMI and visual attention were included as a control tract and task to demonstrate a correlational double dissociation. This study also examined the relationship between the volume of brain regions within the RC-LF network and RC-LF WMI.

Methods. Adult survivors of childhood brain tumors (n= 29, age: M=22 years (SD= 5), 45% female) were treated with neurosurgery, and combinations of radiation therapy and chemotherapy. Age- and gender-matched controls (n=29) were also

included. Tests of auditory attention span, working memory, visual attention, and processing speed served as cognitive measures. Participants completed a 3T MRI diffusion imaging scan. WMI (FA, RD) and volume served as neuroimaging measures. In the survivor group, partial correlations between WMI and cognitive scores included controlling for type of treatment.

Results. A correlational double dissociation was found. RC-LF WMI was associated with auditory attention span (FA: r=.42, *p*=.03; RD: r=-.50, *p*=.01), and was not associated with visual attention (FA: r=-.11, *p*=.59; RD: r=-.11, *p*=.57). SLF II FA WMI was associated with visual attention (FA: r=.44, *p*=.02; RD: r=-.17, p=.40), and was not associated with auditory attention span (FA: r=.24, *p*=.22; RD: r=-.10, *p*=.62). The relationship between RC-LF WMI and auditory attention span robustly dissociated from working memory and visual attention. In the radiation group, thalamic-frontal segment of RC-LF WMI associated with the volumetric measures of each structure of the RC-LF pathway, whereas in the no radiation group cerebellar-rubral segment of RC-LF WMI associated with the volumetric measures.

Conclusions. The current study advances the understanding of structural brain changes following cerebellar tumor resection and treatment because the results show that RC-LF WMI is associated with auditory attention span rather that working memory, provide evidence for a correlational double dissociation, and suggest distinct relationships between WMI and volume based on treatment.

INDEX WORDS: Brain tumor, Structural MRI, Diffusion tractography, Cerebellum, Neurocognitive outcomes, Radiation treatment

DOUBLE DISSOCIATION OF AUDITORY ATTENTION AND VISUAL SCANNING IN LONG TERM SURVIVORS OF CHILDHOOD CEREBELLAR TUMOR: A DETERMINISTIC TRACTOGRAPHY AND VOLUMETRIC STUDY OF THE CEREBELLAR-FRONTAL AND THE SUPERIOR LONGITUDINAL FASCICULUS PATHWAYS

by

ALYSSA AILION

A Dissertation Submitted in Partial Fulfillment of the Requirements for the Degree of

Doctor of Philosophy

in the College of Arts and Sciences

Georgia State University

2017

DOUBLE DISSOCIATION OF AUDITORY ATTENTION AND VISUAL SCANNING IN LONG TERM SURVIVORS OF CHILDHOOD CEREBELLAR TUMOR: A DETERMINISTIC TRACTOGRAPHY AND VOLUMETRIC STUDY OF THE CEREBELLAR-FRONTAL AND THE SUPERIOR LONGITUDINAL FASCICULUS PATHWAYS

by

ALYSSA AILION

Committee Chair: Tricia Z. King

Committee: Bruce Crosson

Jessica Turner

Christopher Conway

Electronic Version Approved:

Office of Graduate Studies

College of Arts and Sciences

Georgia State University

May 2018

ACKNOWLEDGEMENTS

This work would not have been possible without the assistance of my research mentor Tricia King, Ph.D. This work was shaped by the valuable input from Bruce Crosson, Ph.D., Jessica Turner, Ph.D., and Christopher Conway, Ph.D., who all served on my dissertation committee. I would also like to thank Simone Roberts, M.A. who taught me diffusion network tractography and Kristen Smith, Ph.D. who shared her scripts and neuroimaging manuals. Kyle Hortman, Alexandria Cook, Anoohya Kalidindi, and Brian Tang helped with neuroimaging processing. I would like to thank Jaemin Shin and the Center for Brain Imaging team (CABI) for their patience and assistance with computer resource management. Many others provided support and suggestions for the current project, including: Ryan Brewster, Reema Jayakar, Sabrina Na, Michelle Fox, Eric Semmel and the King laboratory research team at Georgia State University. I would also like to express gratitude to my friends and family for their support throughout my graduate career. I would like to thank Jonathan Kincade and Samantha Alter for their unwavering support and assisting with copy editing this document. Lastly, I would like to thank the research participants and their families who willingly volunteered their time and effort to participate in the current study. Funding for this project was provided by the American Cancer Society (PI: T.Z. King, #RSGPB-CPPB-114044), and I was supported by the Doctoral Fellowship provided by the Georgia State University Language Literacy Initiative.

TABLE OF CONTENTS

LIST OF TABLES

LIST OF FIGURES

1 INTRODUCTION

1.1 Childhood Brain Tumors in the Cerebellum

Cerebellar brain tumors are the most common brain tumor in children (Gurney, Smith, and Bunin, 1999; Ostrom et al., 2015). Tumors in the cerebellum account for 18.7% of all brain and central nervous system tumors (Ostrom et al., 2015). Etiology remains poorly understood, although genetic vulnerabilities have been proposed as one possible mechanism (Mueller and Chang, 2009). From 1973-1976, the 10-year survival rate for childhood cerebellar tumors was 43.9% (Ostrom et al., 2015). In contrast, from 1997-2001 the 10-year survival rate for childhood cerebellar tumors was 76.8% (Ostrom et al., 2015). Therefore, medical advances have significantly improved survival outcomes, but there continue to be poor neurocognitive and neuroanatomical outcomes associated with survivorship (Duffner, 2004).

Tumor pathology has been shown to be related to treatment and subsequent outcomes. Different tumor pathologies have different cellular biologies, malignancies, and treatments (Nejat, Khashab, and Rutka, 2008). Commonly studied tumor pathologies include the benign pilocytic astrocytoma and the more aggressive, invasive, and malignant medulloblastoma (Mueller and Chang, 2009). Based on large population studies and descriptive reports of peak incidence rates, medulloblastoma tumors account for 40% of all cerebellar tumors and on average are most commonly diagnosed at 3-4 and 8-9 years old (Mueller and Chang, 2009; Nejat, Khashab, and Rutka, 2008; Ostrom et al., 2015). Astrocytoma tumors account for 20-35% of cerebellar tumors and on average are most commonly diagnosed at 4 years old (Mueller and Chang, 2009; Nejat, Khashab, and Rutka, 2008; Ostrom et al., 2015). Both tumor types are usually in

the posterior fossa, which includes the cerebellum, brain stem, and fourth ventricle, but occasionally occur in cortical brain regions. Across all pathologies, standard treatment includes one or a combination of the following: resection, radiation, chemotherapy, and shunt, all of which is based on age at presentation, location, malignancy, and intracranial pressure. However, many benign tumors require gross total resection followed by no adjuvant treatment at all (Mueller and Chang, 2009).

1.2 Functional Neuroanatomy of the Cerebellum and Cerebellar Pathways

All vertebrates have a cerebellum with a similar cellular architecture and relative size (Clark et al., 2001). The evolutionary success of the structure of the cerebellum suggests that it serves essential functions. The cerebellum consists of three overarching cellular layers—cortex, deep nuclei, and pedunculi (Blumenfeld, 2010). The cortex and the nuclei of the cerebellum are composed of grey matter and contain a large number of neurons that process information (Blumenfeld, 2010). Estimates for the number of neurons in the human cerebellum range from 70 billion to 101 billion, and consist of 82%-84% of all of the neurons in the brain, despite being only about 11% of the total brain volume (Andersen et al., 1992; Lange, 1975).

The cerebellar hemispheres are functionally related to the coordination between the cerebellum and the cortex via reciprocal pathways. The cerebellar hemispheres have three microstructural cellular layers: Molecular, Purkinje, and Granule (Blumenfeld, 2010). The molecular layer contains a number of different interneurons as well as the axons of granule cells (parallel fibers) and the dendrites of the Purkinje cells (Blumenfeld, 2010). The mossy fibers that synapse on Granule cells and climbing fibers that synapse on the Purkinje cells forms the excitatory synaptic inputs to the cerebellum

(Blumenfeld, 2010). The Purkinje cells provide output pathways for the grey matter in the lateral cerebellar hemispheres to the more anterior cerebellar white matter (Blumenfeld, 2010). The dentate is the largest nuclei and receives projections from the cerebellar hemispheres (Blumenfeld, 2010). The cerebellum also is connected to three peduncles: superior, middle, and inferior. The middle peduncle is the largest and carries inputs to the dentate from the cortex (Afferent pathway; Blumenfeld, 2010). Decussation occurs in the superior cerebellar peduncle, which carries many outputs from the cerebellar hemispheres to the dentate. Outputs project from the dentate nucleus to the contralateral thalamus (ventrolateral nucleus and ventral anterior portion) as well as the red nucleus, and then to the cortex (Efferent pathway; Alexander, DeLong, & Strick, 1986; Blumenfeld, 2010; Kelly and Strick, 2003; Parent, 1996). Decussation of neural tracts in general, including the crossing of the pathways from the cerebellum, has been theorized to be the result of an evolutionary rotation of the head of all vertebrates (de Lussanet & Osse, 2012; Kinsbourne, 2013).

The evolutionary history and structure of the cerebellum highlight its importance for essential functions across species. Further, the connections between the cerebellum and the cortex suggest that this structure has some role in supporting the functions of cortical brain regions. Therefore, from evolutionary, neuron-centered, and neuroanatomical perspectives, researchers have called for a more integrated view of the brain that accounts for the structural and functional role of the cerebellum in coordination with the cortex (Herculano-Houzel, 2009; Whiting and Barton, 2003).

1.2.1 Efferent Pathways from the Cerebellum

Review of the animal literature has suggested that pathways from the dentate nucleus divide into three separate bundles that project to the midbrain, red nucleus, and thalamus (Chan-Palay 1977). The current study focused only on the bundles that project to the red nucleus (cerebellar-rubral) and the thalamus (cerebellar-thalamic) because of their cortical involvement. Evidence for the cerebellar-rubral pathway and the cerebellar-thalamic pathway has been well documented in the animal literature across species (See Table 1). Studies of cerebellar degeneration in the cat estimate that approximately 75% of the dentate projections terminate in the red nucleus and 25% continue and terminate in the thalamus (Chan-Palay, 1977; Mussen, 1927).

The cerebellar-rubral pathway refers to the pathways from the dentate nucleus that project to and synapse on the red nucleus. Most of the pathways from the dentate nucleus synapse on the magnocellular portion of the lateral red nucleus (~50%) and a portion of the other pathways from the dentate nucleus (~25%) synapse on the parvocellular portion of the rostral part of the red nucleus (Mussen, 1927; Rand, 1954; Voogd, 1964). The remaining pathways from the dentate nucleus (~25%) form **the cerebellar-thalamic pathway.** These pathways leave the ventrolateral portion of the dentate nucleus, bypass the red nucleus, and divide into smaller bundles. There remains controversy in the animal literature regarding whether cerebellar-thalamic pathways travel around and bypass the red nucleus (Carpenter and Stevens, 1957), or travel through the rostral and lateral portions of the red nucleus without a synaptic terminal (Chan-Palay, 1977; Parent, 1996). Regardless, there has been consensus that projections from the dentate terminate on a variety of nuclei in the thalamus (e.g.,

ventral lateral, ventral anterior, dorsal medial, and midline; Alexander, DeLong, & Strick, 1986; Carpenter and Stevens, 1957; Chan-Palay, 1977; Earle and Matzke, 1974; Rand 1954). The thalamus then projects to a number of different cortical regions, including the dorsolateral prefrontal cortex (Kelly and Strick, 2003; Middleton & Strick, 2002). The current study focused on the pathways between the cerebellum and the dorsolateral prefrontal cortex because of their established involvement in cognitive functions (Salmi et al., 2010).

Table 1 Animal evidence for cerebellar-thalamic and cerebellar-rubral pathways

Author(s)	Year	Species	Evidence for Pathway
Carpenter and Stevens	1957	Rhesus monkey	Cerebellar-thalamic
Earle and Matzke	1974	Hedgehog	Cerebellar-thalamic
Harding	1973	Rhesus monkey	Cerebellar-thalamic
Rinvik and Grofova	1974	Cat	Cerebellar-thalamic
Evrard and Craig	2008	Macaque monkeys	Cerebellar-thalamic
Kelly and Strick	2003	Monkey	Cerebellar-thalamic
Mussen	1927	Cat	Cerebellar-thalamic and Cerebellar-rubral
Chan-Palay	1977	Rat	Cerebellar-thalamic and Cerebellar-rubral
Brodal and Gogstad	1954	Cat	Cerebellar-rubral
Caughell and Flumerfelt	1967	Rat	Cerebellar-rubral
Courville	1966	Cat	Cerebellar-rubral
Flumerfelt and Gwyn	1973	Rat	Cerebellar-rubral
King et al	1973	Opossum	Cerebellar-rubral
Tredici et al	1973	Cat	Cerebellar-rubral
Voogd	1964	Cat	Cerebellar-rubral
Rand	1954	Monkey	Cerebellar-rubral and Cerebellar-thalamic

Note. Adapted from information summarized in Chan-Palay (1977)

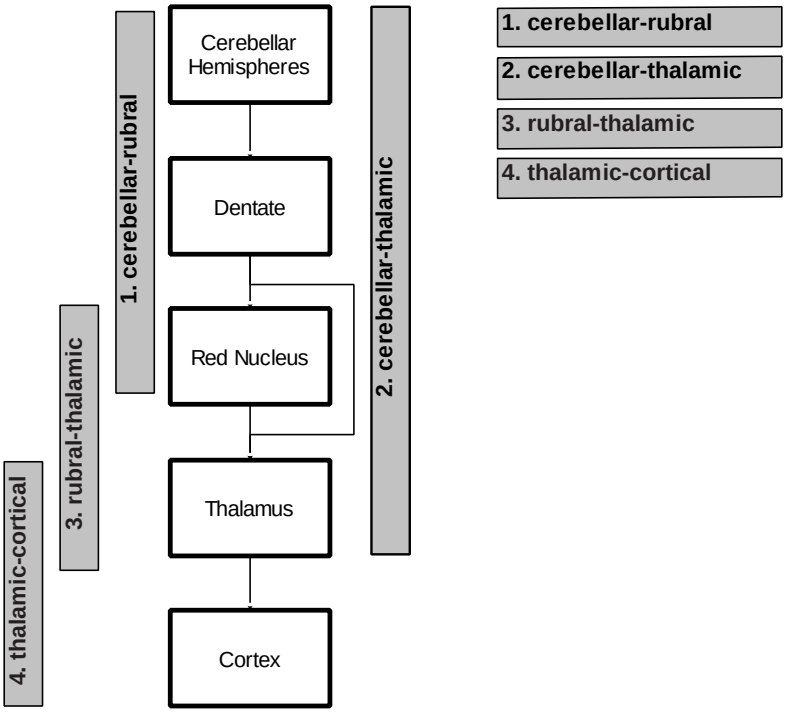

Figure 1 Summary of the segments of the cerebellar efferent pathway
Note. White boxes represent the structures in the brain, and grey boxes represent the white matter pathways that connect the structures in the brain.

1.3 Tractography of the Efferent Cerebellar-Cortical Pathway in Healthy Adults

To provide further support for the animal literature, four prior studies have used diffusion weighted tractography in humans to identify portions of the multisynaptic cerebellar-thalamic-cortical pathway (See Table 2). Two of these prior studies successfully segmented portions of the cerebellar-thalamic (Salmi et al., 2009) and the rubral-thalamic pathways (Habas and Cabanis, 2006) in healthy adults; however, the sections below focused on findings from the two tractography studies that constructed the most complete representation of the efferent cerebellar-cortical pathways based on the animal literature (Habas and Cabanis, 2007; Jissendi, Baudry, and Balriaux, 2008).

Diffusion weighted imaging is an image acquisition method that can be used to provide a measure of the rate and directionality of water molecules; theoretically, a

lower rate of water diffusion and strong directionality indicated myelinated axons (Cascio, Gerig, and Piven, 2007). Tractography uses an algorithm to construct the inferred axonal anatomy from the diffusion weighted data. The algorithm typically employs either an atlas-based or user-generated regions of interest (ROI) to include or eliminate white matter pathways based on their connection to specific brain structures. See Table 2 for the specific ROIs that were included in the human tractography studies.

Consistent with the animal literature, Habas and Cabanis (2007) found evidence for two separate pathways from the dentate to the red nucleus (cerebellar-rubral) and from the dentate to the thalamus (cerebellar-thalamic) in five healthy adults. In contrast to the inconsistencies reported in the animal literature, Habas and Cabanis (2007) reported that the cerebellar-thalamic pathway very closely bypasses the dorsomedial face of the red nucleus before entering the thalamus and then the prefrontal cortex (cerebellar-thalamic-cortical). However, Habas and Cabanis (2007) did not include a thalamic ROI; therefore, in their study, the rubral-thalamic portion of the pathway was not separately segmented and thus difficult to clearly discern from the cerebellar-thalamic pathway.

Jissendi, Baudry, and Balriaux (2008) have included the most precise ROIs to construct the multisynaptic cerebellar-frontal pathway in 10 healthy adults. However, rather than constructing the cerebellar-thalamic and rubral-thalamic pathways separately, the authors traced both the red nucleus and the region surrounding the red nucleus as a singular path in an effort to capture the cerebellar-thalamic pathways that do not pass through the red nucleus. Furthermore, the authors focus exclusively on Brodmann area (BA) 9 and do not construct the cerebellar projections to BA 46,

although both of the areas have been functionally implicated in working memory (Brunoni and Vanderhasselt, 2014).

Therefore, human tractography studies have provided support for each of the segments of the multisynaptic cerebellar-frontal pathway that have been described in animal studies. While each of the cerebellar-rubral, cerebellar-thalamic, rubral-thalamic, and thalamic-frontal have been identified using tractography, no researchers to date have constructed all of the individual segments of this pathway separately. The most notable limitations of the human tractography studies have been the inconsistencies and lack of clarity in the neuroanatomical representations of each segment of the efferent cerebellar-frontal pathways. Specifically, there have been methodological inconsistencies regarding the segmentation of the dentate projections to the red nucleus and the thalamus, despite the evidence for neuroanatomical distinction (Carpenter and Stevens, 1957; Habas and Cabanis, 2007; Parent, 1996).

Table 2 Tractography of the efferent multisynaptic pathway in healthy human populations

Author	Method	Pathways	Segmentation	Seed points	Inclusion masks	Exclusion masks
Habas and Cabanis (2006)	Probabilistic	Rubral-thalamic	None	Bilateral red nuclei	None	None
Habas and Cabanis (2007)	Probabilistic	Cerebellar-rubral Cerebellar-thalamic Thalamic-prefrontal	None	Bilateral red nuclei and dentate nuclei	None	None
Jissendi, Baudry, and Balriaux (2008)	Probabilistic	Cerebellar-rubral-thalamic-cortical	Cerebellar-rubral Rubral-thalamic Thalamic-cortical	Left thalamus	Dentate nucleus, superior cerebellar peduncle, red nucleus + surrounding area, prefrontal paraventricular area, anterior and medial prefrontal cortex (BA 9), and inferior posterior parietal cortex	None
Salmi et al. (2009)	Probabilistic	Cerebellar-thalamic-cortical Cortical-pontine-cerebellar	Cerebellar-thalamic Cerebellar-pontine	Bilateral cerebellum	Thalamus Pons	None

1.4 Diffusion Imaging of the Multisynaptic Cerebellar-Frontal Pathway in Brain Tumor Survivors

The multisynaptic cerebellar-frontal pathway has been of particular interest in the childhood cerebellar tumor population because of its involvement in verbal working memory. The most notable limitations of the human tractography studies on the cerebellar-frontal network has been the inconsistencies and lack of clarity in the neuroanatomical representations of the multisynaptic cerebellar-frontal pathway. Some studies within this population have constructed pathways based on only prefrontal and cerebellum ROIs (Rueckriegel et al., 2015; Soelva et al., 2013). Construction of the multisynaptic cerebellar-frontal pathway based only on prefrontal and cerebellar ROIs makes it impossible to differentiate between the contributions of the afferent versus efferent pathways, as well as the aforementioned cerebellar-frontal segmentations.

Two additional tractography studies have used similar ROIs but added the thalamus as an inclusion mask (Law et al., 2011; Law et al., 2012). It was possible that the addition of the thalamus captures the cerebellar-rubral, cerebellar-thalamic, rubral-thalamic, and thalamic-frontal tracts in one metric; however, it also was possible that this thalamic ROI based approach excludes the cerebellar pathways that synapse on the red nucleus. If the cerebellar-rubral pathway was excluded, then the studies were only measuring about 25% cerebellar output to the cortex based on animal models (Mussen, 1927; Rand, 1954; Voogd, 1964).

To address the methodological limitations of prior studies, Law et al. (2015a; 2015b) segmented the afferent and efferent portions of the multisynaptic cerebellar-frontal pathways. The afferent portion begins in the dorsolateral prefrontal cortex and

projects to the cerebellum via the pontine nuclei and middle cerebellar peduncle. Law et al. (2015a; 2015b) divided the afferent pathways into two segmentations- the frontal lobe to the pons and then the pons to the cerebellar hemispheres. For the efferent portion, the authors segmented three portions of the fiber tract: cerebellar-rubral, rubral-thalamic, and thalamic-cortical. Similar to the aforementioned limitation in healthy controls, these studies were limited by the lack of inclusion of the cerebellar-thalamic portion of the cerebellar-frontal pathway, which does not synapse on the red nucleus, and, neuroanatomically, may not pass through the red nucleus. Although there have been six tractography studies of the cerebellar-cortical pathways to date, no prior study has imaged the complete efferent pathways in healthy or cerebellar tumor populations. Table 3 summarizes methods, pathways, and segmentations across cerebellar brain tumor tractography studies.

With regard to methodology, almost all cerebellar tumor studies that have investigated the multisynaptic cerebellar-frontal pathways employed probabilistic tractography (Law et al., 2011; Law et al., 2012; Law et al., 2015a; Law et al., 2015b), and only two studies have used deterministic tractography (Rueckriegel et al., 2015; Soelva et al., 2013). Deterministic tractography provides a streamlined way to construct the most probable pathway based on user-defined white matter fiber trajectories; in contrast, probabilistic tractography uses the connection probability within a voxel to determine the most probable pathway from all possible paths between ROIs (Mukherjee et al., 2008). While both seek to find the most probable pathway, deterministic tractography infers the most likely axon pathway based on in-vivo virtual dissection of the brain fiber pathway (Abhinav et al., 2014). The comparison of approaches is

particularly noteworthy given that deterministic methods have been recommended over probabilistic methods for long-range pathways, such as the multisynaptic cerebellar-frontal pathway (Khalsa et al., 2014; Morris et al., 2008; Yo et al., 2009). While probabilistic methods have been described as vulnerable to factors unrelated to actual fiber connectivity, deterministic methods have been found to be more accurate at reconstructing tract connectivity (Jbabdi and Johansen-Berg, 2011; Jones et al., 2013). Therefore, additional research using deterministic tractography was necessary to confirm the current research using probabilistic methods in this population.

Lastly, the 6 prior studies of brain tumor survivors have been conducted by only two research groups. The Law et al. (2011; 2012; 2015a; 2015b) research group used a subset of participants from their 2011 study in their 2012 study, and similarly used a subset of participants from their 2015a study in their 2015b study. Soelva et al. (2013) and Rueckriegel et al. (2015) did not state whether there was sample overlap across their studies. Therefore, the existing studies appear to be based upon a relatively small subset of brain tumor survivors.

Table 3 Tractography of the multisynaptic efferent cerebellar-frontal pathways in cerebellar tumor populations

Author	Method	Pathways	Segmentation	Seed points	Inclusion masks	Exclusion masks
Law et al. (2011)	Probabilistic	Cerebellar-thalamic-frontal	None	DLPFC	Thalamus & cerebellar hemisphere	Corpus callosum, inferior medulla
Law et al. (2012)	Probabilistic	Cerebellar-thalamic-frontal	None	DLPFC	Thalamus & cerebellar hemisphere	None reported
Law et al. (2015a)	Probabilistic	Frontal-pontine-cerebellar				None reported
			Frontal-pontine	Frontal hemisphere, pons	Pons	
			Ponto-cerebellar		Pons, cerebellar hemisphere	
		Cerebellar-rubral-thalamic-frontal				
			Cerebellar-rubral	Cerebellar hemisphere	Superior cerebellar peduncle, red nucleus	
			Rubral-thalamic		Red nucleus, thalamus	
			Thalamic-frontal		Thalamus, frontal hemisphere	
Law et al. (2015b)	Probabilistic	Same as Law et al., 2015				None reported
Rueckriegel et al (2015)	Deterministic	Frontal-cerebellar	None	Prefrontal cortex	Entire cerebellum	None reported
Soelva et al. (2013)	Deterministic	Frontal-cerebellar	None	Prefrontal cortex	Entire cerebellum	None reported

Note. All studies included bilateral pathways. Law et al. (2011; 2012) defined the Dorsolateral PreFrontal Cortex (DLPFC) as followed: medial prefrontal cortex, inferior prefrontal gyrus, the superior and middle frontal gyri, and parts of the inferior frontal gyrus (i.e. pars opercularis and pars triangularis); Rueckriegel et al. (2015) and Soelva et al. (2013) defined the prefrontal cortex as volume delineated by the frontal cerebral pole, the interhemispheric fissure, and the temporal pole.

1.5 Theories of the Cerebellum and Working Memory

Precise and accurate construction of the multisynaptic cerebellar-frontal pathway has been important because of its involvement in cognition. There have been a number of theories regarding the role of the cerebellum in cognition. One theory proposed that the cerebellum increases brain efficiency. The efficiency theory posited that the whole cerebellum works to support the efficiency of other brain regions, and individual regions within the cerebellum are not responsible for any specific functions (Bower, 1997). Similarly, researchers have proposed that the cerebellum likely helps to automate learned processes (Koziol et al., 2014). One other study found that the cerebellum has been involved in the initiation of movement in monkeys who have rehearsed a ballistic wrist movement task (Mink and Thach, 1991), and this finding also could be explained by cerebellar activation as a result of learning the rehearsed motor task.

However, the evidence for homogenous cerebellar function has been mixed; for example, single pulse synchronized transcranial magnetic stimulation (sTMS, 1 pulse, 120% MT Intensity, double cone, 110 mm/ handle up) of lobes VI and crus I in the cerebellum resulted in slowed processing speed on verbal working memory tasks, but did not change processing speed on motor tasks (Desmond, Chen, and Shieh, 2005). The cerebellar-cortical pathways have been implicated in motor and cognitive functions (D'Angelo and Casali, 2013; Koziol and Budding, 2009). Furthermore, specific lobes within the cerebellum have been differentially implicated in these pathways in primates (Kelly and Strick, 2003). Therefore, other researchers have proposed functionally heterogeneous lobes of the cerebellum because they connect to different cortical brain

regions associated with either motor or cognitive processing (D'Angelo and Casali, 2013; Kelly and Strick, 2003).

Desmond et al. (1997) proposed a theoretical functional relationship between the frontal lobe and lobe VI and crus I of the cerebellum that supports verbal working memory (Desmond, Chen, and Shieh, 2005; Chen and Desmond, 2005a). Furthermore, this research group found evidence that superior cerebellar activation, which was structurally and functionally associated with the Brodmann area (BA) 44/6, corresponded with an articulatory control process, particularly during task encoding (Chen and Desmond 2005a; Chen and Desmond, 2005b). This evidence was consistent with their theory that the cerebellar-frontal pathway supports articulatory control for working memory.

In sum, the cerebellum has a number of different functions that potentially contribute to working memory. Some research has suggested that the cerebellum supports learning and cognitive efficiencies broadly (e.g., Bower, 1997), and other studies have suggested more specific cerebellar functions (D'Angelo and Casali, 2013; Desmond, Chen, and Shieh, 2005; Kelly and Strick, 2003). With regard to working memory, there was evidence to suggest that the cerebellum and frontal regions are activated during encoding and articulatory control (Chen and Desmond 2005a; Chen and Desmond, 2005b; Desmond, Chen, and Shieh, 2005; Desmond et al., 1997). While the evidence has remained mixed, the consensus has suggested a cerebellar involvement in learning or efficiency.

1.6 Behavioral associations with the Cerebellar-Frontal Pathway

Prior studies have documented lower white matter integrity in bilateral multisynaptic cerebellar-frontal pathway following brain tumor treatment, and researchers have found associations between this pathway and measures of verbal working memory (Law et al., 2011; Law et al., 2015b; Rueckriegel et al., 2015). While prior studies have provided valuable information on the relationship between cerebellar-frontal white matter integrity and verbal working memory, additional research is necessary to understand and integrate these findings from neuroanatomical, methodological, and theoretical perspectives.

Cerebellar tumor survivors have lower white matter integrity in the bilateral frontal–cerebellar tract when compared to controls (Law et al., 2011; Law et al., 2015a; Soelva et al., 2013). Correspondingly, lower white matter integrity in the right cerebellar-left frontal pathway has been correlated with cerebellar resection and radiation treatment (Law et al., 2011; Law et al., 2015a; Law et al., 2015b); this finding applies to survivors treated with cranial radiation and those treated with only surgical resection (Law et al., 2011). Furthermore, longer time since treatment correlated with lower white matter integrity in the right cerebellar-left frontal pathway regardless of treatment (e.g., surgery alone vs. radiation; Law et al., 2011; Law et al., 2015a). Within the right cerebellar-left frontal pathway, posterior segments (e.g., cerebellar-rubral and pontine-cerebellar) had lower white matter integrity when compared to other segments (e.g., rubral-thalamic and thalamic-cortical), which was attributed to both surgery and radiation (Law et al., 2015a). Taken together, lower white matter integrity in the right cerebellar-left frontal pathway has been well documented and appeared to be related to

the segment of the pathway, radiation treatment, as well as time since treatment in both cranial radiation and surgery only treatment groups.

The relative sensitivity of the pathways that directly connect to the cerebellum is important for the current study. While, Law et al. (2015a; 2015b) found that posterior segments (e.g., cerebellar-rubral) had lower white matter integrity when compared to other segments (e.g., rubral-thalamic), they did not include a direct cerebellar-thalamic segment of the pathway. Similar to the cerebellar-rubral segment, the cerebellar-thalamic segment also likely has lower white matter integrity when compared to more distant segments (e.g., rubral-thalamic or thalamic-cortical), due to the direct connection to the cerebellum. Therefore, the current study sought to add to the findings of Law et al. (2015a; 2015b) by including the white matter integrity of the cerebellar-thalamic segment.

Longer time since diagnosis has been identified as a predictor of lower white matter integrity within the cerebellar-frontal pathway (Law et al., 2015a); however, in the above literature, the average time since diagnosis and treatment was only 5.71 years (*SD*= 3.8 years). In brain tumor populations, white matter volume may fail to develop normally and continue to decline with a longer time since diagnosis (Reddick et al., 2005). Therefore, additional research with a longer follow-up period is important to examine the long-term impact of tumor treatment on white matter integrity within this pathway.

Lower white matter integrity in the cerebellar- frontal pathway has been associated with lower verbal working memory (Law et al., 2011, Law et al., 2015b; Rueckriegel et al., 2015). In cerebellar tumor populations, one study has found that

lower white matter integrity in the bilateral cerebellar-frontal pathways did not correlate with either processing speed (Amsterdam Neuropsychological Tasks, baseline speed reaction time) or attention (Amsterdam Neuropsychological Tasks, shifting attentional set; Rueckriegel et al., 2015). Instead, bilateral cerebellar-frontal white matter integrity correlated with an intelligence measure that included a component of working memory and processing speed among other skills (Rueckriegel et al., 2015; i.e., WISC-III FSIQ which included Similarities, Arithmetic, Vocabulary, Comprehension, Picture Completion, Coding, Picture Arrangement, Block Design, and Object Assembly). Another study, using different methods (probabilistic instead of deterministic tractography) found that lower white matter integrity in the right cerebellar-left frontal pathway associated with poorer working memory performance, but not poorer vocabulary performance (Law et al., 2011). Law et al. (2015b) expanded on these findings and investigated the relationship between bilateral reciprocal pathways separately (cortical-pontine-cerebellar and cerebellar-rubral-thalamic-cortical) in relation to working memory. The authors found that only white matter integrity in the left cerebellar-rubral-thalamic-frontal pathway was related to working memory (measured by Working Memory Test Battery for Children, Forward Digit Recall, Word List Recall, Block Recall, and Backward Digit Recall). Therefore, the most recent and methodologically specific literature (Law et al., 2015b) has suggested that only the left lateralized efferent pathway from the dentate to the cerebellum to the frontal lobe specifically related to working memory. Law et al. (2015b) concluded based on findings across studies that brain tumor survivors, and more specifically posterior fossa medulloblastoma survivors, display a diffuse disruption in the cerebellar-frontal network

that was correlated with lower working memory performance (Law et al., 2011; 2012; 2015a; 2015b).

From a neuroanatomical perspective, the findings from Rueckriegel et al. (2015) were obscured by the averaging of the left and right pathways. Laterality should be an important consideration because the right frontal lobe, and potentially corresponding cerebellar pathway, has been related to attention (Mannarelli et al., 2015) and the right cerebellar-left frontal pathway has been related to verbal working memory (Law et al., 2011). Correspondingly, two prior studies have documented that cerebellar-frontal white matter integrity in the left, but not the right pathway related to working memory in short-term survivors (Law et al., 2011 & 2015b). However, since these studies were conducted by the same research group, their results may be based on a subset of the same sample. Lastly, some prior studies did not report tumor location within the posterior fossa (e.g., Law et al., 2011; Rueckriegel et al., 2015), and the two studies that did report tumor location studied tumors located primarily in the midline of the posterior fossa (91% midline - Law et al., 2015a; 96% midline - Law et al., 2015b). Therefore, additional research is necessary to determine if these findings apply to lateralized cerebellar tumors.

From a theoretical perspective, prior studies have been primarily exploratory without a guiding theoretical framework. As a result, no study has differentiated whether the relationship between right cerebellar-left frontal white matter integrity and verbal working memory has been explained by measures of processing speed or attention. Differentiation of these relationships is important because there was one model that suggested that cerebellar tumor survivors have deficits in working memory due to

underlying difficulties with processing speed and attention (Palmer, 2008), whereas another model suggested that processing speed, attention, and working memory were independent factors (Wolfe et al., 2012).

1.7 Theoretical Framework

Theoretical models of cognition and knowledge in healthy children have suggested that attention, working memory, and speed/efficiency are either facilitators or inhibitors of overall cognition or knowledge—such that deficits or strengths in these skills would inhibit or facilitate learning and cognition (Miller, 2013). Similarly, theoretical models based on childhood cerebellar tumor survivors have suggested that the domains of processing speed, attention, and working memory underlie difficulties across broad neurocognitive domains (Palmer, 2008; Wolfe et al., 2012). However, to date, only one of these tractography studies has included measures of attention and processing speed (Rueckriegel et al., 2015).

In healthy children, processing speed and working memory rapidly develop in parallel during ages 6-12 (Fry and Hale, 1996), and correspond with increases in intelligence (Fry and Hale, 2000). This period of rapid cognitive development is critical considering 74% of cerebellar tumors are diagnosed before 10 years of age (Ostrom et al., 2015). In general, brain regions are more susceptible to damage if they myelinate later in development and receive a higher dosage of radiation (Mulhern et al., 2004; Reinhold et al., 1990). While the cerebellum develops prenatally (Blumenfeld, 2010), researchers have found that the cerebellar-cortical white matter pathways continue to develop from adolescence to adulthood (Stevens et al., 2009). In further support of

these theoretical models (Miller, 2013; Palmer, 2008), the cerebellar-cortical white matter pathways have been associated with the automation of learned processes and thus indirectly related to the speed of processing (Koziol et al., 2014). Therefore, early cerebellar-cortical white matter injuries in cerebellar tumor survivors may be related to slowed processing speed and underlie poor attention and working memory, which then has a cascading impact on broad learning and cognition (Palmer, 2008; Miller, 2013). Given the importance of processing speed and attention in theoretical models, as well as the early vulnerability to white matter injury, additional research is necessary. The current study investigated whether white matter integrity of the cerebellar-frontal pathway is specific to working memory, and not disrupting the underlying skills of processing speed or attention, which in turn may disrupt many cognitive skills, including working memory.

1.7.1 Processing Speed

Processing speed is a behavioral description across task performance rather than a discrete neurocognitive skill. Neuropsychological tests do not measure discrete and unitary mental skills but instead have been designed to provide a multifactorial assessment of a variety of skills that require interpretation by a neuropsychologist (Lezak et al., 2012). These multifactorial assessments are useful and efficient for neuropsychologists who use within-person (intraindividual) and between-person comparisons (interindividual) across a full battery of neuropsychological tests to determine individual patterns of strengths and weaknesses (Lezak et al., 2012). However, research on neuropsychological tests requires special considerations because systematic within-person comparisons are untenable. For instance, measures

of processing speed often have been combined with motor functioning and often require executive functioning. Therefore, difficulties on measures of processing speed could be explained by the other skills involved in task performance.

To address these concerns, researchers have utilized factor and principal component analytic approaches to determine the best measures of processing speed. Luciano et al. (2009) used principal component analysis with 1,013 participants to derive a speed factor that included the following measures: Symbol Search, Digit Symbol, Mean Simple Reaction Time, Mean Choice Reaction Time, and Inspection Time. Similarly, Philips (2012) tested a confirmatory factor analysis based on a sample of 235 children with neuropsychological concerns. Philips (2012) tested three models (single processing speed factor, Cattell–Horn–Carroll (CHC) theory, and the School Neuropsychology/CHC model), and reported that the following neuropsychological measures had a strong factor loading (>.5): WISC-IV Cancellation, WISC-IV Coding WISC-IV Symbol Search, DKEFS Stroop Color Naming, DKEFS Stroop Word Reading, DKEFS Fluency Letters, and DKEFS Fluency Categories. However, another study that included younger and older adults (n= 104) found that phonemic fluency highly loads on an executive functioning factor and only WAIS-R Digit Symbol and Choice Reaction Time loaded on the processing speed factor (Bunce and Macready, 2005). Therefore, the prior literature suggested that the best available neuropsychological measures of processing speed were: Digit Symbol Decoding, Choice Reaction Time, Visual Scanning, Rapid Color Naming, and Rapid Word Naming (Bunce and Macready, 2005; Luciano et al., 2009; Philips, 2012). Due to the difficulties operationalizing processing speed using multifactorial neuropsychological assessments, a measure of processing

speed was computed in the current study. The measure included an average of the neuropsychological assessments with a high factor loading on the processing speed factor based on the prior literature.

1.7.2 Attention and Working Memory

In addition to the problems with the measurement of processing speed, there have been inconsistencies in the measurement of attention and working memory. Specifically, only one study explicitly tested attention using the Amsterdam Neuropsychological Tasks, shifting attentional set (Rueckriegel et al., 2015). While other researchers did not intend to test attention, all of the aforementioned studies have included measures of attention (e.g., Digit Span Forward) within their measure of working memory (e.g., Law et al., 2011; Law et al., 2015b; Rueckriegel et al., 2015). Therefore, additional research is necessary to examine the relationship between the cerebellar-frontal pathway and measures of working memory that have not been combined or averaged with measures of attention span.

1.8 Summary and Gaps in Prior Literature

In sum, additional research is necessary to understand and integrate findings from neuroanatomical, methodological, and theoretical perspectives. To advance on the prior studies from a neuroanatomical perspective, the current study sought to include cerebellar-rubral, cerebellar-thalamic, rubral-thalamic, and thalamic-frontal segments of the efferent cerebellar-frontal pathway. Furthermore, only the efferent right cerebellar connections to the left frontal lobe were included to address the lack of specificity of prior studies that included bilateral or reciprocal (afferent and efferent together) pathways. The efferent connections were selected based on the

empirical evidence that lower white matter integrity in these connections alone was related to verbal working memory (Law et al., 2015b). The current study uses deterministic instead of probabilistic tractography methods to advance on prior studies from a methodological perspective. Furthermore, the current study uses a longer follow-up period (*M*=13 years post diagnosis) to advance the literature on long-term survivor outcomes following cerebellar tumor treatment. Lastly, to advance on the theoretical and methodological limitations of prior studies, the current study tests theoretical models (Miller, 2013; Palmer, 2008) of working memory deficits by including measures of processing speed and attention, with careful selection of the measurement of these constructs. Overall, the current study is an important next step to address a number of the limitations of the existing literature.

1.9 Aim 1

Expand on prior finding that white matter integrity in the right cerebellar-left frontal pathways has been associated with working memory by incorporating theory, neuroanatomy, and methodological advancements.

1.9.1 Hypothesis 1

Lower white matter integrity in the right cerebellar-left frontal pathways (sum of cerebellar-rubral, rubral-thalamic, cerebellar-thalamic, and thalamic-frontal pathways) should be associated with lower working memory, but not processing speed or attention span.

1.10 Brain Tumor Risk Factors

The complexity of treatment factors is important to consider for the current study on childhood cerebellar tumor survivors. Researchers have found that surgery, younger

age at diagnosis, radiation dosage, and longer time since treatment have been related to lower whole brain white matter volume and integrity (e.g., Aukema et al., 2009; Khong et al., 2003; Law et al., 2011; Merchant et al., 2008; Palmer et al., 2012; Reddick et al. 2005). Lower whole brain white matter integrity has been correlated with lower Full-Scale Intelligence (FSIQ), processing speed, and attention (Palmer et al., 2012; Rueckriegel et al., 2015).

Palmer (2008) proposed that age at diagnosis and treatment was a direct proxy for the rapid brain myelination that occurs during childhood (Casey, Giedd, & Thomas, 2000; Moore, 2005; Pfefferbaum et al., 1994). Some research has suggested that an early age at neurological insult would result in an abnormal trajectory for the development of any skills acquired after the brain insult (Dennis, Yeates, Taylor and Fletcher, 2006; Taylor and Alden, 1997). Therefore, younger children are considered at greater risk for lower white matter integrity as well as lower academic and intellectual performance (Palmer, 2008).

Radiation treatment appears to have a neurotoxic impact that continues over time. Therefore longer time since treatment (Mulhern et al., 2001), and higher radiation dosage has been associated with lower whole brain white matter volume (Reddick et al., 2000; Palmer et al., 2002). Consistently, survivors of posterior fossa medulloblastoma have lower whole brain white matter volume than controls (Reddick et al., 2005; Riggs et al., 2014). Reductions in white matter appear to be related to both a loss of white matter volume and failure to develop age expected growth in white matter. For example, using a single MRI slice estimate, survivors of childhood medulloblastoma had a 1.1% decrease in white matter volume each year and a failure to develop the

typical 5.4% white matter volume gains per year that were observed in healthy children (Reddick et al., 2005). One caveat of these findings was that a single slice MRI might result in the erroneous conclusion that these findings were consistent throughout the brain.

Nonetheless, reductions in whole brain white matter volume also were related to increases in fractional geometry, a mathematical index of structure complexity (Shan et al., 2006). Researchers have inferred that fractional geometry related to the neurobiological process of cellular or vascular pathogenesis, demyelination, and reduced white matter density (Shan et al., 2006). Correspondingly, in animal studies radiation-induced cellular and vascular compromise related to demyelination (Reinhold et al., 1990). Specifically, demyelination occurred following the initial radiation-induced cellular and vascular injury, which then created a negative feedback loop in which the cells, blood vessels, and myelin continued to degenerate for at least one year following treatment (Reinhold et al., 1990). Vascular injury may differentially impact different tissue types in the brain, because the white matter vasculature has a lower density and fewer connections among blood vessels when compared to the grey matter vasculature (Blumenfeld, 2010; Reinhold et al., 1990). Correspondingly, one brain tumor study found that whole brain grey matter was more resilient to brain tumor treatment when compared to white matter (Riggs et al., 2014). Other researchers have proposed that grey matter resiliencies were related to the developmental trajectory of grey matter, which usually develops by age 4, as opposed to white matter which continues to develop through early adulthood (Palmer, 2008; Pfefferbaum et al., 1994). Therefore, radiation-induced cellular and vascular pathogenesis early in development may explain

the loss of whole brain white matter volume and the failure to develop age expected gains in white matter, as well as the relative resiliencies of whole brain grey matter in brain tumor populations.

While grey matter was arguably more resilient (Riggs et al., 2014), grey matter and white matter regions have been shown to be affected by tumor treatment. Consistent with animal and human studies that suggested that subcortical regions were susceptible to radiation neurotoxicity (e.g., Jayakar et al., 2015; Reinhold et al., 1990), the regions of grey matter vulnerability in cerebellar tumor populations were located primarily in subcortical and posterior fossa regions. Grey matter volume ROI findings included the cerebellum, cerebellar vermis (anterior and posterior), bilateral thalamus, bilateral entorhinal cortex, bilateral hippocampus, and bilateral putamen (Ailion et al., 2016; Horska et al., 2010; Jayakar et al., 2015; Riggs et al., 2014).

In sum, longitudinal studies of whole brain volume have suggested both a progressive loss of white matter and a failure to develop normal white matter volume gains. These changes may be related to an underlying neurobiological process of vascular or cellular pathology. While in general, these findings appear diffuse researchers also have found that subcortical grey matter regions appeared to be at risk for greater radiation-induced volume loss.

The literature suggesting diffuse white matter volume loss in brain tumors populations highlights the need to determine the specificity of the relationship between the cerebellar-frontal white matter integrity and working memory. Lower white matter integrity in the cerebellar-frontal pathway could simply be indicative of lower whole brain white matter integrity; similarly, poorer working memory performance could be indicative

of lower whole brain white matter integrity. Therefore, lower whole brain white matter integrity presents as a potential confound to lower white matter volume within specific pathways. To date, no prior studies on the cerebellar-frontal pathway have reported a double dissociation with a comparison white matter pathway and cognitive measure. The current study adds to the prior literature by testing a theoretically and empirically informed double dissociation with a comparison white matter pathway and comparison cognitive task to test the specificity of the brain-behavior relationship.

A number of criteria were used to select the comparison brain-behavior relationship for the double dissociation. First, the comparison white matter pathway needed to have long-range connections between brain regions to be similar and comparable to the cerebellar-frontal pathway. Second, the long-range pathway needed to be correlated with a behavior, and that behavior needed to be distinct from working memory performance. The task that was selected for Aim 1 was verbally-mediated, and the goal of the control task was to have minimal overlap both with the brain systems involved and the cognitive task demands. Therefore, a visually-mediated task would be more likely to identify a double dissociation when compared to another verbal task, because visual tasks are more likely to recruit distinct brain systems and more likely to have minimal overlap with verbal task demands. Lastly, an ideal behavior would be grossly intact following cerebellar tumor treatment, as another impaired behavior may not provide adequate variance or differentiation to identify a double dissociation. A number of different relationships were considered to select the best possible comparison pathway to identify a double dissociation. Table 4 provides the rationale as to how a number of tracts were not selected for the double dissociation.

Table 4 Possible comparison pathways

Pathway	Behavior	Pros	Reasons pathway was not selected
Anterior supramarginal gyrus- Posterior supramarginal gyrus	Vocabulary	Single dissociation was found with vocabulary in one prior study (Law et al., 2011)	1. Short range pathway 2. Brain regions have been associated with verbal working memory (Chen and Desmond, 2005)
Cortico- Spinal	Motor Performance	Long range tract; involves cortical and subcortical regions	1. A prior study on this sample did not find this pathway to be associated with motor performance (Smith et al., 2014). 2. A double dissociation was unlikely with this pathway because motor skills are often impaired following cerebellar tumor treatment.
Cerebellar-Frontal (motor cortex)	Motor Performance	Long range tract; involves cortical and subcortical regions	1. A double dissociation was unlikely with this pathway because motor skills are often impaired following cerebellar tumor treatment. 2. This pathway also was likely too similar to the cerebellar-dorsolateral prefrontal pathway.
Cerebellar-Temporal	Naming	Long range tract; involves cortical and subcortical regions	1. There was evidence that the dentate has very limited output to the temporal lobe (Glickstein et al., 1985; Ramnani et al., 2006). 2. Naming involved verbal output.
Cerebellar-Parietal	Visual Attention	Long range tract; involves cortical and subcortical regions	1. A prior study was only able to identify this pathway in 60% of healthy participants (Jissendi, Baudry, and Balriaux, 2008)

Within the cortex, one long-range pathway was selected that has been correlated with a cognitive skill that was distinct from working memory and was responsible for visually-mediated information. This pathway is the superior longitudinal fasciculus (SLF), which has been associated with the dorsal stream, also known as the “where” pathway (Hoeft et al., 2007; Thiebaut de Schotten et al., 2011). The SLF has been divided into three separate branches (SLF I, II and III) based on animal and human models (Thiebaut de Schotten et al., 2011). The current study focused on the SLF II, which connects the angular gyrus in the parietal lobe to the dorsolateral prefrontal area (Doricchi et al., 2008; Hoeft et al., 2007; Kamali et al., 2014; Makris et al., 2005). Within this pathway, the parietal region (caudal inferior parietal lobe) has been involved in spatial attention on the basis of human and animal studies (Bisley and Goldberg, 2003; Mesulam, 1981), and the SLF II links visual information to the prefrontal cortex (Makris et al., 2005). One theory regarding the function of this reciprocal pathway has been that the right prefrontal cortex regulates visual attention (Makris et al., 2005).

The right SLF II has been associated with spatial processing, and has been associated with target search tasks in monkeys (Gaffan and Hornak, 1997) as well as target cancellation (Doricchi and Tomaiuolo, 2003), line bisection (Thiebaut de Schotten et al., 2011; Thiebaut de Schotten et al., 2005), visuospatial construction (Hoeft et al., 2007), and visual attention tasks (Urbanski et al., 2008) in humans. To address the concern that visual attention measures, such as cancellation, have a motor and speed component, the number errors independent of the speed on the cancellation measure was included in the current study (DKEFS Visual Scanning).

Based on prior literature, white matter integrity in the right SLF II and visual cancellation task performance should be correlated (Doricchi and Tomaiuolo, 2003; Makris et al., 2005; Thiebaut de Schotten et al., 2011; Urbanski et al., 2008). Furthermore, the right SLF II has not been correlated with measures of verbal working memory (Karlsgodt et al., 2008). Additionally, untimed measures of visual cancellation should not be correlated with measures of working memory. Lastly, no literature has suggested that the cerebellar-frontal pathway should be related to an untimed measure of visual cancellation. Therefore, based on all available evidence, the cerebellar-frontal relationship to working memory should demonstrate a double dissociation from the relationship between SLF II and visual attention. This proposed double dissociation would suggest that lower white matter integrity was both pathway and task specific, and would provide evidence against the argument that diffuse white matter reductions were correlated with gross reductions in neurocognitive performance.

1.11 Aim 2

Double dissociation between the cerebellar-frontal and the right SLF II pathways with both working memory and visual attention performance.

1.11.1 Hypothesis 1

Lower white matter integrity (WMI) in the cerebellar-frontal pathways should be associated with lower working memory, but not visual attention performance.

1.11.2 Hypothesis 2

Lower WMI in the right SLF II should be associated with lower visual attention performance, but not lower working memory performance.

All of the aforementioned aims and hypothesis have focused on diffusion tractography methods to measure white matter integrity. For the remaining aim, measures of brain volume have been incorporated to advance the understanding of neuroanatomical relationships among the volume of brain regions, the pathways that have been constructed to connect them, and their corresponding behaviors.

Prior studies have documented damage to the brain structures involved the cerebellar-frontal pathways including lesions in the hemispheres, vermis, and dentate of the cerebellum (Puget et al., 2009; Kirschen et al., 2008; Konczak et al., 2005; Küper et al., 2013), lower white matter integrity in the pons (Khong et al., 2003; Morris et al., 2009), and lower volume in the bilateral thalamus (Zhang et al., 2008). Furthermore, a number of researchers have reported lower white matter integrity in the frontal lobe (King et al., 2015; Qiu et al., 2007; Soelva et al., 2013). Lower white matter integrity in the frontal lobe has been found in survivors regardless of radiation treatment (Rueckriegel et al., 2015), but for survivors treated with radiation, frontal lobe white matter integrity has appeared to be uniquely vulnerable when compared to the parietal lobe white matter integrity (Qiu et al., 2007).

With regard to neurocognition, lesions in the cerebellum and lower frontal lobe white matter integrity have been associated with lower attention and working memory performance. Kirschen et al. (2008) investigated how cerebellar damage following benign cerebellar tumors affected verbal working memory and found that damage to the left hemispheric lobe VIII was correlated with lower auditory attention (experimental digit span forward task). With regard to the whole frontal lobe, white matter integrity

correlated with lower executive functioning as measured by the Wisconsin Card Sorting Test and the Trail Making Test, Part B (e.g., working memory, shifting attention, cognitive flexibility; Brinkman et al., 2012). However, shifting also was associated with fractional anisotropy (FA) in the bilateral temporal and parietal lobes and Trails B was associated with radial diffusivity (RD) in the bilateral temporal lobe (Brinkman et al., 2012). While the authors justified their findings based on literature that suggests that the frontal-parietal network supports executive control processes (Barbey et al., 2012), this theory was not mentioned as an a priori hypothesis, and the specific regions within the *left lateralized* frontal-parietal network were not investigated (e.g., frontopolar, anterior prefrontal, dorsolateral prefrontal, medial prefrontal, inferior parietal, superior parietal); rather, the authors only reported findings in relation to the *entire bilateral* frontal and parietal lobes. These findings, which were inconsistent with the literature that suggests that executive function corresponds with the left lateralized frontal-parietal network, were likely due to the large number of exploratory analyses conducted, the lack of correction for statistical comparison, and a large ROI approach.

While these studies have provided valuable information about the relationships between the cerebellum, the frontal lobe, and working memory, they have noteworthy limitations. First, findings from Kirschen et al. (2008) were inconsistent with the literature that suggested that the cerebellar lobe VIII projects to the motor cortex (Kelly and Strick, 2003), as well as the extensive literature that suggested that the posterior lobes of the cerebellum (e.g., Crus I and II) project to the dorsolateral prefrontal cortex and are involved in verbal working memory (Desmond et al., 1997; Hoang et al., 2014; Kelly and Strick, 2003; Stoodley and Schmahmann, 2009). However, other research has

suggested that the right VIII and the left inferior parietal lobe are activated during encoding and maintenance phases of a verbal working memory task (Chen and Desmond, 2005).

Furthermore, Kirschen et al. (2008) did not include a control region or a control task, but rather used Bonferroni correction and regressed each of the 24 lobes of the cerebellum on the cognitive measures. Similarly, while Brinkman et al. (2012) found a number of relationships, the authors computed correlations on 6 different brain lobes (left and right frontal, parietal, and temporal lobes), for two different diffusion metrics (FA and RD), across 30 neurocognitive domains, which resulted in 360 correlations but no statistical correction for multiple comparisons was reported. These limitations highlight the need for hypothesis-driven research and the issue of multiple comparisons in neuroimaging research.

1.12 Theoretical Relevance

One explanation for lower volume and white matter integrity within the brain regions in the cerebellar-frontal pathways originates in the functional neuroimaging literature. Theories of brain function suggest that a lesion can disrupt neural activity, which in turn disrupts functional connections between the lesioned region and its distant functional connections, a concept known as diaschisis (von Monakow, 1914). One functional imaging study reported that diaschisis occurs in the forebrain after stroke in the cerebellum (Rehme and Grefkes, 2013). Therefore, possible diaschisis following cerebellar tumor resection may underlie or relate to reductions in white matter integrity and volume in the brain structures involved in the cerebellar-frontal pathway.

One study on cerebellar atrophy following traumatic brain injury (TBI) has provided valuable insights on the relationships among the volume of the pons, cerebellum, thalamus, and dorsolateral prefrontal cortex following cerebellar atrophy. Cerebellar atrophy was of particular relevance because researchers also have found significant cerebellar atrophy in cerebellar tumor survivors (Ailion et al., 2016; Dietrich et al., 2001; Szathmari et al., 2010). Spanos and colleagues (2007) inferred based on their volumetric results that the cerebellum and corresponding regions included in cerebellar-cortical pathways, particularly the pons and the dorsolateral prefrontal cortex, may be vulnerable to a cascading impact of cerebellar atrophy following a moderate to severe TBI. The authors report correlations between white matter volume in the cerebellum and the frontal lobe, as well as the cerebellum and the thalamus in healthy children, but these relationships were not found in children with moderate to severe TBI. In contrast, the volume of the thalamus was correlated with the volume of the frontal lobe in both groups (TBI and controls). The authors proposed that atrophy in the cerebellum may result in disconnection and may be related to lower volume in the other brain regions in the cerebellar-frontal pathways; one possible explanation for this finding was myelin or axonal degeneration (Spanos et al., 2007).

While Spanos and colleagues' (2007) study illuminated a possible association between the volumes of the structures within the cerebellar-frontal network, conclusions from their study were limited by a few important considerations. First, the authors only investigated the volume of the pons, cerebellum, thalamus, and dorsolateral prefrontal lobe. As previously described, the efferent connections between the cerebellum and the frontal lobe also synapse on the red nucleus, which was not included in their study. The

lack of inclusion of the red nucleus may explain why the authors did not find a relationship between the volume of the cerebellum and the volume of the thalamus in the TBI group. Second, the authors mention possible myelin or axon degeneration as one explanation for their findings, but this theory was never tested. As the authors mention in their conclusion, diffusion tractography could be used to construct the cerebellar-frontal fiber pathways to test whether the measures of myelin or axon degeneration were correlated with lower volume within these structures.

To review, prior literature provides evidence for 1) reduced volume in the brain structures involved in the cerebellar-frontal pathway following cerebellar tumor treatment, 2) lesions and lower white matter integrity in the cerebellum and the frontal lobe related poorer working memory performance, 3) diaschisis or cellular degeneration, and 4) cerebellar atrophy may explain reduced volume in the thalamus and dorsolateral prefrontal cortex. While prior research has investigated the relationship between working memory and white matter integrity of the cerebellar-frontal pathway (e.g., Law et al., 2015b) and volumetric measures of brain structures along the pathway (e.g., Kirschen et al., 2008), no study had combined diffusion and volumetric measures to determine the relationship between volume of brain regions, the pathways that connect the regions, and verbal working memory. In addition to the substantial empirical evidence, theories suggesting vulnerability to structural and functional disconnections within the cerebellar-frontal network support the rationale to test these relationships.

1.13 Aim 3

Test the neuroanatomical relationships among the volume of brain regions, the pathways that connect them, and working memory.

1.13.1 Hypothesis 1

There should be positive relationship between the volume of the right cerebellum and the known white matter output pathways (cerebellar-rubral, cerebellar-thalamic, rubral-thalamic, and thalamic-frontal white matter integrity), as well as the volume of structures that receive projected cerebellar output along the pathway (right dentate, left red nucleus, left thalamus, and left frontal lobe). Furthermore, the volume of structures that received projected cerebellar output should have positive relationships with the white matter integrity of connected pathways (e.g., left red nucleus volume would be related to rubral-thalamic white matter integrity; See Figure 2).

1.13.2 Hypothesis 2

Similar to hypothesis 1, cerebellar atrophy should be negatively correlated with white matter integrity in each segment (cerebellar-rubral, cerebellar-thalamic, rubral-thalamic, and thalamic-frontal).

1.13.3 Hypothesis 3

Right cerebellar volume should mediate the relationship between cerebellar-frontal white matter integrity and working memory (See Figure 3).

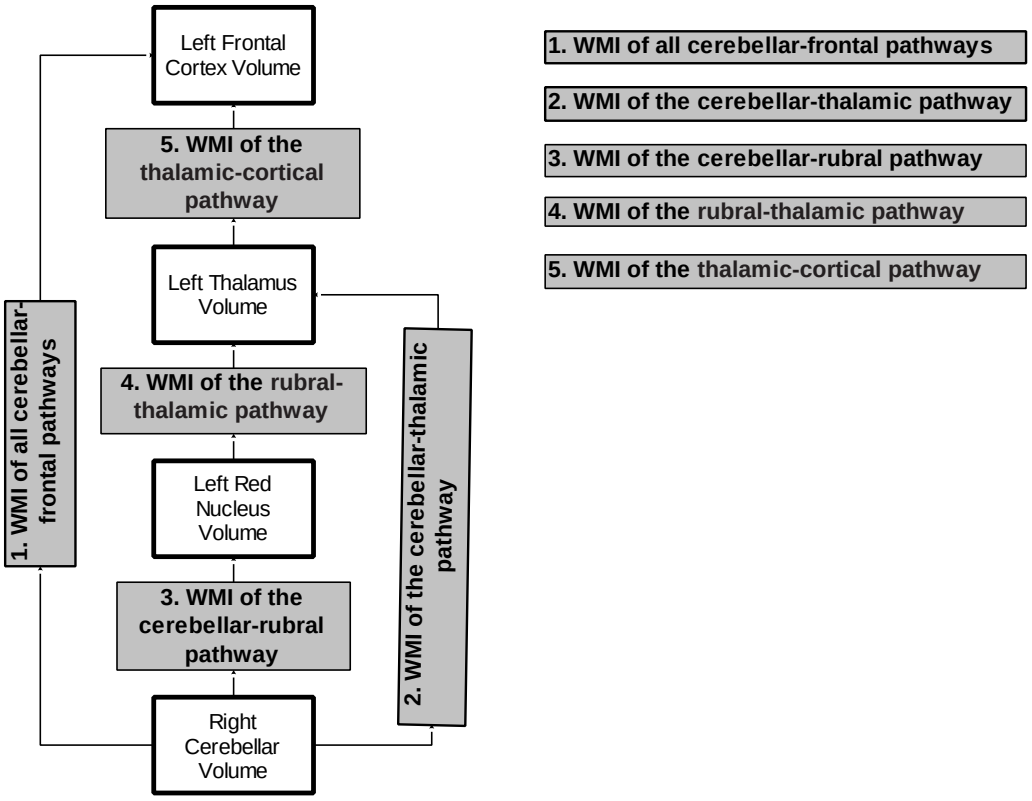

Figure 2 Hypothesized relationships between structures volume and white matter pathways in the cerebellar-frontal network
Note. WMI= White Matter Integrity; White boxes represent the structures in the brain, and grey boxes represent the white matter pathways that connect the structures in the brain.

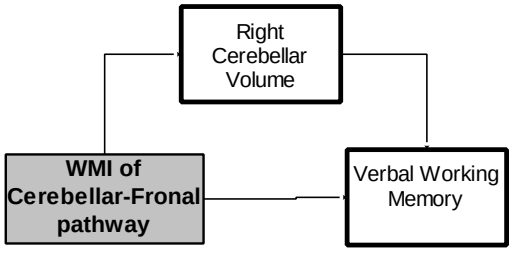

Figure 3 Hypothesized mediation model for working memory in the cerebellar-frontal network
Note. WMI= White Matter Integrity; White boxes represent the structures in the brain, and grey boxes represent the white matter pathways that connect the structures in the brain.

1.14 Aim 4

Test a double dissociation between the cerebellar-frontal network and the SLF II network with both working memory and visual attention performance.

1.14.1 Hypothesis 1

Right parietal lobe volume should mediate the relationship between right SLF II white matter integrity and visual attention.

1.14.2 Hypothesis 2

Cerebellar volume should not mediate the relationship between right SLF II white matter integrity and working memory.

1.14.3 Hypothesis 3

Right parietal lobe volume should not mediate the relationship between cerebellar-frontal white matter integrity and visual attention.

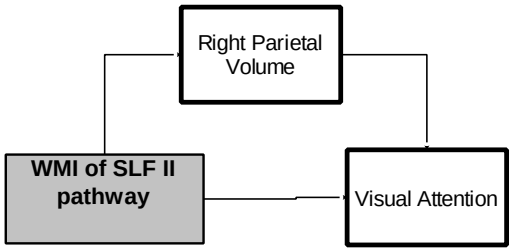

Figure 4 Hypothesized mediation model for visual attention in the right SLF II network
Note. WMI= White Matter Integrity; White boxes represent the structures in the brain, and grey boxes represent the white matter pathways that connect the structures in the brain.

2 SUMMARY OF SPECIFIC AIMS

Aim 1: Expand on prior finding that white matter integrity in the right cerebellar-left frontal pathways has been associated with working memory by incorporating theory, neuroanatomy, and methodological advancements.

Hypothesis 1: Lower white matter integrity in the right cerebellar-left frontal pathways (sum of cerebellar-rubral, rubral-thalamic, cerebellar-thalamic, and thalamic-frontal pathways) should be associated with lower working memory, but not processing speed or attention span.

Aim 2: Double dissociation between the cerebellar-frontal and the right SLF II pathways with both working memory and visual attention performance.

Hypothesis 1: Lower white matter integrity (WMI) in the cerebellar-frontal pathways should be associated with lower working memory, but not visual attention performance.

Hypothesis 2: Lower WMI in the right SLF II should be associated with lower visual attention performance, but not lower working memory performance.

Aim 3: Test the neuroanatomical relationships among the volume of brain regions, the pathways that connect them, and working memory.

Hypothesis 1: There should be a positive relationship between the volume of the right cerebellum and the known white matter output pathways (cerebellar-rubral, cerebellar-thalamic, rubral-thalamic, and thalamic-frontal white matter integrity), as well as the volume of stuctures that receive projected cerebellar output along the pathway

(right dentate, left red nucleus, left thalamus, and left frontal lobe). Furthermore, the volume of structures that receive projected cerebellar output should have positive relationships with the white matter integrity of connected pathways (e.g., left red nucleus volume would be related to rubral-thalamic white matter integrity; See Figure 2).

Hypothesis 2: Similar to hypothesis 1, cerebellar atrophy should be negatively correlated white matter integrity in each segment (fractional anisotropy (FA) of cerebellar-rubral, cerebellar-thalamic, rubral-thalamic, and thalamic-frontal).

Hypothesis 3: Right cerebellar volume should mediate the relationship between cerebellar-frontal white matter integrity and working memory (See Figure 3).

Aim 4: Test a double dissociation between the cerebellar-frontal network and the SLF II network with both working memory and visual attention performance.

Hypothesis 1: Right parietal lobe volume should mediate the relationship between right SLF II white matter integrity and visual attention.

Hypothesis 2: Cerebellar volume should not mediate the relationship between right SLF II white matter integrity and working memory.

Hypothesis 3: Right parietal lobe volume should not mediate the relationship between cerebellar-frontal white matter integrity and visual attention.

3 METHODS

Data for the current study was obtained from a larger study on the long-term outcomes following pediatric brain tumor diagnosis and treatment (PI: T.Z. King #RSGPB-CPPB-114044). Survivors either were part of a long-term follow-up of a prior longitudinal study of childhood brain tumors, or survivors were recruited from a

database of brain tumor survivors obtained from Children's Healthcare of Atlanta (CHOA). Prior to participation, survivors of childhood brain tumors completed a screening form. Candidates were excluded if they had any of the following conditions: pervasive developmental disabilities, neurofibromatosis, MRI incompatible medical implants, serious health complications that would make an MRI scan unsafe, or impairment in hearing or vision that would make them unable to complete components of the study. It was common for survivors with a diagnosis of hydrocephalus to have a metal shunt placed in their skull to drain excess fluid. The participants with shunts were asked to provide the serial number for their implant, which was provided to the MRI technician to ensure that the participant would be safe in the 3 Tesla MRI scanner.

Control participants were recruited from the Georgia State University community through the psychology participant pool, fliers posted around the community, and the Georgia State University/Georgia Institute of Technology Joint Center for Advanced Brain Imaging (CABI). Inclusion criteria included fluency in English and adequate hearing and vision to complete the study. Controls were excluded if they endorsed substance use, had medical illnesses, or psychiatric problems. Georgia State University (IRB# H03177) and Georgia Institute of Technology (IRB# H14088) Institutional Review Boards reviewed and approved all studies.

3.1 Procedure

Participants were asked to come to 2 separate study visits. Informed consent was obtained at both visits. At the first visit, all participants completed a structured clinical interview (SCID-II; First, Spitzer, Gibbon, and Williams, 2002) and a battery of cognitive testing with a trained graduate student. This testing session took

approximately 4 hours. Participants who preferred not to complete an MRI (e.g. due to claustrophobia, safety concerns, or scheduling conflicts) did not continue to the second visit and were compensated for their time. Survivors received $50 and controls received research credit for the first visit.

The second visit of the study took place at the Georgia State University/Georgia Institute of Technology Shared Center for Advanced Brain Imaging. Upon arriving, each participant completed an additional MRI safety screening form, which required approval from an MRI technician to complete the scan. Once cleared for the MRI scan, a graduate student explained the MRI study procedures and completed an informed consent form with the participant. Following the scan, a member of the research team debriefed and compensated each participant. Survivors and controls received $50 for the second visit.

3.2 Participants

A total of 44 participants with tumors in the cerebellum, brain stem, or posterior fossa completed the second visit of the study. Tumors across these regions were included in the current study because the distinction of tumors within structures in the posterior fossa may not be clinically meaningful because tumor compression often damages the surrounding structures due to the spatial constraints of the posterior fossa (Blumenfeld, 2011). Participants were excluded based on the following criteria: global functional impairment (n=2), pervasive developmental disorder (n=1), English as a second language (n=1), less than 5 years from diagnosis (n=1), or younger than 16 years old (n=6). An additional three participants (n=3) had poor quality imaging data due to motion, and one participant had significant hydrocephalus that resulted in abnormal

brain structure (n=1; very enlarged ventricles). The remaining 29 survivors were selected for inclusion in the current study. Survivors were matched with controls on demographic factors that included age, sex, level of education, and handedness. See demographic information for survivors and controls in Table 5.

Table 5 Sample demographics

Group	Survivors	Controls	*t*-test
N	29	29	
Gender	45% Female	45% Female	
Age	*M*=21.34 (*SD*=5.35)	*M*=22.42 (*SD*=5.20)	*t*(56)=.78, *p*>.05
Level of Education	*M*=13.28 (*SD*=2.79)	*M*=14.34 (*SD*=1.68)	*t*(45.08)=1.90, *p*>.05
Handedness	79% Right	83% Right	*t*(56)=.33, *p*>.05

Note. M=mean; SD=Standard Deviation

3.3 Survivor Demographics

The survivor participants were on average 8.55 years old (*SD*=4.88; range 0-18) at diagnosis, and their average age at exam was 21.34 (*SD*=5.35; range 16-35). The average Full-Scale IQ (Wechsler Abbreviated Scale of Intelligence-2; WASI; Wechsler, 1999) was 99.07 (*SD*=13.32). Thirteen individuals were diagnosed with astrocytoma tumors, 12 with medulloblastoma, and the remaining 4 individuals were diagnosed with an ependymoma, a glioma, a primitive neuroectodermal tumor (PNET) - not otherwise specified, and a choroid plexus tumor. Ethnicity in the sample was 72% Caucasian, 14% African-American, 7% Hispanic, and 7% Asian. With regard to treatment, 83% of the sample had a history of hydrocephalus, 52% had a history of radiation treatment, 48% had a history of chemotherapy (only 1 participant had chemotherapy without radiation therapy), 55% had a hormone deficiency, and 3% had a history of seizure disorder. Of the participants who had radiation treatment (n=15), 80% had whole brain

radiation therapy and an additional focal boost of radiation to the posterior fossa, the remaining 20% of participants (n=3) received only focal radiation. Radiation dosage ranged from 5040-6300. Treatment protocol numbers included: 9961 Arm A (n=2), CCG 9961 Arm A (n=3), CCG 9961 Reg B (n=1), CCG 9892 (n=1), CCG 88703-NOS (n=1), POG 8633 (n=1), POG 8695 (n=1), POG 8930 (n=1), ACNS 0331 (n= 1), and three participants did not have protocol numbers listed in their medical records (n=3). The Neurological Predictor Scale (NPS; Micklewright et al., 2008) was a cumulative measure that included treatment complications such as hydrocephalus, hormone deficiency, seizures, as well as the amount of brain surgery, presence and type of radiation therapy, and chemotherapy. The NPS values range from 0 (no treatments or complications) to 9 (high degree of treatments and complications). The average NPS score for the sample was 6 (*SD*=2.54; Range 2-9).

Treatment factors, white matter integrity, brain structure volume, and cognitive performance in adult survivors of childhood posterior fossa tumors may be related. The current study investigated treatment variables (e.g., age at diagnosis, radiation, chemotherapy, seizures) descriptively and in relationship to findings. Small sample size limited the number of treatment factors that can be included as covariates; therefore, NPS was investigated as a cumulative measure of treatment severity. Prior research that included a subset of this sample found that the NPS was associated with measures of white matter integrity (King et al., 2015), subcortical volume (Jayakar et al., 2015) and cerebellar atrophy (Ailion et al., 2016).

3.4 Processing Speed Measures

As discussed in the introduction, the prior literature suggested that the best available neuropsychological measures of processing speed were Digit Symbol Decoding, Choice Reaction Time, Visual Scanning, Rapid Color Naming, and Rapid Word Naming (Bunce and Macready, 2005; Luciano et al., 2009; Philips, 2012). The current study measured processing speed using two methods. To be consistent with prior studies, the Oral Symbol Digit Modality Test was used as a standalone measure of processing speed. Additionally, a composite measure of processing speed was computed as a more multifaceted measure of processing speed.

The composite measure included neuropsychological measures of processing speed based on prior literature (Bunce and Macready, 2005; Luciano et al., 2009; Philips, 2012). The composite measure of processing speed was an average of Oral Digit Symbol Decoding, Choice Reaction Time, Visual Scanning, and Rapid Color Naming. The study used Oral Symbol Digit Decoding rather than Written Symbol Digit Decoding because many survivors of posterior fossa tumors have motor weaknesses. Despite prior literature suggesting that rapid word naming loads on the processing speed factor, Rapid Word Naming was not included in the processing speed measure. The rationale for excluding Rapid Word Naming was because of the task similarities with Rapid Color Naming, which were both part of the Delis-Kaplan Executive Function System (DKEFS) Color-Word Interference subtest. The study used Rapid Color Naming rather than Rapid Word Naming because Rapid Color Naming had a higher factor loading on processing speed (Philips, 2012). The composite measure was computed based on an average of z-scores for each measure to maintain a consistent scale of

measurement. Z-scores were based on the manual norms for all of the measures, except for the 0-Back Choice Reaction Time z-scores, which were based on the healthy control sample (described below).

3.4.1 Symbol Digit Modality Test

Oral digit symbol decoding was measured using the Symbol Digit Modality Test (Smith, 1982). In this 90-second speeded number-symbol task, participants were given a sheet of paper with series of symbols with a blank box beneath each one. At the top of the page, there was a key where each symbol corresponded to a number. Participants were first asked to write the number that corresponded to the symbol (written processing speed). For oral processing speed, participants said the number that corresponded to the symbol in the box as fast as possible. The same form and the same order were used for all participants. The test-retest reliability was .76 for the Oral Symbol Digit Modality Test and .80 for the written portion (Smith, 1982). Prior research suggested that performance on the Symbol Digit Modality Test correlated to performance on the Digit Symbol subtest of the Wechsler Adult Intelligence Scale-Revised (WAIS-R; Morgan and Wheelock, 1992).

3.4.2 DKEFS Subtests – Trail Making Test #1: Visual Scanning

The Visual Scanning subtest of the Trail Making Test consisted of two pages (11 x 17 in) of scattered letters and numbers. Participants were required visually to scan the array of 53 letters and numbers and identify a target number 24 times with a pencil mark. This measure produced two scores, the time to complete the task and the number

of errors (omissions or commissions). The DKEFS manual provided norms based on a standardization sample (Delis, Kaplan, and Kramer, 2001) that was used to obtain standard scores. The standard score based on time to complete the task was converted to a *z*-score and used ito calculate the composite processing speed measure. While the Visual Scanning subtest also required a component of visual attention, it was included in the processing speed measure on the basis of the prior literature, which has found that measures of time to complete visual cancellation tasks have a high factor loading on a general processing speed factor (Luciano et al., 2009; Philips, 2012). The test-retest reliability was .56 for the Visual Scanning subtest (seconds to complete; all ages; Delis, Kaplan, and Kramer, 2001).

3.4.3 DKEFS Subtests –Color-Word Interference #1: Color Naming

The Color Naming subtest of the Color-Word Interference test consisted of a page of colored squares, and participants were required to name the colors as quickly as possible. The examiner recorded completion time and number of errors, but only completion time was be used in the current study. The norms from the DKEFS manual were used to obtain standard scores based on the normalization sample. Similar to the Trail Making Visual Scanning subtest, the color naming subtest had a component of visual attention but was included based on the prior literature that found that measures of color naming have a high factor loading on a general processing speed factor (Luciano et al., 2009). The test-retest reliability was .76 for the Color Naming subtest (seconds to complete; all ages; Delis, Kaplan, and Kramer, 2001).

3.4.4 0-Back Choice Reaction Time

Simple reaction time was measured using the 0-Back Average Choice Reaction Time over 5 runs. The 0-Back task was conducted in the MRI scanner as the simplest portion of the complete N-Back task (0,1,2,3-back). 0-Back reflects basic attention or vigilance. Participants were trained on the N-Back task outside of the scanner before completing the task in the scanner. During the 0-Back condition, participants were shown a target letter and a series of letter stimuli. For each of the letter stimuli, the participants were asked to press “yes” with their index finger when they see the target letter or “no” with their middle finger if the letter was not the target letter. Response reaction time to this task was measured in milliseconds.

Prior research has suggested that the raw 0-Back Reaction Time was not correlated with measures of attention span (*r*= .12; Digit Span Forward) or working memory (*r*=0.06; Digit Span Backward; Miller et al., 2009), but was correlated with one of the other measures of processing speed (*r*=-.33; Stroop Word Reading; Miller et al., 2009). Of note, the 0-Back was not correlated with some measures of processing speed included in the current processing speed composite measure (*r*=-.12; Stroop Color Naming; Miller et al., 2009). However, prior researchers have used the 0-Back Reaction Time as a measure of simple processing speed (e.g., Miller et al., 2009; Shucard et al., 2011).

A *z*-score was computed for all participants based on the mean and standard deviation of all of the controls that completed the task in the larger study (*n*=53). Three controls from the larger sample were excluded due to impairment (>1.5 *SD* below the mean), on measures of intelligence (WASI; Wechsler, 1999), or adaptive functioning

(Scales of Independent Behavior-Revised; Bruininks et al., 1996), and one control was excluded due to age >35 years. The development of the norms for the processing speed measure was based on the technique described in the DKEFS manual (Delis, Kaplan, and Kramer, 2001). First, normality was checked for the score distribution of all the control participants, and the data followed a normal distribution, W=.98, p=.41. Since the data followed a normal distribution, the mean and standard deviation, M=569.01 and SD=92.40, was used instead of the 50th percentile point. 0-back z-scores were calculated based on the mean and standard deviation of the control population.

Table 6 0-Back Reaction Time sample averages

Group	All Controls	Matched Controls	Survivors
N	53	29	29
Gender	53% Female	48% Female	45% Female
Age *M* (*SD*)	21.89 (3.52)	22.43 (5.20)	21.34 (5.35)
Level of Education *M* (*SD*)	14.43 (1.66)	14.17 (1.63)	13.28 (2.79)
0-Back Reaction Time *M* (*SD*)	569.01 (92.40)	563.48 (89.94)	568.24 (95.58)

Note. M=mean; SD=Standard Deviation; age and level of education are reported in years; 0-Back Reaction Time is reported in milliseconds

Other *z*-score computations were considered (e.g., scores relative to the whole sample, matched controls and survivors, or matched controls alone), however all of the controls were selected in an effort to make the reaction time z-score as similar as possible to the other z-scores in the processing speed measure (e.g., based on population norms of healthy individuals). A noteworthy limitation of this approach was the overlap between the controls used in the norm reference group and the matched controls that were used in the analyses. Therefore, the measure was calculated as a preliminary check to determine if the 0-Back z-score and processing speed measures

correlated with other measures of processing speed. High correlations were found, which increased the confidence in the 0-Back *z*-score and composite measure calculations (see Table 7).

Table 7 Correlations of processing speed measures

	Matched Survivors and Controls (*n*=58)	Survivors (*n*=29)	Matched Controls (*n*=29)
	Composite Processing Measure	Composite Processing Measure	Composite Processing Measure
0-Back Reaction Time	.56**	.60**	.51**
Oral-Symbol Digit	.72**	.69**	.72**
Written Symbol Digit	.47**	.51**	.32
DKEFS Visual Scanning	.52**	.46*	.68**
DKEFS Color Naming	.60**	.68**	.29
DKEFS Word Reading	.60**	.68**	.22

Note. Pearson correlation *r* values are reported; z-scores were used in all correlation analyses; *indicates $p<.05$ and **indicates $p<.01$; DKEFS= Delis-Kaplan Executive Function Scale

3.5 Auditory Attention Span

3.5.1 Wechsler Memory Scale Digit Span Forward

The Digit Span Forward subtest from the Wechsler Memory Scale was used as a measure of basic auditory attention span for the first aim and hypothesis (Wechsler, 1997). The examiner read the participant a string of numbers, at a pace of one second per number, and the participant recalled the numbers immediately after the presentation. The test ranged from 2 digits to 9 digits. The highest number of digits repeated accurately was used as a measure of attention span. Prior researchers have found that the Digit Span Forward average number of digits accurately repeated in a

healthy population was 7 with a standard deviation of 2 (Miller, 1956; Shiffrin & Nosofsky, 1994). Digit Span Forward raw scores were used in all analyses. The test-retest reliability for the digits forward measure was .83 (Wechsler, 1997).

3.6 Working Memory

3.6.1 Auditory Consonant Trigram

The Auditory Consonant Trigrams required the examiner to say three consonant letters, and then instruct the participant to count backward from an established starting number (Brown, 1958; Peterson and Peterson, 1959). After a period of distraction by counting backward (for 9, 18, or 36 seconds), the examiner asked the participant to recall the three consonants. The number of consonants accurately recalled for each trial (9, 18, or 36 seconds) was added together to obtain a raw score for each trial, which was then converted into a *z*-score based on population norms (Stuss et al., 1988; Spreen and Strauss, 1998). *Z*-scores of the 36-second trial were used as a measure of working memory. Test-retest reliability for the ACT was .71.

3.7 Visual Attention

3.7.1 D-KEFS Subtests – Trail Making Test #1: Visual Scanning

The Visual Scanning subtest of the Trail Making Test was described above. For Aim 2, two scores from this measure were used to provide a measure of visual attention. First, the number of errors (omission and commissions) was used to obtain a measure of visual scanning with a minimal time component. Then, the z-score that is based on the time to complete the Visual Scanning task was investigated as a visual attention measure with a time component. Based on the theory and evidence that the

pathway between the parietal lobe and the frontal cortex regulates visual attention (Bisley and Goldberg, 2003; Makris et al., 2005; Mesulam, 1981), this measure of visual attention was hypothesized to be associated with white matter integrity in the SLF II. Furthermore, prior research found that letter cancellation (raw number of correct targets) was associated with the right SLF II (Doricchi and Tomaiuolo, 2003; Urbanski et al., 2008).

3.8 Diffusion Weighted Imaging

Diffusion-weighted imaging (DWI) provided an in-vivo methodology that measured the rate and directionality of water diffusion to infer microstructural features of white matter (Cascio, Gerig, and Piven, 2007). This indirect measure of white matter microstructure was used to infer the integrity of the white matter connections. Three principle eigenvectors were used to quantify directionality (λ_1, λ_2, λ_3). The first or principal eigenvector measured parallel directionality and corresponded to the principal eigenvalue, and axial diffusivity (AD), whereas the second two eigenvectors measured diffusion in the perpendicular direction and corresponded to the secondary eigenvalues that comprise radial diffusivity (RD). Four common diffusion measures include radial diffusivity (RD=$[\lambda_2+ \lambda_3]/2$), axial diffusivity (AD=λ_1), fractional anisotropy (FA= $\sqrt{(3/2)}*\sqrt{((\lambda_1-D)^2+(\lambda_2-D)^2+(\lambda_3-D)^2)/(\lambda_1^2+\lambda_2^2+\lambda_3^2)}$); where D=$[\lambda_1+ \lambda_2+ \lambda_3]/3$), and mean diffusivity (MD=$[\lambda_1+ \lambda_2+ \lambda_3]/3$). Higher AD or FA and lower RD or MD were considered proxies for greater white matter integrity (Bartzokis et al., 2012; Mukherjee et al., 2008; Viallon et al., 2015).

FA measured water directionality of diffusivity in all three directions, where greater FA indicated greater white matter integrity on a scale from zero, which indicated isotropy, to one, which indicated anisotropy. MD quantified water diffusion in 10–3mm^2/s, such that higher values indicated unrestricted diffusion regardless of direction (Mukherjee et al., 2008). While some researchers have interpreted AD and RD as general metrics for white matter pathology (Madden et al., 2012; Viallon et al., 2015), other researchers suggested that RD ([λ_2+ λ_3]/2) corresponds with myelination and AD (λ_1) corresponds with axon degeneration (Song et al., 2005; Bartzokis et al., 2012). In support of this idea, researchers found evidence to suggest that changes in RD were associated with myelin growth or loss (e.g., Bartzokis et al., 2012; Gao et al., 2009; Klawiter et al., 2011; Song et al., 2005), RD and AD loaded onto separate factors, and degenerative brain changes differentially impacted AD and RD (Bartzokis et al., 2012).

Each of the metrics has noteworthy strengths and limitations. The most common measures reported in the literature have been FA and MD despite criticism that composite measures are less sensitive and more difficult to interpret due to their combination of multiple eigenvectors that potentially measured different components of brain biology (Bartzokis et al., 2012). One study proposed that RD provided the best measure of myelination in frontal white matter regions based on the correlation with transverse relaxation rate (Bartzokis et al., 2012). The biggest criticism of RD and AD has been that their estimates are strongly affected by crossing fibers (Bartzokis et al., 2012). In the current study, the primary diffusion metric used in the analyses is FA so that the results of the study can be comparable to prior literature. However, due to the importance of frontal lobe myelin degeneration for brain tumor populations, all primary

analyses are replicated with RD using appropriate statistical correction and reported as supplementary information.

Tractography provides a DWI technique that allows for evaluation of white matter integrity within a specific pathway using inferred anatomy. Deterministic tractography was selected over probabilistic tractography because it was more accurate and recommended for long-range fibers (Khalsa et al., 2014; Morris et al., 2008; Mukherjee et al., 2008; Yo et al., 2009).

3.9 Image Acquisition

Participants completed an MRI scan using a 3-Tesla Siemens Trio system with a standard head coil, which included a T1-weighted MPRAGE sagittal sequence (FOV=256mm, voxel size=1x1x1mm, TR/TE=2250ms/3.98 ms, flip angle=9°), a diffusion-weighted sequence with 30 directions acquired along the anterior-to-posterior phase encoding direction (FOV=204mm, voxel size=2x2x2, TR/TE=7700ms/90ms, flip angle=2.4°, b value=1000s/mm^2, GRAPPA parallel imaging acceleration factor=2, number of slices=60), one un-weighted diffusion volume acquired with equivalent parameters (T2-weighted image; b = 0s/mm^2). The same method described in a prior DWI study on this sample (Smith et al., 2016) was used to co-register the diffusion image and the T1 image using the fMRI data and field map. This co-registration method was based on the principle that the echo-planar imaging (EPI) artifacts that affect functional imaging were similar to the magnetic field inhomogeneities that impacted diffusion data. Therefore a similar unwarping method was used to approximate the geometric distortion. Co-registration was an important step so that the ROIs aligned to both the diffusion volumes and T1 images. The co-registration method used the

acquired fMRI sequence (FOV=204mm, voxel size=3x3x3mm, TR/TE=2130ms/30ms, flip angle=90°, number of slices=40, slice gap=0, EPI=180 volumes), and corresponding fMRI field map (FOV=204mm, voxel size=3x3x3mm, TR/TE1/TE2=488ms/4.92ms/ 7.38ms, flip angle=60°) to apply the estimated phase shift to the diffusion scan.

3.10 Preprocessing

Participants selected for the current study excluded those who had been previously excluded based on motion (Smith et al., 2016). Therefore the sample selected for inclusion had no significant motion artifact on their MPRAGE or DWI images. Before participant selection, three survivor participants were excluded because they had greater than 10 DWI volumes with artifact, and three survivors and two controls with 1-10 volumes containing artifact were corrected by removing those volumes from the dataset. The total sample included 29 survivors and 29 controls with neuroimaging data for processing. Image preprocessing was completed using the procedure described in detail by Smith et al. (2016). In brief, the preprocessing pipeline included eddy current correction (FDT FMRIB's Diffusion Toolbox FSL 5.0), skull stripping, fitting the tensor model using DTFIT, and co-alignment of DWI and T1 images using the fMRI field map.

3.11 Region of Interest Procedure

The cerebellar-frontal pathway was constructed based on 5 ROIs: right cerebellar hemisphere, right dentate, left red nucleus, left thalamus, and the left medial frontal gyrus (See Figure 5). The right SLF II was constructed based on three ROIs: the right

parietal lobe white matter, the right middle frontal gyrus, and the right temporal lobe (as an exclusion mask; See Figure 6).

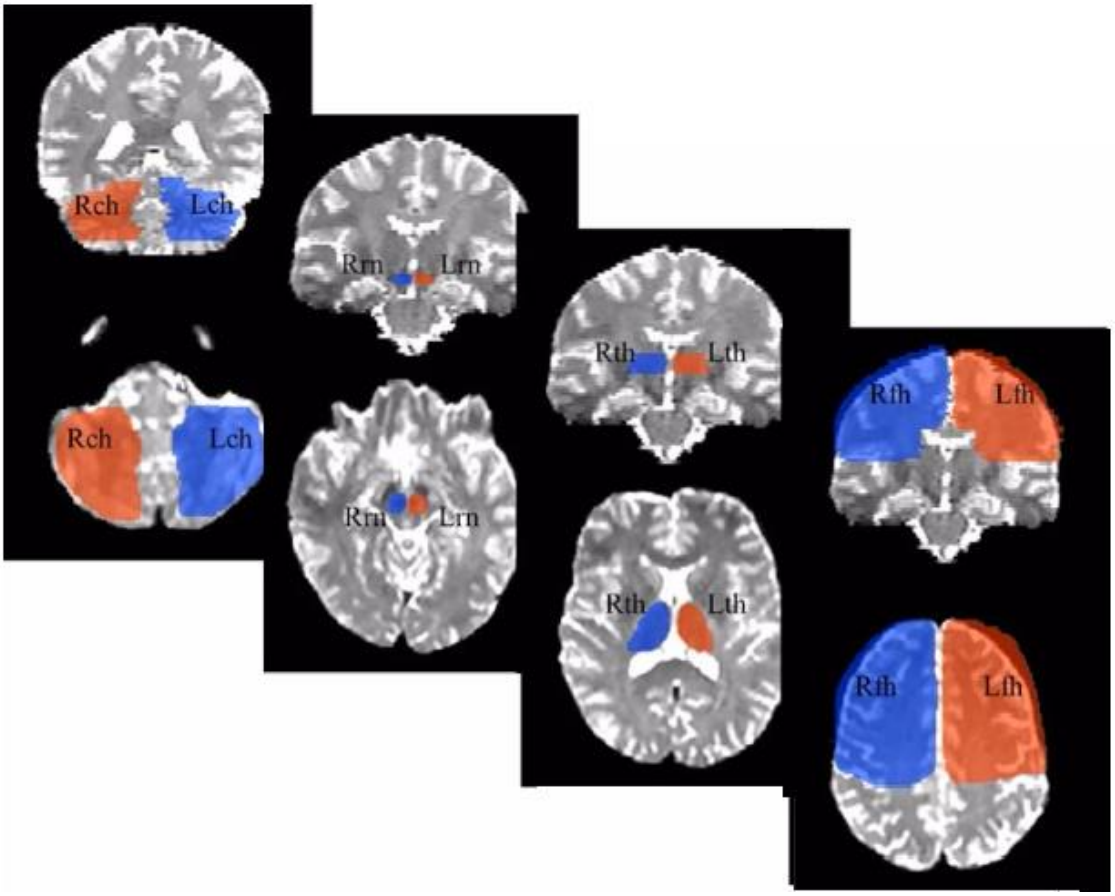

Figure 5 Regions of interest for the cerebellar-frontal pathway (adapted from Law et al., 2015a; reprinted with permission)
Note. R= right, L= left, ch= cerebellar hemisphere, rn=red nucleus, th=thalamus, fh=frontal hemisphere. The dentate nucleus is not pictured but was included as an ROI. While bilateral ROIs are displayed, only the right cerebellum, left red nucleus, left thalamus, and left frontal hemisphere were included.

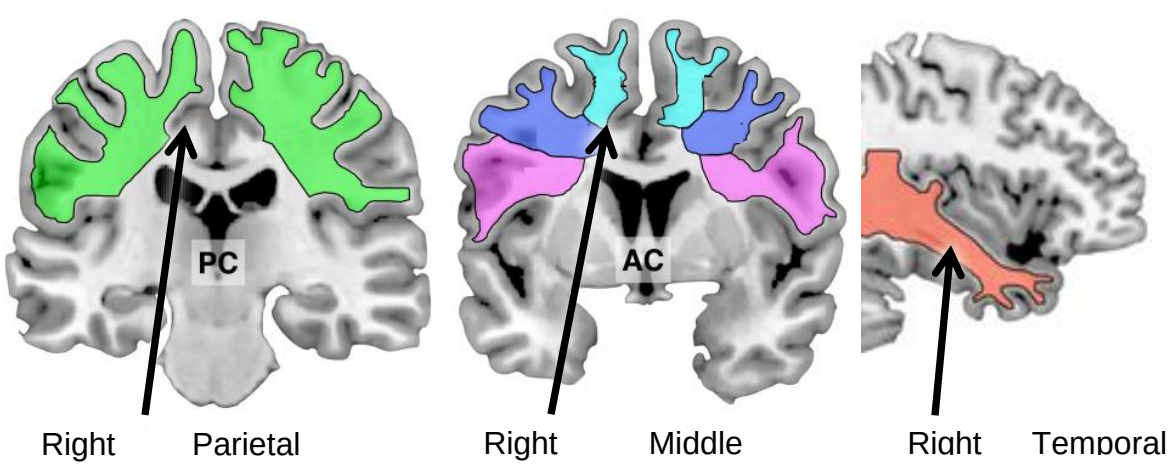

Figure 6 Regions of interest for the right superior longitudinal fasciculus II (adapted from Thiebaut de Schotten et al., 2011; reprinted with permission)

Note. While bilateral ROIs are displayed, only the right hemisphere SLF II was included. The right temporal lobe was included as an exclusion mask.

While prior tractography studies defined the frontal ROI as the entire frontal lobe (e.g., Figure 5), the current study refined this region by including more specific anatomical boundaries for the ROI within the frontal lobe (BA 46; Brodmann, 1909; Catani et al., 2012; Desikan et al., 2006; Turken and Dronkers, 2011). The dorsolateral prefrontal cortex (BA 46) was selected as the specific region within the frontal lobe because BA 46 received input from the cerebellum based on an animal virus tracing study (Kelly and Strick, 2003), and because BA 46 was associated with working memory performance in human fMRI studies (Marvel and Desmond, 2010; Zhang, Leung, and Johnson, 2003). BA 46 was estimated using sulci boundaries of the rostral division of the middle frontal gyrus (Catani et al., 2012; Desikan et al., 2006). The boundaries included the rostral portion of the superior frontal sulcus (front), caudal portion of the middle frontal gyrus (back), dorsal boundary as the superior frontal sulcus

(top), and ventral boundary as the inferior frontal sulcus (bottom; Catani et al., 2012; Desikan et al., 2006; See Figure 7a-d).

There was one noteworthy limitation of the selection of only the middle frontal gyrus. The prior literature suggested that the cerebellum also connects to BA 9, and cerebellar projections to BA 9 have been found in one tractography study on healthy adults (Jissendi, Baudry, and Balriaux, 2008). Furthermore, activation in BA 9 also corresponded with working memory (Marvel and Desmond, 2010; Zhang, Leung, and Johnson, 2003; Ziemus et al., 2007). BA 9 was not included in the frontal ROI for three reasons. First, the sulci boundaries of BA 9 were more difficult to define clearly and most closely corresponded with the superior frontal gyrus, which also included BA 8 and 10 (Canti et al., 2012; See Figure 7a-b). Second, portions of BA 9 were included within the previously described rostral division of the middle frontal gyrus. Lastly, the right middle frontal gyrus was used as the right frontal ROI for the SLF II. Therefore, including only the left middle frontal gyrus in the left frontal ROI makes the two pathways more directly comparable.

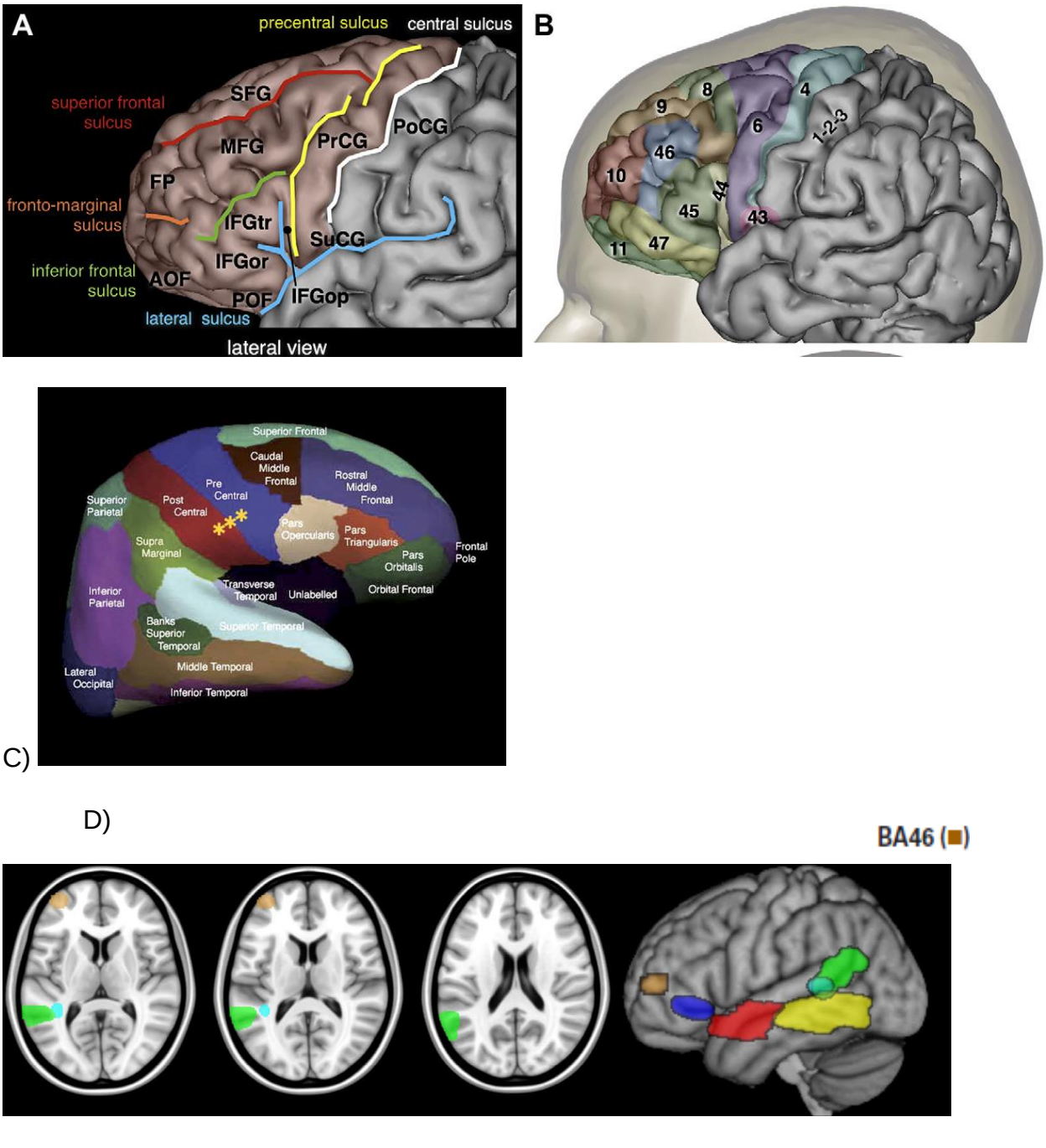

Figure 7 Surface anatomy of the dorsolateral prefrontal cortex (Brodmann area (BA) 46)
Note. Image A and B replicated from Catani et al. (2012; reprinted with permission), and image C replicated from Desikan et al. (2006; reprinted with permission), and image D replicated from Turken and Dronkers (2011; reprinted with permission)

3.11.1 Right Cerebellum

The cerebellum was drawn beginning with the right-most coronal slice where the cerebellum could be identified. The superior portion of the cerebellum was defined using the cerebellar tentorium as a guide. The pons was used as the anterior boundary, and the midline of the cerebellar vermis was used to delineate the left boundary of the ROI.

3.11.2 Right Dentate

The dentate was relatively easy to identify, as a grey matter structure that was surrounded by white matter. The dentate was drawn beginning with the brainstem in the axial view, and the midline of the cerebellum in the sagittal and coronal view. The ROI mask was placed over the crescent-shaped figure in the middle of the cerebellar white matter in the right hemisphere. This mask was drawn to include a 1-2 voxel border into the white matter to ensure the mask would capture the dentate connections to white matter pathways that continue to the cortex.

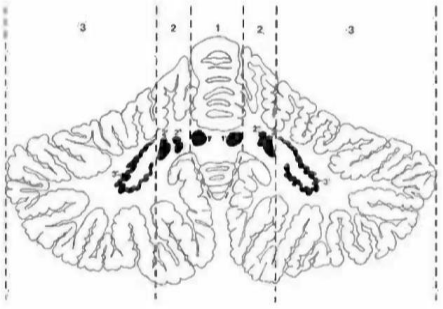

Figure 8 Image of Dentate Nucleus from Duvernoy's Atlas of the Human Brain Stem and Cerebellum (Naidich et al., 2009; reprinted with permission)

3.11.3 Left Red Nucleus

The red nucleus was identified by selecting the first rostral midbrain slice in which it becomes visible in the axial view, using the cerebral peduncles and substantia nigra as anterior/rostral and posterior/caudal reference points, respectively. The structure was circular, which made it easier to define the edges. For this structure, the T2 image was also used as a guide, because the red nucleus contains iron it appeared grey on the T2 image. Similar to the dentate, this mask was drawn to include a 1-2 voxel border into the white matter to ensure the mask would capture the connections to white matter pathways that continue to the cortex. For neuroanatomical reference, see page Figure 6.10B on page 234 of Blumenfeld (2010).

3.11.4 Left Thalamus

The third ventricle defined the right boundary of the thalamus. The internal capsule defined the left boundary of the thalamus. The anterior boundary was defined using the differentiation between the grey matter of the thalamus and surrounding white matter of the internal capsule. Dorsal and ventral boundaries were based on continuous slices of the differentiation between the grey and white matter boundaries on the T1 images, with the posterior commissure as another reference point for the ventral boundary. For neuroanatomical reference points, please see Figure 10-19B on page 144 of Waxman et al. (2009).

3.11.5 Left Middle Frontal Gyrus

The anterior boundary was defined as the rostral portion of the superior frontal sulcus, the posterior portion was defined by the caudal part of the middle frontal gyrus, the superior frontal sulcus defined the dorsal boundary, and the ventral boundary was defined as the inferior frontal sulcus. The MFG was drawn in the sagittal view, using the coronal view of the MFG as a guide (See Figure 7).

3.11.6 Reduced size MFG

The initial delineation of the left middle frontal gyrus was too large for PanTrack processing. Therefore, this ROI was reduced in size during processing. This ROI was reduced to include the first 10-slices of the anterior portion of the middle frontal gyrus. The previous MFG boundaries were used, with the addition of a 10-slice anterior-posterior cut-off. The anterior portion of the ROI began on the 1st coronal slice where lateral ventricles connected and continued on the contiguous 10 slices in the coronal view towards in the anterior direction.

The reduction of the size of the MFG was modeled after the ROI slice procedure described by Ford et al. (2013). While one could argue that a larger ROI is more precise and includes more fibers, it could also be argued that smaller more precise ROI boundaries increase neuroanatomical specificity. The use of PanTrack for network tractography addresses some of these concerns. PanTrack dices the ROI at the voxel level, so there is a decreased reliance on all-inclusive ROI boundaries. In other words, PanTrack is able to capture all the fibers that go each voxel within the reduced size ROI. To date, all prior studies have only used the outer edge boundary of the ROI, which would be more sensitive to changes in ROI boundaries. Even with a reduced size

ROI for the MFG, this ROI method is far superior to prior studies that have used a single slice estimate of ROIs (Jissendi et al., 2008), or defined the frontal ROI too broadly as the dorsal anterior half of the cortex (Law et al., 2015a).

3.11.7 Right middle frontal gyrus

The same parameters described for the left MFG were used in the right hemisphere for the right MFG on the contralateral side. The reduced size MFG was used for both pathways.

3.11.8 Right parietal lobe white matter

The right parietal lobe white matter parameters were based on the anatomical guidelines described by Thiebaut de Schotten et al. (2011), and Kamali et al. (2014). The middle of the splenium of the corpus callosum was used as a starting reference point. The triangle shaped fiber pathway at the inferior portion of the top right bundle of fibers in the parietal lobe was defined as the angular gyrus (See Figure 9-10). This fiber bundle was followed on 10 contiguous slices toward the anterior portion of the brain in the coronal view.

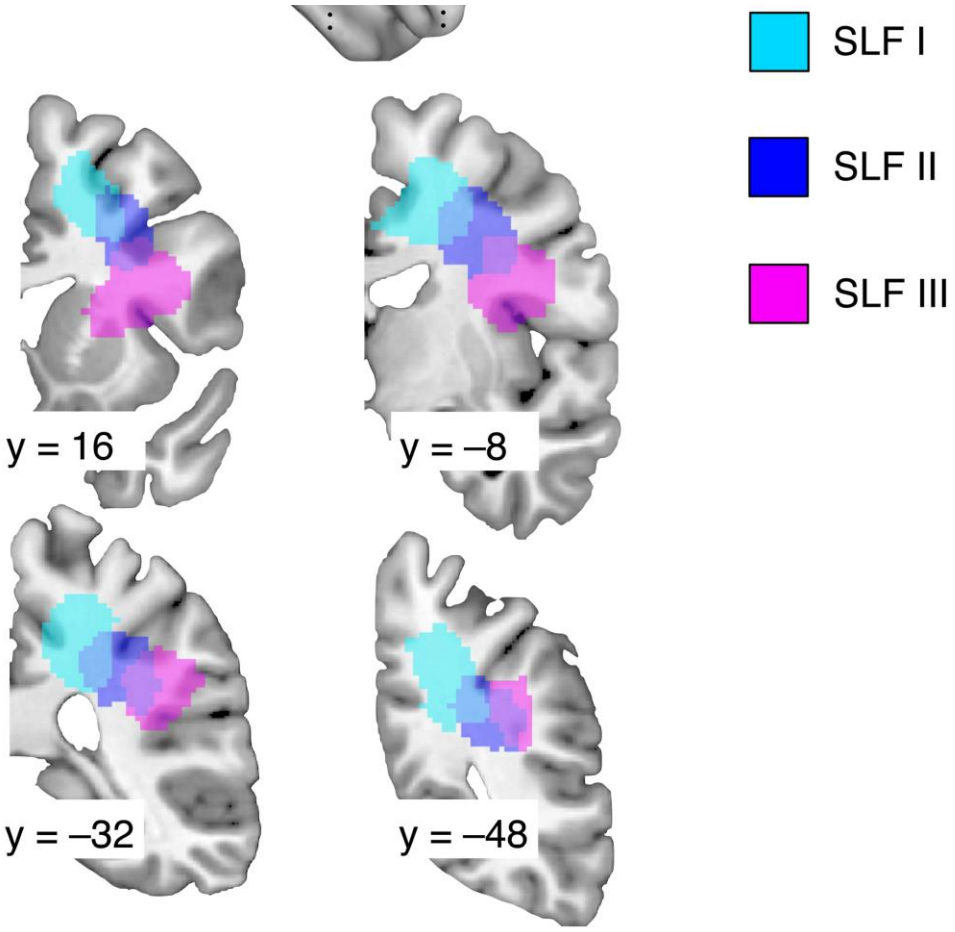

Figure 9 Middle branch of superior longitudinal fasciculus (SLF) II parietal lobe white matter region of interest (ROI) as described by Thiebaut de Schotten et al. (2011; reprinted with permission)

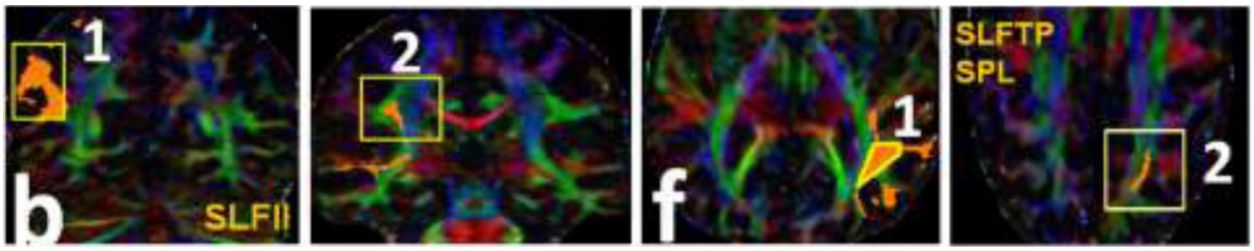

Figure 10 Angular gyrus as defined by Kamali et al. (2014; reprinted with permission)

3.11.9 Right temporal lobe

The first coronal slice where the temporal pole could be defined was used as a starting point and the anterior boundary. The dorsal boundary was defined as the superior temporal gyrus. The posterior boundary was defined as the parieto-occipital sulcus. The left boundary was defined as the first sagittal slice where the corpus callosum became visible (See Figure 6).

3.11.10 ROI Template Method

The method of ROI template generation was based on Law et al. (2015a), which involved manually drawing the ROIs on 10 healthy controls, registering the ROIs to the standard MNI brain to create an ROI template, then registering the template to each participant's native space, and manually editing when necessary (Woods et al., 1998; http://bishopw.loni.ucla.edu/air5/). While this technique was successful in a brain tumor population in one prior study (Law et al., 2015a), one possible limitation of this approach was the potential inaccuracies when converting the template image from standard MNI to native space, due to structural brain abnormalities (e.g., lesions from surgical resection, inter-individuals in sulcal anatomy; Ono et al., 1990). However, a systematic semi-automated approach to ROI reduces the time intensive nature of manual ROI drawings and provides a more objective and standardized approach to ROI generation.

Ten healthy controls were randomly selected to develop the ROI templates. The regions of interest were drawn on the FA image for each control, and co-registered T1 images were used as an anatomical guide. All ROIs were delineated by referencing anatomical guidelines provided by neuroanatomical atlases (e.g., Naidich et al., 2008).

Then, all images and ROIs were co-registered and resliced to the MNI brain template. Once all images were in MNI space, each of the ROIs was combined across participants to obtain an average ROI template across the 10 randomly selected controls. Each of these ROI templates was then visually verified and manually edited when necessary to be consistent with the aforementioned ROI boundaries on the MNI brain to create the template ROIs.

Next, the AFNI non-linear registration program was used (auto_warp.py; Cox, 1996; Cox and Jesmanowicz, 1999) to register each participant's FA image to the standard MNI FA image (1x1x1mm). Following registration, AFNI 3dNwarpApply was used to calculate the inverse normalization warp matrix from standard space to native space. The inverse matrix was then applied to the template ROIs to bring the template ROIs into native space for each participant. Once the ROIs were in native space, each ROI was checked for accuracy. This method was used for all the ROI templates. In general, the template ROIs registered accurately to the participants' native space based on a visual investigation of the images, and ROIs were manually corrected when necessary.

All ROIs were carefully checked and edited after each transformation. Corrections and edits were made at the following steps:

Step 1. Drew ROIs in native space for 10 healthy controls

Step 2. Transformed ROIs into MNI space

****Checked and corrected ROIs according to defined ROI boundaries****

Step 3. Combined ROIs across 10 healthy controls to create template ROIs

****Checked and corrected ROIs according to defined ROI boundaries****

Step 4. Transformed template ROIs into participants' native space

****Checked and corrected ROIs according to defined ROI boundaries****

3.12 Deterministic Tractography: Preprocessing

Pre-processing and white matter fiber reconstruction methods described below were based on the deterministic tractography pipeline developed by Roberts (2016), which was modeled after the methods from Ford et al. (2013) and Bohsali et al. (2015). TrackTools, developed in Dr. Thomas Mareci's research lab at the University of Florida, was used to reconstruct white matter pathways by characterizing local diffusion according to a Mixture of Wisharts (MOW) probability distribution and applying a spherical deconvolution algorithm, prior to filtering estimated pathways to exclude streamlines that do not directly connect ROIs in a network. Network tractography was completed using PanTrack (software developed in Dr. Bruce Crosson's research lab at Georgia State University/Emory University/the Department of Veterans Affairs), which dices ROIs into smaller units for processing similar to Bohsali and colleagues' methods. Reconstruction methods and tracking algorithms similar to those described are available with software that is publicly available (e.g., MRI Analysis Software (MAS) http://marecilab.mbi.ufl.edu).

The FMRIB Software Library (FSL) Diffusion Toolbox (FDT 2.0) was used to complete tractography preprocessing (Smith et al., 2004). First, diffusion images were checked using FSL view for movement and image artifact. Next, the FSL Eddy Current Correction tool was used to correct for motion and eddy current artifacts (Jenkison et al., 2002; Viallon et al., 2015). Then, the FSL voxel-based morphometry Brain

Extraction Tool (FSL-VBM BET) was used to complete skull stripping (Smith et al., 2004).

3.13 Deterministic Tractography: Measures of white matter integrity

The FSL DTIFIT software was used to fit tensors for each scan. The white matter pathways were reconstructed using a Mixture of Wisharts (MOW) signal attenuation model using TrackTools (http://marecilab.mbi.ufl.edu). The MOW model provided a type of high angular resolution reconstruction method that reconstructs eigenvectors based on a spherical deconvolution approach that allows for crossing and branching fibers, which was more accurate when compared to other common tractography methods (Jian et al., 2007; Jian and Vermuri, 2007a; Jian and Vermuri, 2007b). Furthermore, prior studies have used the MOW model to construct the connections from Broca's area to the thalamus via the internal capsule (Bohsali et al., 2015) as well as the superior cerebellar peduncle pathway to the thalamus and the cortex (Ford et al., 2013).

Next, whole brain tractography files were generated using TrackTools. The angular deviation was a cutoff threshold used to determine when to cease tracing a streamline. Therefore, streamlines that had a curvature of more than 65 degrees between steps were excluded. The step length threshold launched streamline estimations in 0.25 voxel increments in the direction of local maxima. The optimal parameters for the angular deviation and step length for the data set were 65 degrees and 0.25, respectively. These parameters were the same as those used by Bohsali et al. (2015) for successfully tracing cortical-thalamic/thalamic-cortical streamlines from $2mm^3$ resolution DWI images. To reduce the computing demands, number of files generated, the size of the input file, and overall time of processing, TrackTools

track_intersect script was used to create two input files for PanTrack processing. The track_intersect scripts eliminated streamlines that did not intersect with a specified ROI and were useful for eliminating unnecessary data before PanTrack processing. The first whole brain file was reduced to include all streamlines that intersected with the right cerebellum and was used for the cerebellar-frontal white matter pathway. The second whole brain file was reduced to include all streamlines that intersected with the right middle frontal gyrus and was used for the SLF II white matter pathway.

Lastly, PanTrack was used for network tractography. PanTrack, an in-house software developed by Roberts et al. (2016) in Dr. Bruce Crosson's research lab, allows the user to infer white matter pathways both within each ROI and between ROIs. This differed from the methodology described by Bohsali and colleagues (Ford et al., 2013; Bohsali et al., 2015) because PanTrack diced ROIs into voxel-sized nodes prior to networking with Tracktools to eliminate streamlines that do not directly connect ROIs (Colon-Perez et al., 2015). This method was more accurate because Tracktools did not capture the white matter pathways within each of the ROIs and relied more heavily on accurate segmentation boundaries. Therefore, PanTrack was selected over Tracktools because it provided a more complete and robust estimation of the pathways. PanTrack was run twice on all participants. First, PanTrack was used to generate all of the direct connections between the right cerebellum and the left middle frontal gyrus. Next PanTrack was used to provide all of the direct connections between the right middle frontal gyrus and the right parietal lobe.

PanTrack output was then opened in TrackVis, and each pathway was visually confirmed for every participant, and the streamlines were manually edited and

corrected. The cerebellar-frontal pathway was defined as the fibers that began in the right dentate and continued to the left red nucleus, left thalamus, and terminated in the left middle frontal gyrus. Fibers that crossed through the corpus callosum were excluded. The right SLF II was defined using the boundaries described by Thiebaut de Schotten et al. (2011) as the white matter streamlines that began in the middle frontal gyrus and connected to the middle parietal gyrus. Fibers that crossed into the temporal lobe were excluded. TrackVis was used to create a mask of each edited pathway, which was then binarized using FSLmaths. Then, the cerebellar-frontal pathway was divided into three segments using FSLmaths -ROI function (dentate-red nucleus; red nucleus-thalamus; thalamus-frontal lobe). Lastly, FA, L1, L2, and L3 values were extracted for each pathway mask using FSLmeants to average the intensity value of each voxel within each pathway.

Although the literature above suggested that there should be separate pathways from the dentate to the red nucleus and from the dentate to the thalamus, there was no reliable evidence for distinct cerebellar-thalamic fibers in this sample (see Figure 11). The aforementioned studies may have attempted to find this segment of the pathway and encountered similar difficulties. Without visual confirmation of the separate cerebellar-thalamic fibers, there is a possibility that approximately 25% the cerebellar output from the thalamus is not measured in the current study. In contrast to prior studies, the current ROI approach included every structure along the cerebellar-frontal pathway and was still unable to identify the cerebellar-thalamic segment. Given the extensive animal literature for this distinction, other possible explanations for the inability to find this pathways include: a need for higher resolution image acquisition, a

synaptic distinction that cannot be captured using tractography, and/or inability to distinguish crossing fibers at the level of the red nucleus (Milardi et al., 2016; Wakana et al., 2004).

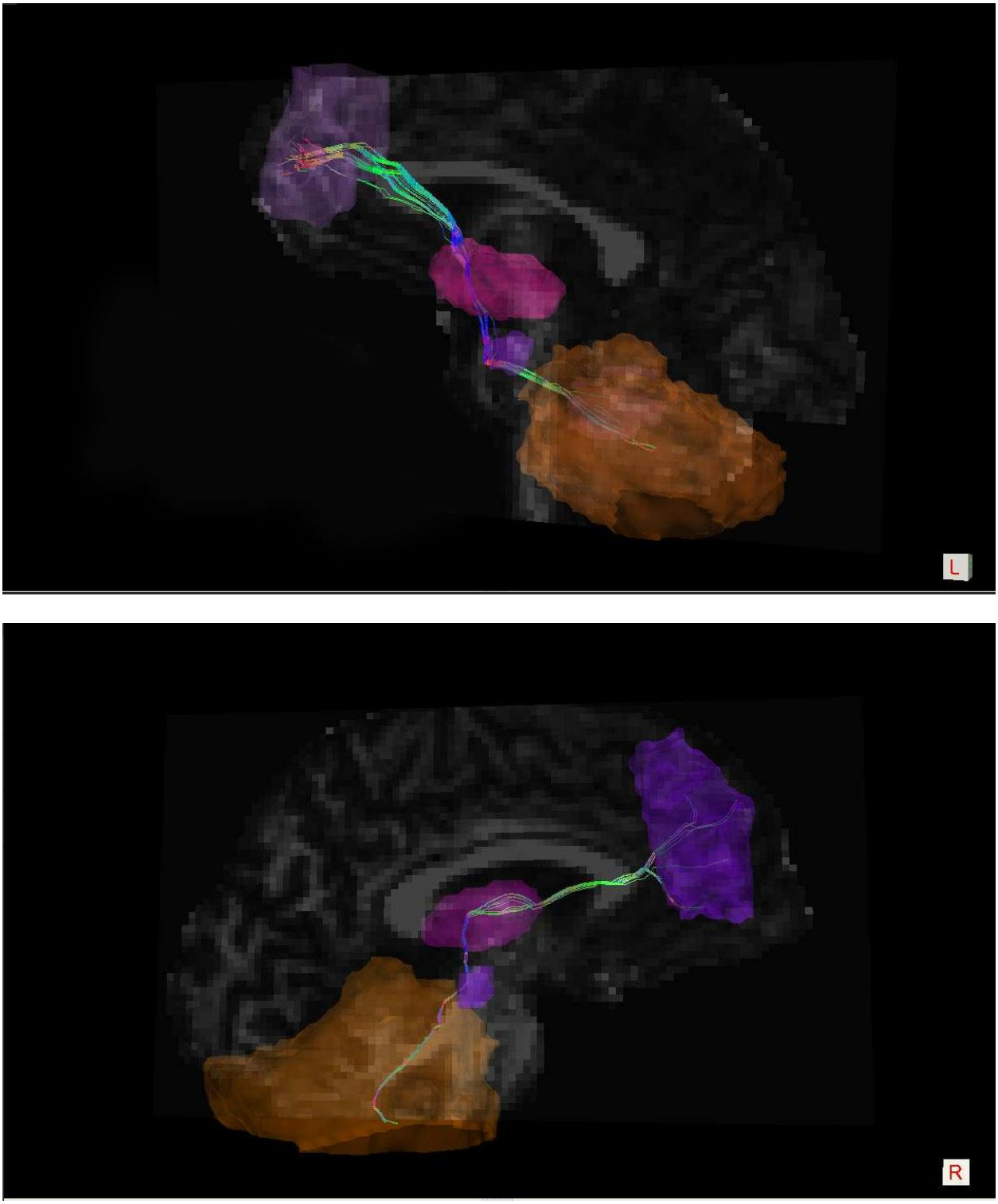

Figure 11 Diffusion tractography of the cerebellar-frontal pathway

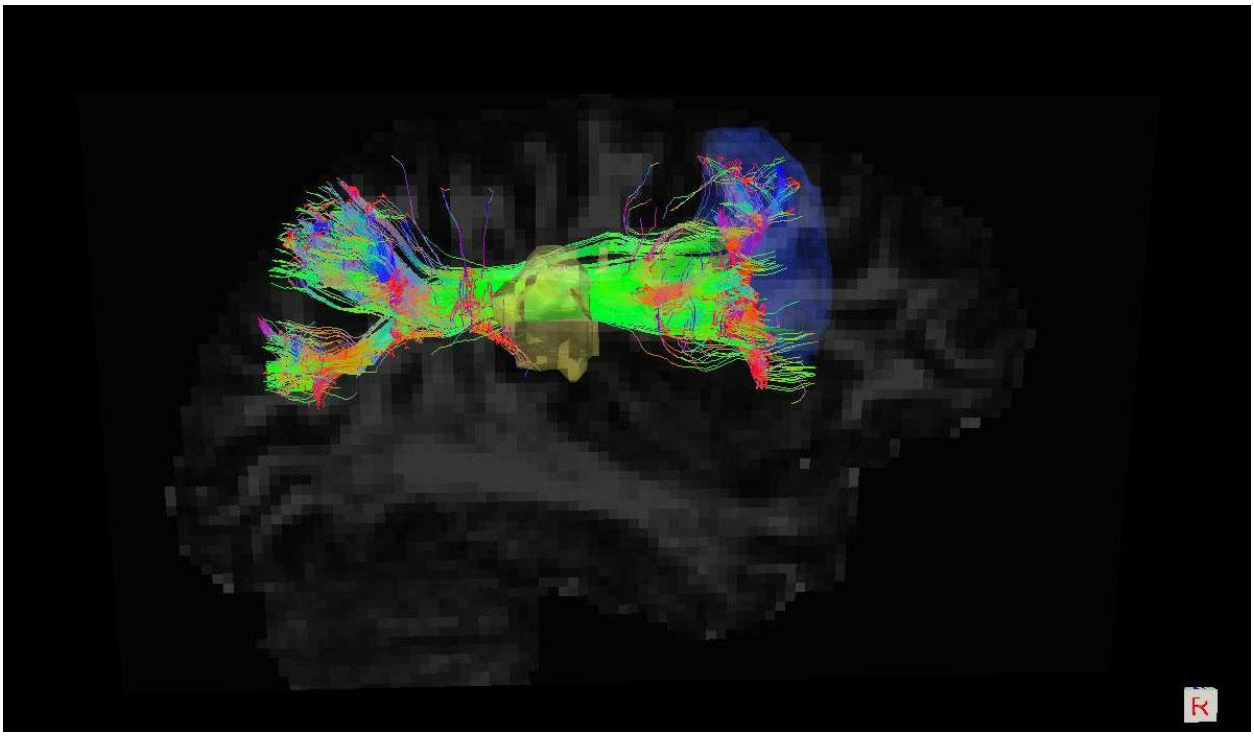

Figure 12 Diffusion tractography of the superior longitudinal fasciculus

3.14 Volumetrics and Cerebellar Atrophy

ROI masks generated for diffusion tractography were used to compute white matter and grey matter volume of each region. First, the T1 image was segmented in Statistical Parametric Mapping (SPM) with Ashburner and Friston's (2005) unified segmentation program. Then a script (Ridgway, 2007; http://www0.cs.ucl.ac.uk/staff/G.Ridgway/vbm/get_totals.m) was used to obtain the voxel counts for participants' whole brain white matter volume, grey matter volume, and cerebrospinal fluid volume, as well as the volume within each ROI. The volume of each ROI was divided by total intracranial vault (Sanfilipo, Benedict, Zivadinov, & Bakshi, 2007) to account for variability in head size. Lastly, a measure of cerebellar atrophy was computed as described in previous research using a subset of this sample (Ailion et al.,

2016). In brief, cerebellar atrophy was defined as the difference between the average of matched controls' cerebellar volume and brain tumor survivors' cerebellar volume (accounting for lesion size) relative to intracranial vault. This measure yielded a percentage of cerebellar atrophy in the survivor group. Detailed equations for the cerebellar atrophy measure can be found in Ailion et al. (2016).

4 ANALYSES

SPSS Statistics version 20 was used for all analyses unless otherwise indicated. Descriptive statistics and scatter plots were used to visualize the distribution of the data and the differences between survivors and controls. The Benjamini-Hochberg statistical correction for family-wise error was used with the recommended 5% false positive rate was used to correct for multiple comparisons because it was less stringent than Bonferroni correction (Benjamini and Hochberg, 1995; Bennett et al., 2009). Analyses were grouped into families by aim, and information related to corrections for multiple comparisons are located at the end of each analysis section.

4.1 Outlier Analyses

Outliers were defined using the outlier labeling rule, in which the interquartile range ($Q3_{75}$-$Q1_{25}$) was multiplied by a factor of 2.2, which was added to or subtracted from $Q2_{50}$ to determine the upper and lower boundary of outliers for each group (Hoaglin and Iglewicz, 1987). Outlier analysis was conducted, and extreme scores for survivors and controls were changed to the next highest or lowest score (Overbay, 2004; see Table 8). Analyses were run both with and without the outliers. The results did not appreciably change when outliers were removed. Therefore, they were included to increase the overall sample size and power in the analyses.

Table 8 Outlier labeling rule change scores

Measure	# of survivors	# of controls	Original scores	Changed scores
Composite processing speed Z-score	2	0	(844) -1.67 (908) 1.87	-1.09 1.42
Whole brain white matter volume relative to ICV	3	0	(833).23 (816) .43 (852).43	.27 .36 .36
Left thalamus volume	0	3	(656) .10 (578) .11 (519) .12	.09 .09 .09
LMFG volume	0	4	(664) .12 (656) .12 (519) .13 (578) .13	.11 .11 .11 .11
Right parietal lobe volume	1	2	(829) .24 (578) .24 (519) .25	.22 .22 .22
RMFG volume	0	2	(519) .14 (578) .15	.13 .13

Note. ICV= intracranial vault; LMFG= left middle frontal gyrus; RMFG= right middle frontal gyrus

4.2 Principal Component Analysis

A principal component analysis (PCA) was computed in the total control sample (*n*=145) to delineate potential factors for each of the hypothesized constructs (Processing Speed, Working Memory, Verbal Attention Span, Visual Attention). Syntax from the UCLA Statistical Consulting Group was used to compute the PCA with 18 test scores from the WMS-III, ACT, OSDMT, DKEFS, and CVLT (List A, Trial 1). The sample was adequate (Kaiser-Meyer-Olkin measure of sampling adequacy= .77), and

Bartlett's test of sphericity was significant ($\chi 2$ (153) = 752.51, $p < .01$). All of the variables except for two loaded onto a single "general executive functioning factor" which explained 26% of the variance. The remaining factor loadings grouped the tests based upon shared test attributes (i.e., the DKEFS subtests grouped together). The lack of differentiation among measures intended to measure separate cognitive functions was likely because measures of executive function are highly correlated in healthy populations and more likely to differentiate in a clinical population. Unfortunately, a PCA in the survivor sample (*n*=29) was not possible because a sample size under 50, which is considered statistically inappropriate (Comrey and Lee, 1992).

4.3 Tests of Statistical Assumptions

Assumptions for analyses were tested for each dependent variable using the explore function within SPSS (e.g., outliers, homogeneity of variance). Variables that did not follow a normal distribution were logarithmetically transformed and rechecked. Variables that still violated the assumption of normality were then square root transformed and rechecked. None of the variables that violated the assumption of normality were successfully transformed to a normal distribution. Therefore, nonparametric statistical tests (Kendall's tau-b and ANOVA) were reported for the variables that violated the assumption of normality (see Table 9).

Table 9 Measures that violated the assumptions of normality

Variable	Kolmogorov-Smirnov	Shapiro-Wilk
Digits Span Z Score	.15, p<.01	.94, p<.01
Digit Span Forward	.15, p<.01	.94, p<.01
Digit Span Backward	.26, p<.01	.87, p<.01
ACT 9 Second Trial Z Score	.17, p<.01	.91, p<.01
ACT 18 Second Trial Z Score	.15, p<.01	.93, p<.01
DKEFS Visual Scanning Z	.28, p<.01	.82, p<.01
DKEFS Visual Errors	.19, p<.01	.82, p<.01

Note. ACT= Auditory Consonant Trigrams; DKEFS= Delis-Kaplan Executive Function Scale

4.4 Survivor and Control Groups

Survivors and controls were matched with regard to age at exam and years of education (see Table 10). Survivors exhibited significantly lower whole brain grey matter volume and whole brain white matter volume when compared to controls. Volume in specific regions, including the left red nucleus and left frontal lobe, were lower in survivors compared to controls. With regard to the diffusion tensor white matter integrity metrics, RD appeared to be more sensitive to demyelination in both white matter pathways. High and low grade tumor groups had similar demographics (see Table 11). Differences in age at diagnosis and treatments were consistent with literature suggesting that high grade tumors are diagnosed at younger ages and receive more aggressive treatment regimens. Subgroup comparisons suggested that survivors with high grade tumors had lower whole brain volume (white and grey matter), cerebellar, frontal, and thalamic volume, and greater white matter disease when compared to low grade tumors and controls.

Of note, Tables 10-11 show that survivors, particularly survivors with high grade tumors, have significantly lower whole brain grey matter volume when compared to controls. These findings were inconsistent with the aforementioned literature that suggested that grey matter should be more resilient to brain tumor treatment. However, the research that suggested relative resiliencies in grey matter used a sample that was on average 5 years post diagnosis (Riggs et al., 2014). Longer-term follow-up studies (Ailion et al., 2016; Jayakar et al., 2015) have found differences in grey matter and whole brain volume. Therefore, it is possible that white matter is more vulnerable to immediate effects of cranial radiation, and findings related to lower grey matter do not appear until a longer time post diagnosis.

In Table 11, percent impairment (defined by greater than 1.5 standard deviations below the mean) of each group is reported for each of the cognitive measures. The low grade tumor group was relatively cognitively intact with only two participants demonstrating impairment on the OSDMT. As expected, the control group was also cognitive intact, with only one participant showing impairment on the Visual Scanning measure. In contrast, the high grade tumor group showed a high degree of impairment on measures of processing speed (OSDMT), auditory attention span (Digit Span Forward), and working memory (ACT 36 Second). These results are consistent with the pattern of weaknesses that has been reported in the literature for high grade tumors (e.g., Palmer, 2008).

In the subsequent analyses, survivors and controls were grouped together unless otherwise specified. Because the hypothesized relationships were not expected to be specific to neurological populations, combining groups was one way to increase

statistical power. Specifically, research on healthy populations reported that cerebellar-frontal white matter integrity was related to working memory, and right SLF II white matter integrity was related to visual attention (Law et al., 2011; Thiebaut de Schotten, 2012). The strength of these relationships was expected to be greater within the survivor group. Therefore, moderations were also tested based on the hypothesis that when estimating cognitive performance survivors would be more affected by lower white matter integrity in both pathways, whereas controls would be less affected by lower white matter integrity in both pathways.

Table 10 Survivor and control demographic and descriptive comparisons

	Survivors *n*=29	Controls *n*=29	Group differences	Cohen's D
Gender	45% Female	48% Female		
Age at exam (years)	*M*=21.34 *SD*=5.35	*M*=22.43 *SD*=5.20	*t*=.79, *p*=.56	-.02
Years of education	*M*=13.28 *SD*=2.79	*M*=14.34 *SD*=2.79	*t*=-1.77, *p*=.08	-.38
Age at diagnosis (years)	*M*=8.55 *SD*=4.88 Range 1-18			
Radiation	*n*=15 52%			
Chemotherapy	*n*=14 48%			
High grade tumor	*n*=14 48%			
Hydrocephalus	*n*=24 83%			
Seizure medication	*n*=1 3%			
Hormone deficiency	*n*=16 55%			
Whole brain grey matter volume**	*M*=.77 *SD*=.05	*M*=.81 *SD*=.02	*t*=4.04, *p*<.01	-1.05
Whole brain white matter volume*	*M*=.31 *SD*=.02	*M*=.32 *SD*=.02	*t*=2.46, *p*=.02	-.50
Right Cerebellar Volume	*M*=.10 *SD*=.03	*M*=.10 *SD*=.05	*t*=.54, *p*=.59	.00
Right Dentate Volume	*M*=.04 *SD*=.02	*M*=.04 *SD*=.03	*t*=.60, *p*=.55	.00
Left Red Nucleus Volume	*M*=.03 *SD*=.02	*M*=.04 *SD*=.03	*t*=.45, *p*=.65	-.39
Left Thalamus Volume	*M*=.04 *SD*=.02	*M*=.04 *SD*=.03	*t*=-.05, *p*=.96	.00
Left Frontal Volume	*M*=.07 *SD*=.02	*M*=.06 *SD*=.03	*t*=-.67, *p*=.51	.39
Cerebellar-Frontal FA	*M*=.32 *SD*=.06	*M*=.32 *SD*=.05	*t*=-.04, *p*=.97	.00
Cerebellar-Frontal RD**	*M*=.0013 *SD*=.0003	*M*=.0011 *SD*=.0001	*t*=-2.64, *p*<.01	.89
SLF II FA	*M*=.28 *SD*=.05	*M*=.26 *SD*=.05	*t*=-1.51, p=.14	.40
SLF II RD	*M*=.0008 *SD*=.0001	*M*=.0007 *SD*=.0001	*t*=3.81, p<.01	1.00

Note. ** indicates p<.01 and * indicates p<.05; All volume measures are regional gray matter plus white matter divided by intracranial vault

Table 11 Subgroup descriptive statistics and effect sizes

	Subgroup descriptive statistics			Subgroup differences Cohen's D		
	Low Grade *n*=15	High Grade *n*=14	Controls *n*=29	Low Grade vs. High Grade	Low Grade vs. Controls	High Grade vs. Controls
Gender	40% Female	50% Female	48% Female			
Age at exam (years)	*M*=21.27 *SD*=5.18	*M*=21.43 *SD*=5.72	*M*=22.43 *SD*=5.20			
Years of education	*M*=13.53 *SD*=2.72	*M*=13.00 *SD*=2.94	*M*=14.34 *SD*=2.79			
Age at diagnosis (years)	*M*=10.00 *SD*=4.63 Range 1-18	*M*=7.00 *SD*=4.82 Range 1-17				
Radiation	*n*=2 13%	*n*=13 93%				
Chemotherapy	*n*=0 0%	*n*=14 100%				
Hydrocephalus	*n*=12 80%	*n*=12 86%				
Seizure medication	*n*=1 7%	*n*=0 0%				
Hormone deficiency	*n*=12 80%	*n*=13 93%				
Whole brain grey matter volume+	*M*=.79 *SD*=.06	*M*=.75 *SD*=.03	*M*=.81 *SD*=.02	0.83**	-0.52*	-2.54**
Whole brain white matter volume+	*M*=.32 *SD*=.02	*M*=.30 *SD*=.03	*M*=.32 *SD*=.02	0.79*	0.00	-0.85**
Right Cerebellar Volume+	*M*=.11 *SD*=.03	*M*=.09 *SD*=.02	*M*=.10 *SD*=.05	0.78*	0.00	-.85**
Right Dentate Volume	*M*=.04 *SD*=.02	*M*=.04 *SD*=.02	*M*=.04 *SD*=.03	0.00	0.00	0.00
Left Red Nucleus Volume	*M*=.03 *SD*=.02	*M*=.03 *SD*=.02	*M*=.04 *SD*=.03	0.00	-0.37	-0.37
Left Thalamus Volume+	*M*=.05 *SD*=.02	*M*=.04 *SD*=.02	*M*=.04 *SD*=.03	0.50*	0.37	0.00
Left Frontal Volume+	*M*=.07 *SD*=.02	*M*=.06 *SD*=.02	*M*=.06 *SD*=.03	0.50*	0.37	0.00
Cerebellar-Frontal FA	*M*=.32 *SD*=.04	*M*=.31 *SD*=.07	*M*=.32 *SD*=.05	0.18	0.00	-.0.18
Cerebellar-Frontal RD+	*M*=.0012 *SD*=.0002	*M*=.0013 *SD*=.0003	*M*=.0011 *SD*=.0001	-0.40	0.71*	1.06**
SLF II FA+	*M*=.30 *SD*=.05	*M*=.25 *SD*=.04	*M*=.26 *SD*=.05	1.10**	0.80**	-0.21
SLF II RD+	*M*=.0007 *SD*=.0001	*M*=.0008 *SD*=.0001	*M*=.0007 *SD*=.0001	-1.00**	0.00	1.00**
Percent impairment on cognitive measures. Impairment defined as ≤ 1.5 SD below the mean						
Processing Speed Composite	*M*=.25 *SD*=.67 *n*=0 0%	*M*=-.30 *SD*=.41 *n*=0 0%	*M*=.31 *SD*=.54 *n*=0 0%	-	-	-
OSDMT	*M*=-.50 *SD*=1.38 *n*=2 13%	*M*=-1.58 *SD*=1.14 *n*=8 57%	*M*=.03 *SD*=1.07 *n*=0 0%	c^2=6.15 Fisher's p=.02	c^2=.21 Fisher's p=.26	c^2=16.45 Fisher's p<.01
Digit Span Forward	*M*=7.00 *SD*=1.20 *n*=0 0%	*M*=5.64 *SD*=1.22 *n*=3 21%	*M*=7.14 *SD*=1.22 *n*=0 0%	c^2=3.58 Fisher's p=.10	-	c^2=6.68 Fisher's p=.03
Working Memory	*M*=.01 *SD*=1.17 *n*=0 0%	*M*=-.98 *SD*=1.09 *n*=5 36%	*M*=.47 *SD*=.92 *n*=0 0%	c^2=3.72 Fisher's p=.08	-	c^2=11.72 Fisher's p<.01
Visual Scanning	*M*=1.07 *SD*=1.22 *n*=0 0%	*M*=.64 *SD*=1.15 *n*=0 0%	*M*=.79 *SD*=1.16 *n*=1 3%	-	c^2=.53 Fisher's p=1.00	c^2=.49 Fisher's p=.67

Note. All volume measures are gray matter plus white matter divided by intracranial vault; + indicates significant difference; Cohen's D: Small=0.2-0.3, Medium=0.5*, Large ≥ 0.8**; OSDMT= Oral Symbol Digit Modality Test; Working Memory= Auditory Consonant Trigrams 36 Second Trial; Visual Scanning= Delis-Kaplan Executive Function System, Trail Making Test, Visual Scanning; c^2 = chi square; Fisher's p is Fisher's Exact Test.

4.5 Confound Analyses

Based on prior literature, potential confounds or covariates included longer time since treatment, younger age at diagnosis, radiation treatment, and radiation dosage (Aukema et al., 2009; Khong et al., 2003; Law et al., 2011; Law et al., 2015a; Merchant et al., 2008; Mulhern et al., 2001; Palmer et al., 2012; Palmer, 2008; Palmer et al., 2002; Reddick et al. 2005; Reddick et al., 2000). These and other treatment factors (e.g., hydrocephalus, seizure disorder, and hormone disorder) were explored in analyses as potential confounds and covariates. A confound was defined as a treatment variable that was correlated with both the independent variable (e.g., white matter integrity) and the dependent variable (e.g., cognitive performance). A covariate was defined as a treatment factor that was correlated with the dependent variable (e.g., cognitive performance) but not the independent variable (e.g., white matter integrity).

Covariate and confound analyses revealed a number of associations between treatment factors and neurocognitive measures (see Table 12-13). Specifically, all treatment factors were correlated with lower processing speed, and tumor grade and the amount of treatment were associated with lower performance across neurocognitive domains. Furthermore, treatment and tumor grade were associated with lower whole brain volume, cerebellar volume, and SLF II white matter integrity (see Table 14; FA and RD). Therefore, the Neurological Predictor Scale (NPS; Micklewright et al., 2008) was selected as a covariate in analyses because it provided a cumulative measure of treatment severity and complications. The NPS quantified hydrocephalus, hormone deficiency, seizures, type of surgical resection, type of radiation therapy, and

chemotherapy on a scale from 0 (no treatments or complications) to 9 (high degree of treatments and complications; Taiwo et al., 2017).

Age at diagnosis was positively correlated with cerebellar-frontal FA and whole brain white matter volume, indicating that children diagnosed at older ages had greater white matter volume and integrity. Therefore, age at diagnosis was investigated as a covariate based on the correlation with cerebellar-frontal FA. Age at diagnosis was associated with both the cerebellar-frontal FA and composite processing speed. Of note, treatment severity and age at diagnosis are both proposed mechanisms for lower white matter and volume in brain tumor survivors when compared to controls. Therefore, the results tables for Aims 1-4 include comparison correlations without the treatment covariates.

Table 12 Correlations between treatment variables and neurocognitive measures (n=29)

	Composite PS Measure	OSDMT	Digit Span Forward	Digit Span Backwards	ACT 36 seconds	DKEFS Visual Scanning Z	DKEFS Visual Scanning Errors
Time Since Diagnosis (years)	r=.48**	r=-.27	τb=-.04	τb=-.03	r=-.29	τb=-.26	τb=-.12
Age at Diagnosis (years)	r=.42*	r=.10	τb=.16	τb=.07	r=.35	τb=.09	τb=.16
Radiation	r=-.45*	r=-.36	τb=-.22	τb=-.15	r=-.35	τb=-.35*	τb=-.37*
Amount of Radiation (rads)	r=-.44*	r=-.35	τb=-.21	τb=-.18	r=-.36*	τb=-.21	τb=-.39*
Hydrocephalus	r=-.39*	r=-.16	τb=-.04	τb=-.29	r=-.32	τb=-.16	τb=-.20
Hormone Disorder	r=-.54**	r=-.31	τb=-.18	τb=-.11	r=-.36*	τb=-.40*	τb=-.37*
WHO Grade	r=-.54**	r=-.44*	τb=-.44**	τb=-.37*	r=-.44*	τb=-.22	τb=-.32*
Seizures	r=.07	r=.04	τb=.28	τb=.28	r=.07	τb=.22	τb=-.12
NPS	r=.63**	r=-.49*	τb=-.32*	τb=-.25	r=-.40*	τb=-.36*	τb=-.38**

Note. *indicates $p<.05$ and **indicates $p<.01$; Radiation, hormone disorder, and seizures are coded as dichotomous variables in which 0= not present and 1= present; WHO= World Health Organization; WHO Grade= 1-4 where 1 is the most benign and 4 is the highest grade tumor; NPS= Neurological Predictor Scale; PS= processing speed; OSDMT= Oral Symbol Digit Modality Test; ACT= Auditory Consonant Trigram; DKEFS= Delis-Kaplan Executive Function Scale; τb = Kendall's Tau

Table 13 Correlations between treatment variables and cerebellar-frontal neuroimaging metrics (n=29)

	Cerebellar-Frontal FA	Cerebellar-Frontal RD	Right Cerebellar Volume	Right Dentate Volume	Left Thalamus Volume	Left MFG Volume	Cerebellar Atrophy	Whole Brain White Matter	Whole Brain Grey Matter
Time Since Diagnosis	r=-.03	r=-.06	r=-.30	r=-.03	r=-.02	r=-.05	r=.08	r=.22	r=-.22
Age at Diagnosis	r=.44*	r=-.26	r=-.06	r=-.16	r=-.15	r=-.12	r=-.11	r=.46*	r=.12
Radiation	r=.02	r=.13	r=-.43*	r=-.12	r=-.14	r=-.11	r=.11	r=-.07	r=-.10
Amount of Radiation	r=.00	r=.15	r=-.45*	r=-.13	r=-.16	r=-.13	r=.11	r=-.07	r=-.11
Hydrocephalus	r=-.21	r=.22	r=-.22	r=-.21	r=-.16	r=-.20	r=.11	r=.09	r=.19
Hormone Disorder	r=-.02	r=.15	r=-.48**	r=-.17	r=-.20	r=-.17	r=.09	r=-.04	r=-.12
WHO Grade	r=-.15	r=.22	r=-.31	r=-.04	r=-.13	r=-.15	r=.19	r=-.42*	r=-.43*
Seizures	r=.13	r=-.05	r=.28	r=.30	r=.31	r=.30	r=-.15	r=-.04	r=.12
NPS	r=-.11	r=.30	r=-.40*	r=-.10	r=-.13	r=-.13	r=.19	r=-.19	r=-.24

Note. *indicates $p<.05$ and **indicates $p<.01$; radiation, hormone disorder, and seizures are coded as dichotomous variables in which 0= not present and 1= present; WHO= World Health Organization; NPS= Neurological Predictor Scale; FA= fractional anisotropy; RD= radial diffusivity; MFG= Middle Frontal Gyrus; Whole brain white and grey matter are measures of volume.

Table 14 Correlations between treatment variables and SLF II neuroimaging metrics (n=29)

	Right Parietal Volume	Right MFG Volume	SLF II FA	SLF II RD	Whole Brain White Matter	Whole Brain Grey Matter
Time Since Diagnosis	r=.07	r=-.02	r=-.41*	r=.42*	r=.22	r=-.22
Age at Diagnosis	r=.06	r=-.10	r=.30	r=.-10	r=.46*	r=.12
Radiation	r=-.08	r=-.03	r=-.59**	r=.36*	r=-.07	r=-.10
Amount of Radiation	r=-.09	r=-.05	r=-.60**	r=37*	r=-.07	r=-.11
Hydrocephalus	r=-.07	r=-.22	r=-.37*	r=.21	r=.09	r=.19
Hormone Disorder	r=-.11	r=-.10	r=-.61**	r=.44*	r=-.04	r=-.12
WHO Grade	r=-.35	r=-.11	r=-.45*	r=.38*	r=-.42*	r=-.43*
Seizures	r=.25	r=.24	r=.27	r=-.19	r=-.04	r=.12
NPS	r=-.20	r=-.09	r=-.58**	r=.43*	r=-.19	r=-.24

Note. *indicates $p<.05$ and **indicates $p<.01$; Radiation, hormone disorder, and seizures are coded as dichotomous variables in which 0= not present and 1= present; WHO= World Health Organization; NPS= Neurological Predictor Scale; MFG= Middle Frontal Gyrus; SLF= Superior Longitudinal Fasciculus; FA= fractional anisotropy; RD= radial diffusivity; Whole brain white and grey matter are measures of volume.

4.6 Aim 1

4.6.1 Hypothesis 1

Lower white matter integrity in the right cerebellar-left frontal pathways (sum of FA for the cerebellar-rubral, rubral-thalamic, and thalamic-frontal pathways) would be associated with lower working memory, but not processing speed or auditory attention span.

Across each correlation, the independent variables were white matter integrity measures of cerebellar-frontal pathways (FA and RD), and the dependent variables were *z*-scores on processing speed (OSDMT and processing speed composite measure), attention span (Digits Forward), and working memory (ACT 36 Second) measures. In the survivor group analyses, auditory attention span was correlated with cerebellar-frontal white matter integrity (FA and RD), and this relationship remained significant after using partial correlations to control for treatment factors (see Table 15). Importantly, Digit Span Backward trial did not correlate with any of cerebellar-frontal white matter integrity (FA or RD), which suggests a unique contribution of auditory attention span. Digit Span combined score is provided to be consistent with prior studies. In the control group analyses, only processing speed was correlated with cerebellar-frontal white matter integrity (FA only). For the control group, higher FA was associated with lower composite processing speed. This relationship appeared strong for the OSDMT as well, although it was not significant (see Table 15 and Figure 14). This relationship is the opposite of what would be expected.

Theoretically, higher FA should be associated with faster processing speed. However, a similar inverse relationship has been found in a neurotypical population.

Similar to the current findings, Imfeld et al. (2009) found an inverse relationship, such that skilled musicians had reductions in corticospinal white matter integrity (FA) when compared to neurotypical controls. Higher FA was thought to represent increased permeability of the axonal membrane secondary to repeated plastic changes within the corticospinal tract (Imfeld et al., 2009). Similarly, white matter pruning of the cerebellar-frontal pathway may result in increased permeability if the axonal membrane. Therefore, it is possible that lower FA in the neurotypical population is measuring axonal membrane permeability secondary to healthy white matter pruning (e.g., Huang et al., 2015). In line with this theory, the frontal portion of the cerebellar-frontal pathway undergoes synaptic pruning from adolescence to adulthood (Willing and Juraska, 2015; Huang et al., 2015).

The inverse relationship highlights the pitfalls of summary diffusion metrics that combine measures of axons, myelin, extracellular spacing, and membrane permeability (Beaulieu, 2002). These results provide support for the criticisms of FA, including the combination of multiple eigenvectors that measure different components of brain biology, which makes it less sensitive and more difficult to interpret as a measure (Tournier, Mori, & Leemans, 2011; Wheeler-Kingshott & Cercignani, 2009). In sum, white matter integrity measures that combine multiple eigenvectors may capture healthy neural processes, such as pruning, as opposed to white matter injury in neurotypical populations. However, more research is needed to better understand how FA may be influenced by membrane permeability or healthy neural processes such as pruning.

Significant relationships are plotted for each group in Figures 13-16. The initially proposed path analysis was unnecessary due to the lack of significant findings across

multiple measures in the combined group or separate group analyses. Fisher's r-to-z transformation was computed to determine if the correlations for cerebellar-frontal white matter integrity and auditory attention span were significantly greater than other measures. The correlation coefficient was significantly larger for auditory attention span when compared to working memory (FA z= 1.74, p=.08; RD z=-2.76, p<.01). However, Fisher's Z was not statistically significant for the other measures (OSDMT FA z=1.74, p=.08; RD z=1.88, p=.06; composite processing speed FA z=1.67, p=.09; RD z=-1.00, p=.31).

Table 15 Summary of correlation results for Hypothesis 1

	Processing Speed Composite (z-score)	Processing Speed OSDMT (z-score)	Working Memory ACT 36 Second (z-score)	Auditory Attention Span Digit Span Forward (raw)	Digit Span Backward (raw)	Combined Digit Span Forward and Backward (z-score)
Survivors only (n=29)						
Right cerebellar-left frontal FA	r=-.06	r=.14	r=.09	τb=.40**	τb<.00	τb=.36
Right cerebellar-left frontal RD	r=.05	r=-.16	r=.11	τb=-.34*	τb=.01	τb=-.32
Survivors only (n=29) partial correlations (controlling for NPS)						
Right cerebellar-left frontal FA	r=.21	r=.02	r=.11	r=.42*	r=.03	r=.39
Right cerebellar-left frontal RD	r=-.26	r=-.16	r=.08	r=-.50*	r=.05	r=-.31
Survivors only (n=29) partial correlations (controlling for NPS and age at diagnosis)						
Right cerebellar-left frontal FA	r=-.05	r=-.11	r=-.07	r=.39*	r=.07	r=.36
Right cerebellar-left frontal RD	r=-.11	r=.10	r=.36	r=-.37*	r=.04	r=-.29
Controls only (n=29)						
Right cerebellar-left frontal FA	r=-.45*	r=-.35	r=.16	τb=-.03	τb=.08	τb=-.02
Right cerebellar-left frontal RD	r=.22	r=.33	r=.08	τb=.06	τb=.06	τb=.11

Note. *indicates $p<.05$ and **indicates $p<.01$; NPS= neurological predictor scale; Processing Speed measured by the Oral Symbol Digit Modality Test (OSDMT); Working Memory measured by the Auditory Consonant Trigrams 36 Second Trial; Auditory Attention measured by the Digit Span Forward subtest.

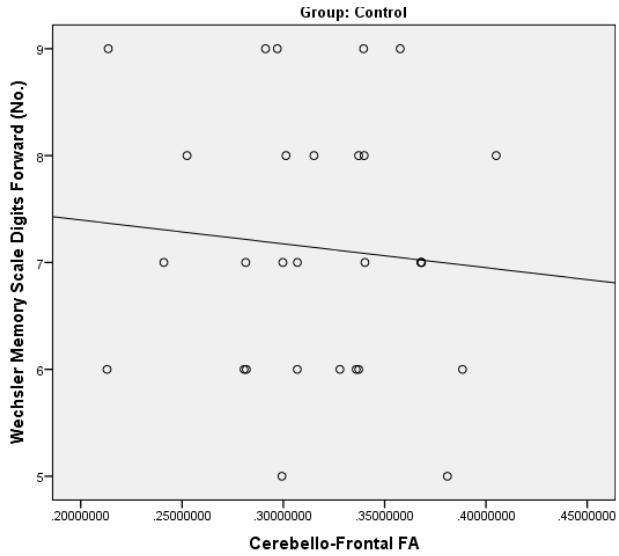

Figure 13 Hypothesis 1: Scatterplot of cerebellar-frontal FA and Digits Span Forward Raw Scores in the control group Note. FA= Fractional Anisotropy

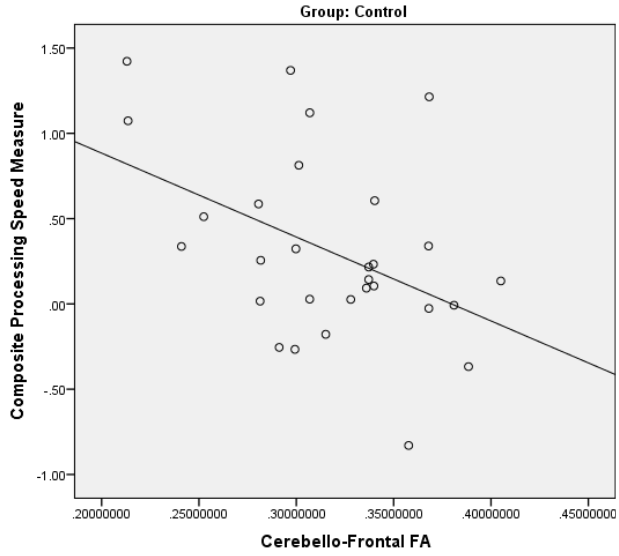

Figure 14 Hypothesis 1: Scatterplot of cerebellar-frontal FA and composite processing speed in the control group Note. FA= Fractional Anisotropy

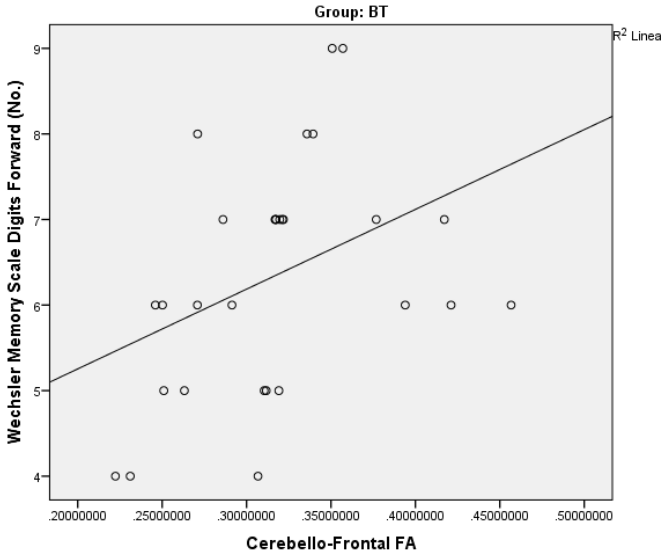

Figure 15 Hypothesis 1: Scatterplot of cerebellar-frontal FA and Digit Span Forward Raw Scores in the survivor group Note. BT= Brain Tumor; FA= Fractional Anisotropy

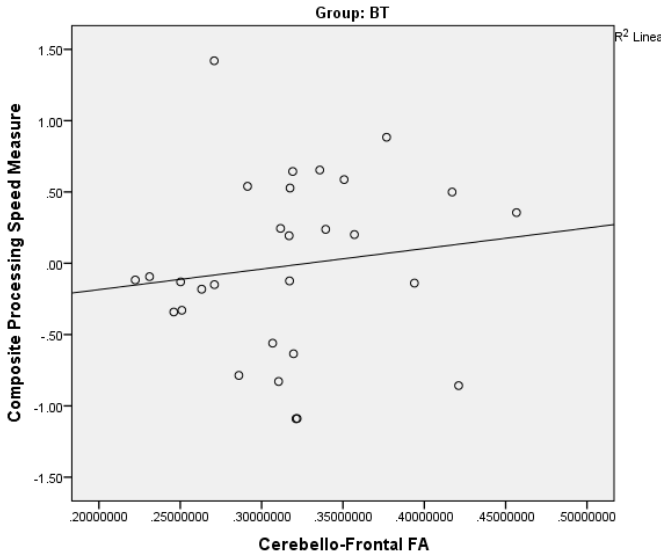

Figure 16 Hypothesis 1: Scatterplot of cerebellar-frontal FA and composite processing speed in the survivor group Note. BT= Brain Tumor; FA= Fractional Anisotropy

Analyses from Hypothesis 1 were replicated with the neurocognitive measures and whole brain white matter volume relative to intracranial vault (see Table 16). In the survivor group analyses, whole brain white matter volume was correlated with auditory attention span (τb=.36, p<.05), and this relationship remained significant when controlling for treatment factors. In the control group, these relationships between neurocognitive measures and whole brain white matter volume did not reach statistical significance.

Table 16 Hypothesis 1: Correlations between whole brain white matter volume and neurocognitive measures

	Processing Speed Composite	Processing Speed OSDMT	Auditory Attention Span Raw Score	Verbal Working Memory
Survivors only (n=29)				
Whole Brain White Matter Volume /ICV	r=.02	r=-.08	τb=.36*	r=-.02
Survivors only (n=29) partial correlations (controlling for NPS)				
Whole Brain White Matter Volume/ICV	r=-.11	r=.02	r=.55*	r<.01
Survivors only (n=29) partial correlations (controlling for NPS and age at diagnosis)				
Whole Brain White Matter Volume/ICV	r=-.31	r=-.20	r=.48*	r=-.27
Controls Only (n=29)				
Whole Brain White Matter Volume /ICV	r=.16	r=.14	τb=.12	r<.01

Note. *indicates *p*<.05 and **indicates *p*<.01; ICV= intracranial vault; NPS= neurological predictor scale; OSDMT= Oral Symbol Digit Modality Test; τb= Kendall's Tau

The initially proposed moderation between groups (survivor vs. control) for cerebellar-frontal white matter integrity and working memory was unnecessary because there were no significant correlations between cerebellar-frontal white matter integrity

and working memory. Instead, group moderations were tested for the significant correlations reported in Table 15 (i.e., cerebellar-frontal white matter integrity and processing speed; cerebellar-frontal white matter integrity and auditory attention span).

First, a forced entry multiple regression was tested with group (control=0, survivor=1), cerebellar-frontal FA, and the interaction term (cerebellar-frontal FA*group) as the independent variables and composite processing speed as the dependent variable (see Table 17). Cerebellar-frontal FA was mean centered to aid interpretation. The model accounted for 12% of the variance in composite processing speed, *Adj* R^2=.12, $F(3,54)=3.57$, p=.02. A main effect of group was significant, B=-.33, SE=.15, Beta=-.27, p=.03 and uniquely explained 8% of the variance in processing speed. Higher FA was associated with lower processing speed in the control group, B=-4.92, SE=2.17, Beta=-.44, p=.03, and uniquely explained 8% of the variance in processing speed. An interaction effect between group and white matter integrity was present in the sample, B=6.36, SE=2.84, Beta=-.43, p=.03, and accounted for 8% of the variance in processing speed. The interaction was probed at both group levels. For controls, higher cerebellar-frontal FA was associated with lower processing speed, whereas for survivors there was no relationship between cerebellar-frontal FA and processing speed, B=1.44, SE=1.84, Beta=.13, p>.05.

Table 17 Regression coefficients for group and cerebellar-frontal FA predicting composite processing speed

Variable	*B*	*SE B*	Beta	*p*	sr^2	*VIF*
Group (0=control, 1=survivor)	-.33	.15	-.28	.03	.08	1.00
Cerebellar-Frontal FA (mean centered)	-4.92	2.17	-.44	.03	.08	2.39
Interaction (group*FA)	6.36	2.84	.43	.03	.08	2.39

Note. FA= fractional anisotropy; SE= Standard Error; sr^2= semi-partial correlation; VIF= Variance Inflation Factor

Next, because the Digit Span Forward measure violated the assumption of normality, a univariate analysis of variance (ANOVA) was tested with group (control=0, survivor=1), cerebellar-frontal FA, and the interaction term (cerebellar-frontal FA*group) as the independent variables and Digit Span Forward as the dependent variable. The model accounted for 12% of the variance in auditory attention span, *Adj* R^2=.12, $F(3,54)=3.68$, $p=.02$. A main effect of group was significant, $B=.80$, $SE=.23$, 95% CI [.13-1.46], $p=.02$. Cerebellar-frontal FA was positively associated with auditory attention span, $B=9.32$, $SE=4.14$, 95% CI [1.03-17.61], $p=.03$. However, the interaction effect between group and white matter integrity was not statistically significant in the model, $B=-11.55$, $SE=6.39$, 95% CI [-24.37-1.27], $p=.08$. Results were similar for cerebellar-frontal RD, *Adj* R^2=.15, $F(3,54)=4.38$, $p<.01$, except group was not significant ($B=-2.71$, $SE=20.2$, 95% CI [-6.751-1.33], $p=.11$).

4.7 Statistical Correction

The Benjamini-Hochberg statistical correction for family-wise error was used with the recommended 5% false positive rate because it was less stringent than Bonferroni correction (Benjamini and Hochberg, 1995; Bennett et al., 2009). A total of 67 analyses were computed for the first aim, and all reported results survived statistical correction for multiple comparisons. The statistical correction was determined by rank ordering the p-values for all analyses and computing the Benjamini-Hochberg critical value using the following formula:

Benjamini-Hochberg critical value = (i/m)*Q

i = the individual p-value rank (1-55)

m = total number of tests (55)

Q = the false discovery rate (5%)

4.8 Aim 2

4.8.1 Hypothesis 1

Lower white matter integrity (WMI) in the cerebellar-frontal pathways would be associated with lower working memory, but not visual attention performance.

4.8.2 Hypothesis 2

Lower WMI in the right SLF II would be associated with lower visual attention performance, but not lower working memory performance.

Double dissociations help to determine the exact roles of brain structures and behavior and help to localize cognitive functions. The goal of the current study was to establish the specificity for the relationship between cerebellar-frontal white matter

integrity and working memory via a double dissociation with the right SLF II pathway and visual attention. Pearson correlations were planned between the measures of white matter integrity of the pathways of interest (FA of the cerebellar-frontal and SLF II pathways) and cognitive performance (working memory, visual attention- number of errors and visual attention-time to complete). However, auditory attention span, rather than working memory, was associated with the cerebellar-frontal white matter integrity in Aim 1. Therefore, auditory attention span, rather than working memory was the measure selected for the double dissociation in Aim 2.

In the survivor group analyses, SLF II FA was associated with visual attention. However, this relationship was not present in the control sample (see Table 18). Based on statistical significance, the results support the hypothesis of a double dissociation with brain-behavior specificity for each pathway in the survivor group. Fisher's r-to-z transformation was used to determine if the correlation between right cerebellar-left frontal FA and RD and auditory attention span was significantly greater than the correlations to visual attention. Fisher's r-to-z transformation indicated that the correlation between cerebellar-frontal FA and auditory attention span was significantly greater than the correlation to visual attention (FA: $z=2.38$, $p=.02$). However, the same analyses for RD did not reach statistical significance ($z=-1.58$, $p=.11$). Similarly, Fisher's Z transformation indicated that correlations for SLF II FA and RD and visual attention were not significantly greater than auditory attention span (FA: $z=.82$, $p=.41$; RD: $z=-26$, $p=.79$).

Table 18 Summary of correlation results for Hypothesis 2

	Auditory Attention Span (raw)	Visual Attention	Visual Attention # of Errors
Survivors only (n=29)			
Right cerebellar-left frontal FA	τb=.40**	τb=-.03	τb=-.18
Right cerebellar-left frontal RD	τb=-.34*	τb=-.04	τb=.04
Right SLF II FA	τb=.19	τb=.31*	τb=.07
Right SLF II RD	τb=-.09	τb=-.22	τb=.03
Survivors only (n=29) partial correlations (controlling for NPS)			
Right cerebellar-left frontal FA	r=.42*	r=-.11	r=-.20
Right cerebellar-left frontal RD	r=-.50*	r=-.11	r=-.02
Right SLF II FA	r=.24	r=.44*	r=.09
Right SLF II RD	r=-.10	r=-.17	r=.24
Controls Only (n=29)			
Right cerebellar-left frontal FA	τb=-.03	τb=-.15	τb=.07
Right cerebellar-left frontal RD	τb=.06	τb=.19	τb=.09
Right SLF II FA	τb=.14	τb=-.03	τb=.08
Right SLF II RD	τb=.21	τb=.27	τb=-.21

Note. τb = Kendall's Tau; *indicates $p<.05$ and **indicates $p<.01$; NPS= neurological predictor scale; τb = Kendall's Tau; FA= fractional anisotropy; RD= radial diffusivity; Visual Attention= Delis-Kaplan Executive Function Scale, Trail Making Test, Visual Scanning Trial z-score

Analyses from Hypothesis 2 were also computed with whole brain white matter volume relative to intracranial vault to determine that the results were not due to overall reductions in whole brain white matter volume. The Aim 1 results from auditory attention span are reported in the first column to ease the comparison of findings. Across the groups, the results did not reach statistical significance (see Table 19).

Table 19 Hypothesis 2: Correlations between whole brain white matter volume and neurocognitive measures

	Auditory Attention Span (raw)	Visual Attention	Visual Attention # of Errors
Survivors only (n=29)			
Whole Brain White Matter Volume/ICV	τb=.36*	τb=-.19	τb=-.01
Survivors only (n=29) partial correlations (controlling for NPS)			
Whole Brain White Matter Volume/ICV	r=.55**	r=-.20	r=-.05
Controls Only (n=29)			
Whole Brain White Matter Volume/ICV	τb=.12	τb<.01	τb=-.12

Note. *indicates $p<.05$ and **indicates $p<.01$; ICV= intracranial vault; NPS= Neurological Predictor Scale; Visual Attention= Delis-Kaplan Executive Function Scale, Trail Making Test, Visual Scanning Trial z-score; τb= Kendall's Tau

Since a significant relationship was found between the right SLF II white matter integrity and visual attention, a group moderation was tested (survivor vs. control). The hypothesis was that the slope of the relationship between right SLF II white matter integrity and visual attention would be steeper for the survivor group when compared to the control group. Right SLF II white matter integrity was grand mean centered to aid interpretation. The interaction variable was computed in SPSS by multiplying the group variable (survivor vs. control) by right SLF II white matter integrity. Because visual attention violated the assumption of normality, an ANOVA was used to test the moderation. Group (control=0, survivor=1), SLF II FA, and the interaction term (SLF II FA*group) were the independent variables, and DKEFS Visual Scanning was the dependent variable. The model did not account for significant variance in visual attention, *Adj* R^2=.04, $F(3,54)=1.74$, $p=.17$. Results were similar when SLF II RD was computed, *Adj* R^2=.03, $F(3,54)=1.66$, $p=.19$.

4.9 Statistical Correction

Similar to Aim 1, the Benjamini-Hochberg statistical correction for family-wise error was be used with the recommended 5% false positive rate. A total of 26 analyses were computed for the second aim, and all reported results survived statistical correction for multiple comparisons. See statistical correction section under Aim 1 for the Benjamini-Hochberg statistical correction formula.

4.10 Aim 3

4.10.1 Hypothesis 1

There would be a positive relationship between the volume of the right cerebellum and the known white matter output pathways (cerebellar-rubral, rubral-thalamic, and thalamic-frontal white matter integrity), as well as the volume of structures that receive projected cerebellar output along the pathway (left red nucleus, left thalamus, and left frontal lobe). Furthermore, the volume of structures that receive projected cerebellar output would have positive relationships with the white matter integrity of connected pathways (e.g., left red nucleus volume would be related to rubral-thalamic white matter integrity).

4.10.2 Hypothesis 2

Similar to hypothesis 1, cerebellar atrophy would be negatively correlated white matter integrity in each segment (cerebellar-rubral, rubral-thalamic, and thalamic-frontal).

4.10.3 Hypothesis 3

Right cerebellar volume would mediate the relationship between cerebellar-frontal white matter integrity and working memory.

The goal of the third aim of the current study was to test a theory of structural neural connectivity using two measures of inferred brain structure (volume and white matter integrity). Theoretically, lesions can disrupt functional connections between the lesioned region and its distant functional connections (von Monakow, 1914), and atrophy may disrupt structural connections (e.g., myelin or axons) between the atrophied region and distant structural connections (Spanos et al., 2007). In support of these theories, cerebellar atrophy has been associated with lower volume in structural connections (Spanos et al., 2007). Furthermore, one prior study has found that volumetric measures and tractography measures of FA are positively correlated in the context of atrophy (Ezzati et al., 2015). Lastly, animal models provide evidence for demyelination following radiation-induced brain injury (Reinhold et al., 1990). Survivors in the current study had cerebellar lesions, cerebellar atrophy, and 52% were treated with radiation; thus, structural disconnection within the cerebellar-frontal pathway was likely. Specifically, cerebellar damage (lesion or atrophy) could have caused demyelination and axonal damage within the cerebellar-frontal pathway as well as cascading reductions in volume on structures along the pathway. For the following hypotheses, the relationships were expected to be different in the control group when compared to the survivors (e.g., controls do not have lesions or atrophy). Consequently, the survivor and control groups were analyzed separately.

4.11 Results of Hypothesis One

Hypothesis 1 focused on testing inferred neuroanatomical connectivity using Pearson correlations. The volume of the right cerebellar hemisphere was expected to be positively correlated with each segment of cerebellar-frontal white matter integrity (cerebellar-rubral, rubral-thalamic, and thalamic-frontal). This hypothesis was not supported. While none of the relationships reached statistical significance in the control group, descriptively, the correlations appeared to become less strong in the more distal segments of the cerebellar-frontal pathway (see Table 20). In the survivor group, cerebellar volume was only significantly associated with the most distal portion, namely the thalamic-frontal segment, of the cerebellar-frontal pathway (see Table 20). These correlations continued to be significant after correcting for treatment factors.

Table 200 Aim 3: Hypothesis 1 correlations between cerebellar volume and the diffusion metrics of the segments of the cerebellar-frontal white matter pathway

	Cerebellar-Rubral		Rubral-Thalamic		Thalamic-Frontal	
	FA	RD	FA	RD	FA	RD
Controls Cerebellar Volume	.35	-.18	-.22	.32	-.15	.04
Survivors Cerebellar Volume	.20	-.07	.01	-.15	.43*	-.49**
Survivors Cerebellar Volume (controlling for NPS)	.15	-.02	.02	-.04	.42*	-.41*
Survivors Cerebellar Volume (controlling for NPS and Age at diagnosis)	.27	-.03	.07	-.10	.47*	-.45*

Note. Reported values are Pearson correlation coefficients; *indicates $p<.05$ and **indicates $p<.01$; NPS= neurological predictor scale; FA= fractional anisotropy; RD= radial diffusivity.

4.12 Results of Hypothesis Two

For the next hypothesis, the volume of the right cerebellar hemisphere was expected to be positively correlated with the volume of regions of interest within the cerebellar-frontal pathway (left red nucleus, left thalamus, and left frontal lobe). Higher correlations were expected for pathways and structures that were closer to the cerebellum (e.g., Law et al., 2015a). Correlations were computed to test for possible cascading damage along the pathway between each of the following: cerebellar-rubral white matter integrity → left red nucleus volume, left red nucleus volume → rubral-thalamic white matter integrity, rubral-thalamic white matter integrity → left thalamus volume, thalamic-frontal white matter integrity → left frontal volume. The ROI volumes used are the same as those that were used for the diffusion tractography, except for the frontal lobe ROI. Since the MFG ROI was only modified to be smaller for deterministic tractography processing, the initial boundaries described in the methods section as the MFG defined the boundaries of the frontal lobe ROI for volumetric processing.

Results were inconsistent with the hypotheses and differed among control and survivor groups. In the control group, only the rubral-thalamic segment white matter integrity (RD only) of the cerebellar-frontal pathway was associated with the volume the red nucleus and the thalamus (see Table 21). For the survivor group, the thalamic-frontal segment (FA and RD) was associated with both thalamus volume and frontal lobe volume. These results are consistent with the study conducted by Law et al. (2015a) that found lower white matter integrity in the cerebellar- rubral and thalamic-cerebral segments.

Table 21 Correlations between volumetric measures and the diffusion metrics of the segments of the cerebellar-frontal pathway

	Cerebellar-Rubral		Rubral-Thalamic		Thalamic-Frontal	
	FA	RD	FA	RD	FA	RD
Controls						
Left Red Nucleus Volume	.12	.08	-.32	.47**		
Left Thalamus Volume			-.32	.48**	-.05	.06
Left Frontal Lobe Volume					-.02	.07
Survivors						
Left Red Nucleus Volume	.28	.03	.14	-.24		
Left Thalamus Volume			.19	-.29	.45*	-.44*
Left Frontal Lobe Volume					.44*	-.41*
Survivors (controlling for NPS)						
Left Red Nucleus Volume	.26	.04	.14	-.24		
Left Thalamus Volume			.20	-.26	.44*	-.42*
Left Frontal Lobe Volume					.43*	-.39*
Survivors (controlling for NPS and age at diagnosis)						
Left Red Nucleus Volume	.40*	.03	.20	-.31		
Left Thalamus Volume			.26	-.34	.49*	-.46*
Left Frontal Lobe Volume					.47*	-.43*

Note. Reported values are Pearson correlation coefficients; *indicates $p<.05$ and **indicates $p<.01$; NPS= neurological predictor scale; FA= fractional anisotropy; RD= radial diffusivity.

4.13 Results of Hypothesis Three

The cerebellar structure may be at high risk for atrophy and may be related to atrophy in other brain regions (e.g., Finnie et al., 2001; Rohkamm, 1977; Spanos et al., 2007). Cerebellar atrophy secondary to cerebellar brain tumor resection is hard to capture with volumetric measures because of the presence of tumor resection. Research based on a subset of this sample developed a measure of cerebellar atrophy independent of lesion size and found atrophy was correlated with processing speed

performance (Ailion et al., 2016). Therefore, some of the analyses proposed in hypothesis one were replicated with a measure of cerebellar atrophy for hypothesis two, and relationships were expected to be stronger. Only the survivor group was analyzed in this hypothesis because controls were not expected to have any cerebellar atrophy. Cerebellar atrophy was expected to be negatively correlated with each segment of cerebellar-frontal white matter integrity (cerebellar-rubral, rubral-thalamic, and thalamic-frontal). Pearson correlations revealed that the high correlation between the cerebellar-rubral RD and cerebellar atrophy, indicating that as cerebellar atrophy increased cerebellar-rubral white matter integrity decreased (see Table 22). While there was a general trend that the portions of the white matter pathway closest to the cerebellum demonstrated the highest correlations with cerebellar atrophy, the relationships among the other portions of the pathway did not reach statistical significance (e.g., rubral-thalamic; see Table 22).

Correlations were also computed for cerebellar lesion size and each portion of the cerebellar-frontal pathway. Similar to the findings from cerebellar volume (see Aim 3 Hypothesis 1, Table 20), correlations became stronger in the portions of the white matter pathway that were most distant to the cerebellum (e.g., thalamic-frontal; see Table 22); however, none of these results reached statistical significance.

Table 22 Correlations between cerebellar atrophy and lesion size and the diffusion metrics for segments of the cerebellar-frontal pathway

	Cerebellar-Rubral		Rubral-Thalamic		Thalamic-Frontal	
	FA	RD	FA	RD	FA	RD
Cerebellar Atrophy	-.32	.53**	.22	-.04	-.04	-.01
Cerebellar Lesion Size	-.08	.07	.06	-.12	.20	-.32
(controlling for NPS)						
Cerebellar Atrophy	-.30	.52**	.22	-.10	.06	-.08
Cerebellar Lesion Size	-.10	.09	.06	-.09	.19	-.30
(controlling for NPS + Age at Diagnosis)						
Cerebellar Atrophy	-.31	.52**	.24	-.12	.07	-.09
Cerebellar Lesion Size	-.17	.10	.03	-.05	.17	-.28

Note. *indicates $p<.05$ and **indicates $p<.01$; pearson r values are reported; NPS= neurological predictor scale; FA= fractional anisotropy; RD= radial diffusivity.

The rationale for hypothesis 3 was based on the same theories for the prior hypotheses but added the cognitive component of auditory attention span. While the prior aims were able to establish that cerebellar-frontal white matter integrity correlated with auditory attention span, they were unable to establish a correlation between the right cerebellar volume and complete cerebellar-frontal pathway. Therefore, the necessary relationship between cerebellar volume and the cerebellar-frontal pathway for the proposed mediation model did not exist in the sample.

4.14 Statistical Correction

Similar to Aims 1-2, the Benjamini-Hochberg statistical correction for family-wise error was be used with the recommended 5% false positive rate. A total of 100 analyses were computed for the third aim, and all reported results survived statistical correction for multiple comparisons. See statistical correction section under Aim 1 for the Benjamini-Hochberg statistical correction formula.

4.15 Aim 4

4.15.1 Hypothesis 1

Right parietal lobe volume would mediate the relationship between right SLF II white matter integrity and visual attention.

4.15.2 Hypothesis 2

Cerebellar volume would not mediate the relationship between right SLF II white matter integrity and working memory.

4.15.3 Hypothesis 3

Right parietal lobe volume would not mediate the relationship between cerebellar-frontal white matter integrity and visual attention.

The goal of aim four was to test a double dissociation between the cerebellar-frontal network (Aim 3, Hypothesis 3) and the right SLF II network with both working memory and visual attention performance. Similar to the findings reported in Aim 3: Hypothesis 3 (no relationship between cerebellar-frontal white matter integrity and cerebellar volume), there was not a statistically significant association between the SLF II white matter integrity and right parietal lobe volume (see Table 23). Fisher's r-to-z transformation was computed to see if relationships between white matter pathways

and volumes (cerebellar and parietal lobes) were significantly higher for the hypothesized relationships, and none of the expected relationships were found (Controls: cerebellar-frontal: FA z=.52 RD z=-.94; SLF II: FA z=.34 RD z=-1.76; Survivors: cerebellar-frontal: FA z=-.33 RD z=.46; SLF II: FA z=.43, RD z=-.58, all p's>.05). For Hypotheses 2 and 3, simple regressions were planned to confirm the specificity of the mediation relationships in Aim 3: Hypothesis 4 and Aim 4: Hypothesis 1. Since the mediations could not be tested, these analyses were no longer warranted.

Table 233 Aim 4: Hypothesis 1 correlations between SLF II and parietal lobe volume

	Parietal lobe volume
Survivors only (n=29)	
SLF II FA	τb=.25
SLF II RD	τb=-.18
Controls only (n=29)	
SLF II FA	τb=-.04
SLF II RD	τb=.05

Note. *indicates *p*<.05 and **indicates *p*<.01; NPS= Neurological Predictor Scale; τb= Kendall's Tau; FA= fractional anisotropy; RD= radial diffusivity; SLF= superior longitudinal fasciculus;

4.16 Post-hoc analyses

To further investigate the findings reported in Aim 3, the survivor group was split into radiation and no radiation groups. In the no radiation group, the volume of each structure along the pathway was associated with the cerebellar-rubral segment. High correlations were also observed in the thalamic-frontal segment. However, these correlations did not reach significance due to small sample size (see Table 24). In the

radiation group, significant correlations were found between each structure and the thalamic-frontal segment of the pathway.

Differences in the radiation and no radiation group are likely due to the type of brain injury associated with each treatment. In the no radiation group, the primary mechanism of injury is the cerebellar tumor growth and resection. Therefore the most proximal connection to that injury (cerebellar-rubral pathway) explained reductions in volume along the pathway. Whereas, the radiation group had a multifactorial brain injury from brain surgery and cranial radiation treatment. Cranial radiation treatment is theorized to have the greatest impact on the latest myelinating pathway (thalamic-frontal pathway). Therefore, the initial injury to the thalamic-frontal white matter and failure to attain normal white matter growth in this white matter segment explained reductions in volume along the pathway. Arguably, the radiation and no radiation groups initially had a similar degree and pattern of damage. However, subsequent radiation-induced demyelination of the thalamic-frontal portion of the pathway appears to demonstrate a stronger relationship with volume loss in the cerebellum, red nucleus, thalamus, and frontal lobe.

To further investigate this theory, a correlation was run between cerebellar-frontal white matter integrity and age at diagnosis in the radiation and no radiation groups. In the radiation group, age at diagnosis was strongly associated with cerebellar-frontal white matter integrity (FA $r=.52$, $p<.05$; RD $r=-.50$, $p=.06$). In contrast, a significant relationship was not found in the no radiation group (FA $r=.40$, $p=.16$; RD $r=.06$, $p=.85$).

Table 24 Radiation subgroup comparisons for the cerebellar-frontal pathway

	Cerebellar-Frontal		Cerebellar-Rubral		Rubral-Thalamic		Thalamic-Frontal	
	FA	RD	FA	RD	FA	RD	FA	RD
No Radiation (n=14)								
Right Cerebellum Volume	.58*	-.28	.59*	-.15	-.26	-.26	.28	-.44
Left Red Nucleus Volume	.72**	-.13	.64*	-.04	-.07	-.28	.41	-.45
Left Thalamus Volume	.66**	-.26	.50	-.21	.07	-.36	.35	-.31
Left Frontal Lobe Volume	.65*	-.18	.56*	-.11	-.07	-.33	.38	-.45
Radiation (n=15)								
Right Cerebellum Volume	.20	-.06	-.20	.00	.26	-.02	.60*	-.46
Left Red Nucleus Volume	.28	-.13	-.13	.11	.33	-.26	.58*	-.58*
Left Thalamus Volume	.30	-.17	-.07	.08	.33	-.30	.55*	-.55*
Left Frontal Lobe Volume	.29	-.14	-.08	.08	.29	-.24	.50	-.44

Note. *indicates $p<.05$ and **indicates $p<.01$; reported values are Pearson correlation coefficients; FA= fractional anisotropy; RD= radial diffusivity; Radiation therapy was coded as dichotomous variables in which 0= not present and 1= present

To investigate whether the primary finding of the double dissociation was due to motor weaknesses in the survivor group partial correlations were computed. The relationship between cerebellar-frontal white matter integrity and auditory attention span remained significant after controlling for dominant hand performance on the Grooved Pegboard (FA: r=-.63, p<.01; RD: r=.38, p<.05).

5 DISCUSSION

The white matter pathway connecting the cerebellum and the frontal lobe is commonly studied in the childhood brain tumor population (Ailion et al., 2017). The current study advances the existing literature on this pathway in a variety of ways. First, the results of Aim 1 provide theory-driven evidence about the specific neurocognitive performance that is associated with cerebellar-frontal white matter integrity. Second, the results of Aim 2 provide specificity for Aim 1 with differential associations for key brain-behavior relationships. Third, the results of Aim 3 elucidate the structural connectivity within the cerebellar-frontal pathway using diffusion-weighted and voxel-based measures of brain structure.

First, with regard to neurocognitive performance, the sample exhibited a pattern that is consistent with the current literature. Such that, survivors with high grade tumors and correspondingly more complex treatment and complications exhibited the highest proportion of individuals with impairment across neurocognitive measures. Survivors with low grade tumors were largely performing within normal limits, with only two participants in the impaired range on oral processing speed and none on the composite processing speed score. Survivors treated for high grade tumors had significantly more impaired processing speed (OSDMT) relative to controls as well as survivors treated for

low grade tumors. Survivors treated for high grade tumors had significantly more impaired auditory attention span and working memory when compared to controls, and these relationships were trending towards significance when compared to survivors treated for low grade tumors.

The results of Aim 1 identified a significant association between auditory attention span and cerebellar-frontal white matter integrity (FA and RD). The relationship between cerebellar-frontal white matter and auditory attention span was a statistically stronger association when compared working memory. These findings challenged the current body of literature that suggested that the cerebellar-frontal white matter connections should be related to working memory. However, methodological limitations may have obscured this finding in prior studies. Specifically, previous studies that reported that cerebellar-frontal white matter integrity is related to working memory used Digit Span Forward and Backward as a combined score (Law et al., 2001; Law et al., 2015). Of note, in the current sample, the results did replicate the relationship between Digit Span total score and the cerebellar-frontal pathway, but also highlight the importance of auditory attention span and showed no relationship with Digit Span Backward (see Table 15).

A combined digit span measure is problematic because these two subtests are theoretically and empirically distinct in neurological populations. Digit Span Forward assesses attention span and corresponds to Baddeley's Phonological Loop, whereas Digit Span Backward assesses mental manipulation and corresponds to Baddeley's Central Executive (Baddeley, 1996; Gerton et al., 2004; Hebben and Milberg, 2009; Mapou and Spector, 1995; Monaco et al., 2013; Strauss et al., 2006). These constructs

overlap in the domain of working memory, and Digit Span Forward and Backward are highly correlated in the healthy normative sample; therefore, during test development, Digit Span Forward and Backward were combined to create the digit span index for a more normal-shaped data distribution (Lezak et al., 2012). However, Digit Span Forward and Backward are often distinct constructs that are not correlated in clinical populations (Black and Strub, 1978; Kiefer et al., 2002). For neurological populations, combined index scores can result in a poor specificity of neurocognitive processes (Dennis et al. 2009) and biased psychometric distributions (Lezak et al., 2012). In fact, combining Digit Span Forward and Backward in neurological populations has been explicitly cited as inappropriate because it obscures the ability to measure important and distinct neuropsychological functions (Lezak et al., 2012; Weinberg et al., 1972).

The current study found that Digit Span Forward, but not Digit Span Backward or ACT 36 Second Trial, is associated with cerebellar-frontal white matter integrity (see Table 15). This relationship is consistent with the theory that the cerebellum's role in working memory is error driven adjustment of information from the phonological store and the articulatory control system (Desmond et al., 1997; see Figure 17). The cerebellar-frontal network has been implicated in the phonological loop, articulatory rehearsal, and mental subvocalization- all of which are required for auditory attention span (Ben-Yehudah et al., 2007; Desmond et al., 1997). The Digit Span Forward task relies on the phonological store and mental subvocalization systems (Gerton et al., 2004). Whereas, Digit Span Backward builds on the task demands of the Digit Span Forward and adds the component of manipulation, which is consistent with Baddeley's (1996) notion of the Central Executive (Gerton et al., 2004).

Correspondingly, the cerebellar-frontal network is activated during encoding and maintenance of verbal information (Chen and Desmond, 2005a). Therefore, the specificity in the relationship between cerebellar-frontal white matter integrity and auditory attention span demonstrated in Aim 1 is consistent with the Desmond et al.'s (1997) theoretical model and prior network activation studies (Chen and Desmond, 2005a).

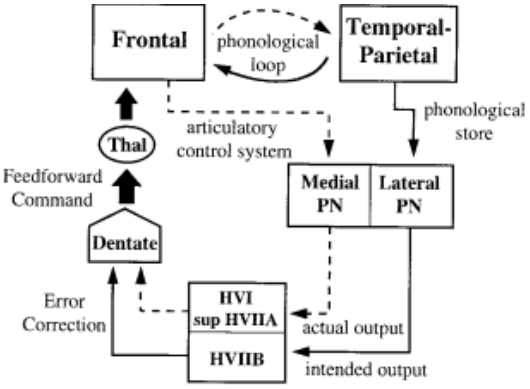

Figure 9. Model of cerebrocerebellar circuit proposed to be involved in verbal working memory. In addition to the phonological loop between frontal lobe structures (such as Broca's area, comprising the articulatory control system and represented by a *dashed line*) and temporal-parietal structures (such as the supramarginal gyrus, comprising the phonological store and represented by a *solid line*), a parallel path from these structures enters the cerebellar cortex via the pontine nuclei. Discrepancies between the actual and intended phonological output are computed and used to update a feedforward articulatory rehearsal command to the frontal cortex via dentatothalamic projections. *PN*, Pontine nuclei; *Thal*, thalamus.

Figure 17 Model of cerebellar-frontal pathway involvement in working memory (Desmond et al., 1997; reprinted with permission)

The association with auditory attention span, but not working memory on the surface seems counterintuitive. Auditory attention span is often considered a prerequisite for working memory and has been theorized to be upstream in the developmental cascade contributing to deficits in working memory (Palmer, 2008). However, there is literature to suggest that the digits backward task employs visuospatial processes to re-sequence the digits in reverse order (Costa, 1975;

Larrabee & Kane, 1986; Mapou and Spector, 1995; Weinberg et al., 1972). Therefore, these findings could be explained by the high verbal demands of the digit forward task, and relatively preserved visuospatial processes that serve as a compensatory mechanism for digits backward performance.

Importantly, both cerebellar-frontal white matter integrity (FA and RD) and whole brain white matter volume were related to auditory attention span. Whole brain volume metrics are problematic because they average all the reductions in white matter volume that may not be equally distributed throughout the brain. In cerebellar brain tumor survivors, lesions and atrophy in posterior fossa regions contribute to a reduction in whole brain volume. Correspondingly, survivor cerebellar-frontal FA demonstrated a moderate correlation with whole brain white matter volume (r=.31), whereas SLF II FA was not correlated with whole brain white matter volume (r=.05). Therefore, white matter volume reductions that were captured in the whole brain white matter volume metric may be concentrated in the posterior fossa and subcortical regions. Given the high correlation between cerebellar-frontal white matter integrity and whole brain white matter volume—the association between whole brain white matter volume and Digit Span Forward, alone, does not suggest that these results are due to diffuse white matter damage.

The current study found that survivors have significantly lower whole brain grey matter volume when compared to controls, which is inconsistent with the reviewed literature that posited grey matter resiliencies. However, the research on relative grey matter volume resiliencies was based on brain tumor survivors who were on average 5 years post diagnosis (Riggs et al., 2014). Longer-term follow-up studies have found

differences in grey matter (Ailion et al., 2016) and whole brain volume (Jayakar et al., 2015). Therefore, white matter may be more vulnerable to the immediate effects of cranial radiation, and reductions in grey matter may emerge with a longer time post diagnosis.

Aim 2 confirmed the specificity of the relationship between cerebellar-frontal white matter integrity and auditory attention span in the survivor group. Fisher's Z confirmed that the association between cerebellar-frontal FA and auditory attention span was stronger than the correlation coefficient for cerebellar-frontal FA and visual attention. The data support a correlational double dissociation between cerebellar-frontal white matter integrity (correlated with auditory attention span) and SLF II white matter integrity (correlated with visual attention). Cerebellar-frontal white matter integrity was not correlated with visual attention performance, and SLF II white matter integrity was not associated with auditory attention span. Together, these results also provide evidence against diffuse white matter damage. If whole brain white matter volume reductions explained auditory attention span (as the correlation between whole-brain white matter and Digit Span Forward suggests), then the right SLF II also should be correlated with auditory attention span. In sum, the results from Aim 2 provide a compelling argument for the brain-behavior specificity of visual and auditory attention span with two distinct brain networks and against diffuse brain disruptions.

Relationships among measures of structural connectivity were much more limited than initially hypothesized. First, only the thalamic-frontal segment of the cerebellar-frontal pathway was associated with the volumetric measures of each structure in the survivor group (see Figure 18 and Table 21). Second, cerebellar atrophy was only

associated with the cerebellar-rubral segment of the cerebellar-frontal pathway (the most proximal segment). This pattern of results suggested that the mechanisms of structural disconnection were more nuanced than initially hypothesized.

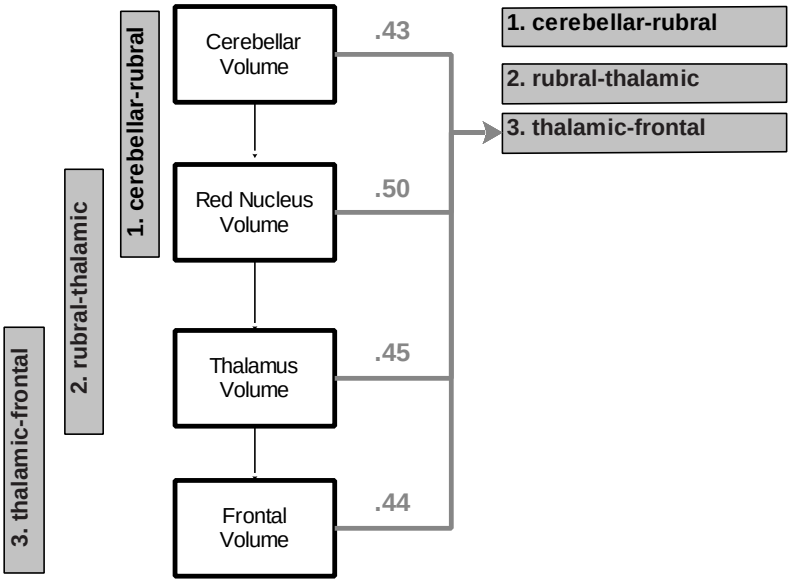

Figure 18 Correlations between volume and diffusion metrics for the survivor group

Note. Values are Pearson correlation coefficients without any control variables between volume (white + grey matter divided by intracranial vault) and white matter integrity (thalamic-frontal fractional anisotropy). White boxes denote volumes, and grey boxes denote white matter integrity.

The disruption of the cerebellar-frontal connections is likely due to multifactorial injury. Moderate correlations were observed between the NPS and both cerebellar volume and cerebellar-frontal RD. Given the proximity to the cerebellum, it is possible that the etiology of cerebellar atrophy extends to the cerebellar-rubral pathway. Alternatively, cerebellar atrophy may reduce cerebellar output, and cause demyelination within the cerebellar-rubral segment. Evidence from the human and animal literature that suggests a combination of these explanations. The initial injury from tumor growth, surgery, and treatment cause demyelination followed by a negative feedback loop in

which the cells, blood vessels, and myelin continue to degenerate over time (Glass et al., 2017; Reddick et al., 2005; Reinhold et al., 1990).

The relationship between volumetric measures and only the thalamic-frontal segment is likely related to differential developmental trajectories of myelination within the cerebellar-frontal pathway. Consistent with this finding, cerebellar-frontal FA correlated with age at diagnosis (see Table 13), particularly for survivors treated with cranial radiation (see page 116). Research suggests that the cerebellum, pons, and cerebellar peduncles exhibit developmentally early myelination, and are present at birth; whereas, the subcortical and frontal regions continue to myelinate into early adulthood (Gao et al., 2009; Hermonye et al., 2009; Kochunov et al., 2012; Paus et al., 2001; Westlye et al., 2010). Similar to Aim 1, the correlations between the volume and white matter integrity in the thalamic-frontal segment are likely related to initial injury, structural disconnection beginning with atrophy in the cerebellum, and a failure to develop normal white matter gains in developmentally sensitive regions (Glass et al., 2017; Reddick et al., 2005; Reinhold et al., 1990).

6 LIMITATIONS

While the current study sought to provide evidence for brain-behavior relationships, the brain regions of interest are part of dynamically interrelated networks; therefore, the results may have been influenced by larger network-related neural abnormalities associated with tumor development and treatment. The current study addressed this limitation by including double dissociation hypotheses with a comparison brain-behavior relationship as well as investigating a measure of whole brain white matter volume and grey matter volume. In addition to a double dissociation and whole

brain volume measures, the current study included a comparison group with no history of neurological injury. While no causal conclusions can be drawn, the synthesis of findings from a double dissociation, comparison whole brain metrics, and a healthy comparison group collectively provided strong support for brain-behavior specificity.

While a double dissociation was found in the survivor group, the expected relationships were not found in the control group. Although there is a similar amount of variation between each group (SD), the control group variation was all within normal limits of performance without any impairments. The lack of a double dissociation in the control group was likely because differences in brain metrics (volume and white matter integrity) and neuropsychological measures are less meaningful in healthy individuals because there is no disease process to explain the statistical variance in either variable. The double dissociation in the survivor group alone suggests that these two brain networks appear necessary for their associated behaviors, meaning that when a disease or treatment process damages the brain networks, there are reductions in corresponding performance measures.

The control region that was selected for the double dissociation had two noteworthy limitations. First, the right SLF II does not connect to subcortical brain regions, which makes it structurally distinct from the cerebellar-frontal pathway. While this structural distinction may be advantageous to identify a double dissociation, a comparison pathway that has structural differences could result in findings that are explained by differences in cortical versus subcortical brain regions. The right SLF II was chosen in light of this limitation because it has a number of other similar structural features to the cerebellar-frontal pathway, such as being a long-range reciprocal

pathway that underlies a component of executive functioning (e.g., visual attention). Additionally, the right SLF II connects to the right frontal lobe (middle frontal gyrus), which was the contralateral equivalent to the frontal ROI that was included in the cerebellar-frontal pathway.

The second limitation was the measure of visual attention. While a robust literature supports the association between the right SLF II and visual attention, other literature suggests that the right SLF II was associated with spatial working memory (Preuss and Goldman-Rakic, 1989; Petrides and Pandya, 2002). Given that the current study initially sought to investigate working memory, a double dissociation of verbal and spatial working memory may have been methodologically superior to the current performance measures. However, the existing data set did not include a measure of spatial working memory, and the primary pathway of interest was associated with auditory attention span and not verbal working memory. In addition, the two available measures of visual attention (cancellation time and cancellation number of errors) were robustly associated with the right SLF II were well suited for the double dissociation with verbal attention span.

An inevitable limitation of research on brain tumor survivors was exclusion based upon poor quality imaging data or inability to obtain an MRI scan due to medical implants. While the current study has a large number of participants for this patient population, a larger sample size would allow for more variables that could be statistically modeled. Although it would be desirable to perform the current study with a larger sample, it is challenging to follow brain tumor survivors on average 13 years post

diagnosis due to difficulty tracking patients over time and across the transition to adulthood.

Brain tumor populations also are difficult to study due to differences in the speed of tumor growth, the age of tumor identification, pathology, and location of the tumor within the posterior fossa. Therefore, heterogeneity among tumor and treatment factors could have contributed to the results. The current study statistically accounted for the influence of treatment factors and analyzed treatment groups separately when appropriate to ensure that tumor and treatment factors do not better explain the results.

The results discussed include white matter measures of FA and RD. However, some results were inconsistent across measures of FA and RD. Cerebellar-rubral RD had a higher correlation to cerebellar atrophy when compared to FA. Furthermore, larger group differences (i.e., high grade, low grade, controls) were present using RD when compared to FA across both white matter pathways. Prior literature suggests that RD is sensitive to demyelination (Song et al., 2005; Bartzokis et al., 2012), so it is possible that these findings reflect a demyelinating process. In the survivor double dissociation, SLF II FA but not SLF II RD was associated with visual attention. The correlation coefficient between SLF II RD and visual attention was in the direction consistent with the hypotheses, although it was weaker than FA and not statistically significant. The RD metric was selected for the current study because of its sensitivity to myelin content in late-myelinating regions; however, RD has demonstrated less sensitivity earlier-myelinating regions in the posterior brain (Bartzokis et al., 2012). Therefore, the discrepancy between SLF II FA and RD is consistent with the literature

that suggests that RD would not be sensitive to white matter changes in early-myelinating posterior brain regions.

Both FA and RD have noteworthy limitations. FA is considered less sensitive and more challenging to interpret because it combines different measurements of brain biology. Whereas, RD is more vulnerable to measurement error related to crossing fibers (Bartzokis et al., 2012). One explanation could be that the RD metric is measuring demyelination associated with the initial injury and continued structural disconnection in the cerebellar-frontal pathway, whereas FA is providing a measure of more general brain disruption that includes axon degeneration.

7 STRENGTHS

This study was among the first to attempt to find a double dissociation of brain-behavior relationships in a childhood brain tumor population. Neurocognitive difficulties in brain tumor populations have been attributed to both focal and diffuse disruptions in brain volume and white matter integrity (Ailion et al., 2017). While focal and diffuse brain differences are well documented, brain-behavior double dissociation studies are absent. The lack of research on double dissociations is likely related to the controversy about whether brain tumor survivors exhibit neurocognitive difficulties as a result of diffuse brain damage. However, brain-behavior double dissociations provide evidence for specificity, particularly in the context of brain disease. Without comparison brain regions and behaviors, prior literature remains obscured by the possible contribution of diffuse neurological injury. The current study investigated the cerebellar-frontal white matter pathway and corresponding neurocognitive measures with a control brain-behavior relationship to account for diffuse neurological injury and found evidence for a brain-

behavior double dissociation. Therefore, neurocognitive performance can be localized to specific and theoretically supported white matter pathways, and the idea that neurocognitive difficulties are due to diffuse neurological injury in this population is overly simplistic.

The current study is the only known study to date to simultaneously investigate the multi-synaptic cerebellar-frontal pathway and the volume of the brain structures along the pathway. The current study found that in the no radiation group the cerebellar-rubral segment correlated with cerebellar, red nucleus, thalamus, and frontal volumes; whereas, in the radiation treatment group the thalamic-frontal segment correlated with the aforementioned volumes. These results are theoretically meaningful because the no radiation group shows a pattern that may reflect a structural equivalent of functional diaschisis (von Monakow, 1914); whereas, the radiation group shows a pattern that may reflect a neurodevelopmental vulnerability to radiation-induced demyelination (Palmer et al., 2002; Qiu et al., 2007; Reddick et al., 2000; Reddick et al., 2005; Reinhold et al., 1990; Stevens et al., 2009). These findings would have been impossible to detect without combining imaging techniques (Tractography and VBM) and segmenting the larger white matter pathway into multi-synaptic pieces. The results also further highlight that more research is needed into the mechanisms underlying distinct brain behavior relationships. The results of the current study provide a strong justification for investigating with greater theoretical and performance based specificity and complementary multimodal neuroimaging methods in general, and specifically with complex neurological populations.

The current study is among the first to segment the cerebellar-frontal pathway at synapse points. A large number of prior studies on this population have investigated the cerebellar-frontal pathway without segmenting the pathway at synapse points (Law et al., 2011; 2012; Rueckriegel et al., 2015; Soelva et al., 2013). Only two prior studies in this population have differentiated the cerebellar-frontal pathway into multi-synaptic segments (Law et al., 2015a; 2015b), and only one of those studies included neurocognitive measures (Law et al., 2015b). Law et al. (2015b) looked at medulloblastoma survivors on average 6.28 years post diagnosis. Therefore, the current study is the first to segment the cerebellar-frontal pathway in long-term survivors (M=13 years post diagnosis) with a sample that includes both low and high grade tumors.

Results of the current study increase the specificity of the prior literature that has suggested that the cerebellar-frontal pathway is associated with verbal working memory (i.e., Digit Span total, Law et al., 2011; Law et al., 2015b; Rueckriegel et al., 2015). The convergence of a number of guiding theoretical models and frameworks provided a rationale to increase the specificity of neurocognitive measurement of these constructs. A theoretical, instead of exploratory approach, allows the results to have conceptually meaningful significance. For instance, the results of the current study provide empirical support for the theory the cerebellum and its frontal white matter connections are implicated in the phonological loop, and more specifically correlated with auditory attention span (i.e., Digit Span Forward). Furthermore, these results increase the specificity of the current knowledge base and suggest that specific white matter pathways correlate with different modalities (i.e. auditory vs. visual) of attentional performance.

The results of the current study are critical to advancing the understanding of structural brain changes following brain tumor treatment. These results are clinically useful for neuropsychologists educating families of posterior fossa tumor survivors about the relationships among affected brain regions, affected pathways, and associated neurocognitive outcomes. These results are of particular relevance because researchers have begun to apply region based volume measures to the clinical interpretation of brain MRIs (e.g., Bigler, 2016), therefore it is increasingly critical to understand how measures of regional volume relate to other complementary neurobiological markers (e.g., white matter integrity), as well as cognition.

7.1 Future Directions

The current study sought to be the first to reconstruct the complete cerebellar-frontal pathway based on each of the four distinct segments (cerebellar-rubral, cerebellar-thalamic, rubral-thalamic, and thalamic-frontal) based on the animal literature. However, the cerebellar-thalamic segment of the cerebellar-frontal pathway could not be identified in the current dataset. In the healthy adult literature, two studies have reported that they were able to visually identify the cerebellar-thalamic segment using probabilistic tractography with different scanner parameters, but segmentation was not possible (Habas and Cabanis, 2007; Jissendi, Baudry, and Balriaux, 2007; see Table 25). Law et al. (2015a) did not attempt to segment or visualize the cerebellar-thalamic segment. The current study attempted to both visualize and segment and was unable reliably find fibers that represented the cerebellar-thalamic segment of the cerebellar-frontal pathway. Therefore, consistent with prior studies no study to date has been able to successfully segment the cerebellar-thalamic portion of the pathway

(Habas and Cabanis, 2007; Jissendi, Baudry, and Balriaux, 2007; Law et al., 2015a). The inability to segment the cerebellar-thalamic fibers is likely related to insufficient imaging acquisition parameters. These fibers, which are located near the brain stem, are also susceptible to pulse and respiratory artifact. More sophisticated imaging methods would provide more accurate imaging of these complex fiber, and better correction for regional artifacts (Jiang et al., 2002). Future studies on the cerebellar-frontal pathway should investigate this pathway with acquisition parameters that would allow for more accurate imaging of the cerebellar-frontal pathway and more precise reconstruction techniques, such as Diffusion Kurtosis Imaging. Further, caution should be used when using the current parameters or less powerful imaging acquisition and reconstruction techniques because they are unable to distinguish similar pathways.

Table 25 Imaging acquisition parameters for studies on the cerebellar-frontal pathway

	Magnet	Head Coil	TE	TR	Slice thickness	Directions	Method
Habas and Cabanis (2007)	3T Signa	8-channel	76.1	9000	3 mm	55	Probabilistic
Jissendi, Baudry, and Balriaux (2007)	3T Philips	8- channel	77	10,200	2 mm	32	Probabilistic
Law et al. (2015a)	1.5T GE	8-channel	4.2	10.056	1.5 mm	25-31	Probabilistic
	3T Siemens	12-channel	3.91	2300	1 mm	30	
Current study	3T Siemens	12-channel	90	7700	2 mm	30	Deterministic

Note. TE= Echo Time; TR=Repetition Time; T= Tesla; Law et al. (2015a) combined two scanner parameters into one study

The current study used single shell diffusion weighted volumes and angular reconstruction for deterministic tractography, which was limited due to *a priori* assumptions about the radial profile of local diffusivity. Diffusion Kurtosis Imaging (DKI) is a DWI method used to estimate kurtosis, which helps address problems associated with crossing fibers, but similarly requires *a priori* assumptions about the angular diffusion profile (Assemlal et al., 2011; Jensen et al., 2005). DKI adds a quadratic dimension to allow a more accurate fit of the tensors and is more sensitive approach when compared to linear DWI (Cheung et al., 2009). However, DKI assumes isotropy along the principal eigenvector and modeling DKI with acceptable precision requires a multi-shell acquisition (e.g., 2+ nonzero b-values; Jensen and Helpern, 2010). For the current study, single shell DWI was acquired with a b-value of 1000s/mm^2. Therefore, the imaging acquisition for the current study was not sufficient to model DKI. Instead, the current study employed a high angular reconstruction method (HARDI) based on a MOW model, which also addressed concerns related to crossing fibers (Jian et al., 2007; Jian and Vermuri, 2007a; Jian and Vermuri, 2007b). Future studies should collect data using a multi-shell acquisition method that would allow for increased sensitivity and specificity of the fiber reconstruction for diffusion tractography.

The scope of the current study did not permit the analysis of functional imaging, although it was collected. Structural and functional neuroimaging methods answer distinct questions about the brain. In the context of the damaged brain, structural neuroimaging findings infer if a brain region is necessary for a cognitive skill; whereas, functional neuroimaging findings infer if a brain region is involved in a cognitive skill (Price et al., 1999; Rorden, Karnath, and Bonilha, 2007). Despite its importance,

functional imaging was not included because the current study focuses on strengthening and expanding the understanding of the relationship between the structural brain measures (e.g., white matter integrity and volume) and cognitive skills. Nonetheless, functional imaging that corresponds with these pathways and cognitive skills (e.g., functional connectivity) will be an important future direction of this research.

REFERENCES

Abhinav, Kumar, et al. (2014). Advanced diffusion MRI fiber tracking in neurosurgical and neurodegenerative disorders and neuroanatomical studies: A review. *Biochimica et Biophysica Acta (BBA)-Molecular Basis of Disease*, *1842.11*, 2286-2297.

Ailion, A. S., Hortman, K., King, T.Z. (2017). Childhood Brain Tumors: a Systematic Review of the Structural Neuroimaging Literature. *Neuropsychology Review. [E-pub before print],* 1-25.

Ailion, A. S., King, T. Z., Wang, L., Fox, M. E., Mao, H., Morris, R. M., & Crosson, B. (2016). Cerebellar Atrophy in Adult Survivors of Childhood Cerebellar Tumor. J *Int Neuropsychol Soc*, 1-11. doi: 10.1017/s1355617716000138

Alexander, G. E., DeLong, M. R., & Strick, P. L. (1986). Parallel organization of functionally segregated circuits linking basal ganglia and cortex. *Annu Rev Neurosci, 9*, 357-381. doi:10.1146/annurev.ne.09.030186.002041

Andersen, B. B., Korbo, L., & Pakkenberg, B. (1992). A quantitative study of the human cerebellum with unbiased stereological techniques. *J Comp Neurol, 326*(4), 549-560. doi:10.1002/cne.903260405

Andersen, S.M., Rapcsak, S.Z., Beeson, P.M. (2010). Cost function masking during normalization of brains with focal lesions: still a necessity? *Neuroimage 53*, 78 – 84.

Ashburner, J. and Friston, KJ. (2005). Unified segmentation. *Neuroimage, 26*(3), 839-51.

Aukema, E. J., Caan, M. W., Oudhuis, N., Majoie, C. B., Vos, F. M., Reneman, L., . . . Schouten-van Meeteren, A. Y. (2009). White matter fractional anisotropy correlates with speed of processing and motor speed in young childhood cancer survivors. *International journal of radiation oncology, biology, physics, 74*(3), 837-843. doi: 10.1016/j.ijrobp.2008.08.060

Baddeley, A. (1996). The fractionation of working memory. *Proceedings of the National Academy of Sciences, 93*(24), 13468-13472. Retrieved from http://www.pnas.org/content/93/24/13468.abstract

Barbey, A.K., Colom, R., Solomon, J., Krueger, F., Forbes, C., Grafman, J. (2012). An integrative architecture for general intelligence and executive function revealed by lesion mapping. *Brain*, *135*, 1154–1164.

Barrett, P. (2007). Structural equation modelling: Adjudging model fit. *Personality and Individual Differences*, *42*(5), 815-824.

Bartko, J. J. (1966). The intraclass correlation coefficient as a measure of reliability. *Psychological reports, 19*(1), 3-11.

Bartzokis, G., Lu, P. H., Heydari, P., Couvrette, A., Lee, G. J., Kalashyan, G., . . . Altshuler, L. L. (2012). Multimodal magnetic resonance imaging assessment of white matter aging trajectories over the lifespan of healthy individuals. *Biol Psychiatry, 72*(12), 1026-1034. doi:10.1016/j.biopsych.2012.07.010

Beaulieu, C. (2002). The basis of anisotropic water diffusion in the nervous system – a technical review. *NMR in Biomedicine, 15,* 435-455.

Benjamini, Y., & Hochberg, Y. (1995). Controlling the false discovery rate: A practical and powerful approach to multiple testing. *Journal of the Royal Statistical Society, 57*(1), 289–300. doi:10.2307/2346101

Bennett, C. M., Wolford, G. L., & Miller, M. B. (2009). The principled control of false positives in neuroimaging. *Social Cognitive and Affective Neuroscience, 4,* 417–422. doi:10.1093/scan/nsp053

Ben-Yehudah, G., Guediche, S., and Fiez, J.E. (2007). Cerebellar contributions to verbal working memory: beyond cognitive theory. *The Cerebellum, 6,* 193-201.

Bigler, E.D. (2016, February). *Clinical Application of Individualized Quantitative Neuroimaging for Neuropsychology – Precision Medicine Meets Neurocognitive Assessment.* Oral presentation at the annual meeting of the International Neuropsychological Society, Boston, MA.

Bisley, J.W. and Goldberg, M.E. (2003). Neuronal activity in the lateral intraparietal area and spatial attention. *Science 299,* 81-86.

Black, F. W., & Strub, R. L. (1978). Digit repetition performance in patients with focal brain damage. *Cortex, 14*(1), 12-21.

Blumenfeld, H. (2010). *Neuroanatomy Through Clinical Cases*, 2nd edition, Sinauer Associates, Inc., ISBN 978-0-87893

Bohsali, A., Triplett, W., Sudhyadhom, A., Gullett, J. M., McGregor, K., FitzGerald, D. B., … Crosson, B. (2015). Broca's area - Thalamic connectivity. *Brain and Language, 141C*, 80–88. doi:10.1016/j.bandl.2014.12.001

Bower, J.M. (1997). Control of sensory data acquisition. *Int Rev Neurobiol. 41*, 489-513.

Brett, M., Leff, A. P., Rorden, C., & Ashburner, J. (2001). Spatial normalization of brain images with focal lesions using cost function masking. *NeuroImage*, *14*(2), 486-500. doi: 10.1006/nimg.2001.0845

Brinkman, T. M., Reddick, W. E., Luxton, J., Glass, J. O., Sabin, N. D., Srivastava, D. K., . . . Krull, K. R. (2012). Cerebral white matter integrity and executive function in adult survivors of childhood medulloblastoma. *Neuro-oncology, 14 Suppl 4*, iv25-36. doi: 10.1093/neuonc/nos214

Brodmann K. Vergleichende lokalisationslehre der großhirnrinde: In ihren prinzipien. Leipzig, Germany: Barth, 1909.

Brown, J. (1958). Some tests of the decay theory of immediate memory. *Quarterly Journal of Experimental Psychology, 10*(1), 12–21. doi:10.1080/17470215808416249.

Bruininks, R.H., Woodcock, R.W., Weatherman, R.F., and Hill, B.S. (1996). S*cales of Independent Behavior-Revised (SIB-R)*. Itasca, IL: Riverside Publishing Company.

Brunoni, A.R., Vanderhasselt, M.A. (2014). Working memory improvement with non-invasive brain stimulation of the dorsolateral prefrontalcortex: a systematic review and meta-analysis. *Brain Cogn, 86*, 1-9.

Bunce, D., & Macready, A. (2005). Processing speed, executive function, and age differences in remembering and knowing. *Q J Exp Psychol A, 58*(1), 155-168. doi:10.1080/02724980443000197

Carpenter, M. B., & Stevens, G. H. (1957). Structural and functional relationships between the deep cerebellar nuclei and the brachium conjunctivum in the rhesus monkey. *J Comp Neurol, 107*(1), 109-163.

Cascio, C. J., Gerig, G., & Piven, J. (2007). Diffusion tensor imaging: Application to the study of the developing brain. *J Am Acad Child Adolesc Psychiatry, 46*(2), 213-223.

Casey, B. J., Giedd, J. N., & Thomas, K. M. (2000). Structural and functional brain development and its relation to cognitive development. *Biological Psychology, 54*, 241–257

Catani, M., Dell'acqua, F., Vergani, F., Malik, F., Hodge, H., Roy, P., . . . Thiebaut de Schotten, M. (2012). Short frontal lobe connections of the human brain. *Cortex, 48*(2), 273-291. doi:10.1016/j.cortex.2011.12.001

Chan-Palay, V. (1977). *Cerebellar Dentate Nucleus: Organization, Cytology and Transmitters*. New York, New York: Springer-Verlag Berlin Heidelberg.

Chen, S. H., & Desmond, J. E. (2005b). Temporal dynamics of cerebro-cerebellar network recruitment during a cognitive task. *Neuropsychologia, 43*(9), 1227-1237. doi:10.1016/j.neuropsychologia.2004.12.015

Chen, S.H. & Desmond, J.E. (2005a). Cerebrocerebellar networks during articulatory rehearsal and verbal working memory tasks. *Neuroimage, 24*(2), 332-8.

Cheung, M.M., Hui, E.S., Helpern, J.A., Qi, L., Wu, E.X. (2009). Does diffusion kurtosis imaging lead to better neural tissue characterization? A rodent brain maturation study. *Neuroimage, 45*, 386-392.

Clark, D. A., Mitra, P. P., & Wang, S. S. (2001). Scalable architecture in mammalian brains. *Nature, 411*(6834), 189-193. doi:10.1038/35075564

Colon-Perez, L. M., Spindler, C., Goicochea, S., Triplett, W., Parekh, M., Montie, E., … Mareci, T. H. (2015). Dimensionless, Scale Invariant, Edge Weight Metric for the Study of Complex Structural Networks. *Plos One, 10(*7), 1-29. doi:10.1371/journal.pone.0131493

Comrey, A. L. & Lee, H. B. (1992). *A first course in factor analysis*. Hillsdale, NJ: Erlbaum

Costa, L. D., & Vaughan, H. G. (1962). Performance of patients with lateralized cerebral lesions. *Journal of Nervous and Mental Disease, 134,* 162-168.

D'Angelo, E., and Casali, S. (2013). Seeking a unified framework for cerebellar function and dysfunction: from circuit operations to cognition. *Front Neural Circuits, 6,* 116. doi: 10.3389/fncir.2012.00116.

de Lussanet, M. H. E., & Osse, J. W. M. (2012). An ancestral axial twist explains the contralateral forebrain and the optic chiasm in vertebrates. *Animal Biology, 62*, 193–216. http://arxiv.org/abs/1003.1872

Delis, D.C., Kaplan, E., and Kramer, J.H. (2001). *Delis-Kaplan (D-KEFS) Executive Function System Technical Manual*. The Psychological Corporation: San Antonio, TX.

Dennis M., Yeates K.O., Taylor H.G., Fletcher J.M. (2006). Brain reserve capacity, cognitive reserve capacity, and age-based functional plasticity after congenital and acquired brain injury in children. In: Stern Y, editor. *Cognitive reserve: Theory and Applications*. New York: Psychology Press.

Dennis, M., Francis, D. J., Cirino, P. T., Schachar, R., Barnes, M. A., & Fletcher, J. M. (2009). Why IQ is not a covariate in cognitive studies of neurodevelopmental disorders. *J Int Neuropsychol Soc, 15*(3), 331-343. doi: 10.1017/S1355617709090481

Desikan, R. S., Segonne, F., Fischl, B., Quinn, B. T., Dickerson, B. C., Blacker, D., . . . Killiany, R. J. (2006). An automated labeling system for subdividing the human cerebral cortex on MRI scans into gyral based regions of interest. *Neuroimage, 31*(3), 968-980. doi:10.1016/j.neuroimage.2006.01.021

Desmond, J., Gabrieli, J., Wagner, A., Ginier, B., & Glover, G. (1997). Lobular patterns of cerebellar activation in verbal working-memory and finger-tapping tasks as revealed by functional MRI. *The Journal of Neuroscience, 17*(24), 9675-9685.

Desmond, J.E., Chen, S.H., Shieh, P.B. (2005). Cerebellar transcranial magnetic stimulation impairs verbal working memory. *Ann Neurol., 58*(4), 553-60.

Dietrich, U., Wanke, I., Mueller, T., Wieland, R., Moellers, M. et al. (2001). White matter disease in children treated for malignant brain tumors. *Child's Nerv Syst, 17,* 731–738.

Doricchi F and Tomaiuolo F. (2003). The anatomy of neglect without hemianopia: a key role for parietal–frontal disconnection? *NeuroReport, 14,* 2239–2243.

Doricchi, F., Thiebaut de Schotten, M., Tomaiuolo, F., & Bartolomeo, P. (2008). White matter (dis)connections and gray matter (dys)functions in visual neglect: gaining insights into the brain networks of spatial awareness. *Cortex, 44*(8), 983-995. doi:10.1016/j.cortex.2008.03.006

Duffner, P. K. (2004). Long-term effects of radiation therapy on cognitive and endocrine function in children with leukemia and brain tumors. *The Neurologist, 10*(6), 293-310. doi: 10.1097/01.nrl.0000144287.35993.96

Earle, A. M., & Matzke, H. A. (1974). Efferent fibers of the deep cerebellar nuclei in hedgehogs. *J Comp Neurol, 154*(2), 117-131. doi:10.1002/cne.901540202

Eickhoff S, Stephan KE, Mohlberg H, Grefkes C, Fink GR, Amunts K, Zilles K (2005). A new SPM toolbox for combining probabilistic cytoarchitectonic maps and functional imaging data. *NeuroImage* 25(4), 1325-1335.

Ezzati, A., Katz, M. J., Lipton, M. L., Zimmerman, M. E., & Lipton, R. B. (2015). Hippocampal volume and cingulum bundle fractional anisotropy are independently associated with verbal memory in older adults*. Brain Imaging and Behavior,* 1-8. doi:10.1007/s11682-015-9452-y

Finnie, J.W., Van den Heuvel, C., Gebski, V., Manavis, J., Summersides, G.E., & Blumbergs, P.C. (2001). Effect of impact on different regions of the head of lambs. *Journal of Comparative Pathology, 124*, 159–164.

First, M. B., Spitzer, R. L., Gibbon, M., & Williams, J. B. W. (2002). *Structured Clinical Interview for DSM-IV-TR.* New York: New York State Psychiatric Institute.

Ford, A., Colon-Perez, L., Triplett, W. T., Gullett, J. M., Mareci, T. H., & Fitzgerald, D. B. (2013). Imaging white matter in human brainstem. *Frontiers in Human Neuroscience, 7*(July), 400. doi:10.3389/fnhum.2013.00400

Fry, A.F. & Hale, S. (1996). Processing speed, working memory and fluid intelligence: evidence for a developmental cascade. *Psychol Sci, 7*, 237–241.

Fry, A.F., & Hale, S. (2000). Relationships among processing speed, working memory, and fluid intelligence in children. *Biological Psychology, 54,* 1–34.

Gaffan, D., & Hornak, J. (1997). Visual neglect in the monkey. Representation and disconnection. *Brain, 120*(Pt 9), 1647-1657.

Gao W, Lin W, Chen Y, Gerig G, Smith JK, Jewells V, et al. (2009). Temporal and spatial development of axonal maturation and myelination of white matter in the developing brain. *AJNR Am J Neuroradiol, 30,* 290 – 296.

Gao, W., Lin, W., Chen, Y., Gerig, G., Smith, J. K., Jewells, V., & Gilmore, J. H. (2009). Temporal and spatial development of axonal maturation and myelination of white matter in the developing brain. *AJNR Am J Neuroradiol, 30*(2), 290-296. doi:10.3174/ajnr.A1363

Garrison, K. A., Rogalsky, C., Sheng, T., Liu, B., Damasio, H., Winstein, C. J., & Aziz-Zadeh, L. S. (2015). Functional MRI Preprocessing in Lesioned Brains: Manual Versus Automated Region of Interest Analysis. *Frontiers in Neurology*, *6*, 196.

Gerton, B. K., Brown, T. T., Meyer-Lindenberg, A., Kohn, P., Holt, J. L., Olsen, R. K., & Berman, K. F. (2004). Shared and distinct neurophysiological components of the digits forward and backward tasks as revealed by functional neuroimaging. *Neuropsychologia, 42*(13), 1781-1787. doi:10.1016/j.neuropsychologia.2004.04.023

Glass, J. O., Ogg, R. J., Hyun, J. W., Harreld, J. H., Schreiber, J. E., Li, Y., . . . Reddick, W. E. (2017). Disrupted development and integrity of frontal white matter in patients treated for pediatric medulloblastoma. *Neuro Oncol*. doi:10.1093/neuonc/nox062

Glickstein, M., May, J. G., 3rd, & Mercier, B. E. (1985). Corticopontine projection in the macaque: the distribution of labelled cortical cells after large injections of horseradish peroxidase in the pontine nuclei. *J Comp Neurol, 235*(3), 343-359. doi:10.1002/cne.902350306

Gurney, G. G., Smith, M. A., & Bunin, G. R. (1999). CNS and miscellaneous intracranial and intraspinal neoplasms. In L. Ries, M. Smith, J. Gurney, M. Linet & T. Tamra (Eds.), *Cancer Incidence and Survival among Children and Adolescents: United States SEER Program 1975-1995* (99-4649 ed.). Retrieved from http://seer.cancer.gov/publications/childhood/cns.pdf

Habas, C., & Cabanis, E. A. (2006). Cortical projections to the human red nucleus: a diffusion tensor tractography study with a 1.5-T MRI machine. *Neuroradiology, 48*(10), 755-762. doi:10.1007/s00234-006-0117-9

Habas, C., & Cabanis, E. A. (2007). Cortical projection to the human red nucleus: complementary results with probabilistic tractography at 3 T. *Neuroradiology, 49*(9), 777-784. doi:10.1007/s00234-007-0260-y

Hayes, A.F. (2013). *Introduction to Mediation, Moderation, and Conditional Process Analysis.* New York: Guilford Press.

Hebben, N., & Milberg, W. (2010). *Essentials of neuropsychological assessment* (A. S. Kaufman, Ed.). Hoboken, NJ: Wiley.

Herculano-Houzel, S. (2009). The Human Brain in Numbers: A Linearly Scaled-up Primate Brain. *Frontiers in Human Neuroscience*, *3*, 31. http://doi.org/10.3389/neuro.09.031.2009

Hermoye, L., Saint-Martin, C., Cosnard, G., Lee, S. K., Kim, J., Nassogne, M. C., . . . Mori, S. (2006). Pediatric diffusion tensor imaging: normal database and observation of the white matter maturation in early childhood. *Neuroimage, 29*(2), 493-504. doi:10.1016/j.neuroimage.2005.08.017

Hermoye, L., Saint-Martin, C., Cosnard, G., Lee, S. K., Kim, J., Nassogne, M. C., . . . Mori, S. (2006). Pediatric diffusion tensor imaging: normal database and observation of the white matter maturation in early childhood. *Neuroimage, 29*(2), 493-504. doi:10.1016/j.neuroimage.2005.08.017

Hoang, D. H., Pagnier, A., Guichardet, K., Dubois-Teklali, F., Schiff, I., Lyard, G., . . . Krainik, A. (2014). Cognitive disorders in pediatric medulloblastoma: What neuroimaging has to offer. *Journal of Neurosurgery. Pediatrics, 14*(2), 136-144. doi: 10.3171/2014.5.peds13571

Hoeft, F., Barnea-Goraly, N., Haas, B. W., Golarai, G., Ng, D., Mills, D., . . . Reiss, A. L. (2007). More is not always better: increased fractional anisotropy of superior longitudinal fasciculus associated with poor visuospatial abilities in Williams syndrome. *J Neurosci, 27*(44), 11960-11965. doi:10.1523/jneurosci.3591-07.2007

Holm, S. (1979). A simple sequentially rejective multiple test procedure. *Scandinavian Journal of Statistics, 6*(2), 65–70.

Horska, A., Laclair, A., Mohamed, M., Wells, C. T., McNutt, T., Cohen, K. J., . . . Kates, W. (2010). Low cerebellar vermis volumes and impaired neuropsychologic performance in children treated for brain tumors and leukemia. *AJNR. American Journal of Neuroradiology, 31*(8), 1430-1437. doi: 10.3174/ajnr.A2114

Huang, H., Shu, N., Mishra, V., Jeon, T., Chalak, L., … He, Y. (2015). Development of human brain structural networks through infancy and childhood. *Cerebral Cortex, 25,* 1389-1404.

Imfeld, A., Oechslin, M. S., Meyer, M., Loenneker, T., & Jancke, L. (2009). White matter plasticity in the corticospinal tract of musicians: A diffusion tensor imaging study. *Neuroimage, 46*(3), 600-607. doi: http://dx.doi.org/10.1016/j.neuroimage.2009.02.025

Jayakar, R., King, T. Z., Morris, R., & Na, S. (2015). Hippocampal volume and auditory attention on a verbal memory task with adult survivors of pediatric brain tumor. *Neuropsychology, 29*(2), 303-319. doi: 10.1037/neu0000183

Jbabdi, S., & Johansen-Berg, H. (2011). Tractography: where do we go from here? *Brain Connect, 1*(3), 169-183. doi:10.1089/brain.2011.0033

Jenkinson M. & Smith S.M. (2001). A global optimisation method for robust affine registration of brain images. *Medical Image Analysis, 5*(2),143-156.

Jenkinson M., Bannister P.R., Brady J.M., & Smith S.M. (2002). Improved optimisation for the robust and accurate linear registration and motion correction of brain images. *NeuroImage, 17*(2), 825-841.

Jensen, J.H., Helpern, J.A. (2010). MRI quantification of non-Gaussian water diffusion by kurtosis analysis. *NMR Biomed., 23*(7), 698-710. doi: 10.1002/nbm.1518.

Jensen, J.H., Helpern, J.A., Ramani, A., Lu, H., Kaczynski, K. (2005). Diffusional Kurtosis Imaging: The Quantification of Non-Gaussian Water Diffusion by Means of Magnetic Resonance Imaging. *Magnetic Resonance in Medicine, 53*, 1432-1440.

Jian, B., & Vemuri, B. C. (2007a). A unified computational framework for deconvolution to reconstruct multiple fibers from diffusion weighted MRI. *IEEE Transactions on Medical Imaging*, 26(11), 1464–71. doi:10.1109/TMI.2007.907552

Jian, B., & Vemuri, B. C. (2007b). Multi-Fiber Reconstruction from Diffusion MRI Using Mixture of Wisharts and Sparse Deconvolution, *Inf Process Med Imaging. 20*, 384–395.

Jian, B., Vemuri, B. C., Özarslan, E., Carney, P. R., & Mareci, T. H. (2007). A novel tensor distribution model for the diffusion-weighted MR signal. *NeuroImage, 37*(1), 164–76. doi:10.1016/j.neuroimage.2007.03.074

Jiang, H.Y., Golay, X., Van Zijl, P.C.M., and Mori, S. (2002). Origin and minimization of residual motion-related artifacts in navigator-corrected segmented diffusion-weighted EPI of the human brain. *Magn.Reson. Med.* 47, 818–822. doi:10.1002/mrm.10102

Jissendi P, Baudry S, Baleriaux D (2008). Diffusion tensor imaging (DTI) and tractography of the cerebellar projections to prefrontal and posterior parietal cortices: A study at 3T. *J Neuroradiol 35,* 42–50.

Jones, D. K., Knösche, T. R., & Turner, R. (2013). White matter integrity, fiber count, and other fallacies: The do's and don'ts of diffusion MRI. *NeuroImage, 73*, 239-254. doi: http://dx.doi.org/10.1016/j.neuroimage.2012.06.081

Kamali, A., Flanders, A. E., Brody, J., Hunter, J. V., & Hasan, K. M. (2014). Tracing superior longitudinal fasciculus connectivity in the human brain using high resolution diffusion tensor tractography. *Brain Struct Funct, 219*(1), 269-281. doi:10.1007/s00429-012-0498-y

Karlsgodt, K. H., van Erp, T. G., Poldrack, R. A., Bearden, C. E., Nuechterlein, K. H., & Cannon, T. D. (2008). Diffusion tensor imaging of the superior longitudinal fasciculus and working memory in recent-onset schizophrenia. *Biol Psychiatry, 63*(5), 512-518. doi:10.1016/j.biopsych.2007.06.017

Kelly, R. M., & Strick, P. L. (2003). Cerebellar loops with motor cortex and prefrontal cortex of a nonhuman primate. *The Journal of neuroscience: The official journal of the Society for Neuroscience, 23*, 8432-8444.

Khalsa, S., Mayhew, S. D., Chechlacz, M., Bagary, M., & Bagshaw, A. P. (2014). The structural and functional connectivity of the posterior cingulate cortex: comparison between deterministic and probabilistic tractography for the investigation of structure-function relationships. *Neuroimage, 102 Pt 1*, 118-127. doi:10.1016/j.neuroimage.2013.12.022

Khong, P. L., Kwong, D. L., Chan, G. C., Sham, J. S., Chan, F. L., & Ooi, G. C. (2003). Diffusion-tensor imaging for the detection and quantification of treatment-induced white matter injury in children with medulloblastoma: A pilot study. *AJNR. American journal of neuroradiology, 24*(4), 734-740.

Kiefer, M., Apel, A., & Weisbrod, M. (2002). Arithmetic fact retrieval and working memory in schizophrenia. *Schizophr Res, 53*(3), 219-227.

King, T.Z., Wang, L., Mao, H. (2015). Disruption of White Matter Integrity in Adult Survivors of Childhood Brain Tumors: Correlates with Long-Term Intellectual Outcomes. *PLOS One, 10*(7), e0131744. doi:10.1371/journal.pone.0131744

Kinsbourne, M. (2013). Somatic twist: A model for the evolution of decussation. *Neuropsychology, 27*, 511–515. http://dx.doi.org/10.1037/a0033662

Kirschen, M. P., Davis-Ratner, M. S., Milner, M. W., Chen, S. H., Schraedley-Desmond, P., Fisher, P. G., & Desmond, J. E. (2008). Verbal memory impairments in children after cerebellar tumor resection. *Behavioural neurology, 20*(1-2), 39-53. doi: 10.3233/ben-2008-0216

Klawiter EC, Schmidt RE, Trinkaus K, Liang HF, Budde MD, Naismith RT, et al. (2011). Radial diffusivity predicts demyelination in ex vivo multiple sclerosis spinal cords. *Neuroimage, 55*, 1454 –1460.

Konczak, J., Schoch, B., Dimitrova, A., Gizewski, E., & Timmann, D. (2005). Functional recovery of children and adolescents after cerebellar tumour resection. *Brain: A Journal of Neurology, 128*(Pt 6), 1428-1441. doi: 10.1093/brain/awh385

Koziol, L. F., Budding, D., Andreasen, N., D'Arrigo, S., Bulgheroni, S., Imamizu, H., . . . Yamazaki, T. (2014). Consensus paper: the cerebellum's role in movement and cognition. *Cerebellum, 13*(1), 151-177. doi:10.1007/s12311-013-0511-x

Koziol, L.F. & Budding, D.E. (2009). *Subcortical Structures and Cognition: Implications for Neuropsychological Assessment.* New York, NY: Springer.

Küper, M., Doring, K., Spangenberg, C., Konczak, J., Gizewski, E. R., Schoch, B., & Timmann, D. (2013). Location and restoration of function after cerebellar tumor removal-a longitudinal study of children and adolescents. *Cerebellum, 12*(1), 48-58. doi: 10.1007/s12311-012-0389-z

Lange, W. (1975). Cell number and cell density in the cerebellar cortex of man and some other mammals. *Cell Tissue Res, 157*(1), 115-124.

Larrabee, G.J. and Kane, R.L. (1986). Reversed digit repetition involves visual and verbal processes. *Int J Neurosci.*, *30*(1-2), 11-5.

Law, N., Bouffet, E., Laughlin, S., Laperriere, N., Briere, M. E., Strother, D., . . . Mabbott, D. (2011). Cerebello-thalamo-cerebral connections in pediatric brain tumor patients: impact on working memory. *NeuroImage, 56*(4), 2238-2248. doi: 10.1016/j.neuroimage.2011.03.065

Law, N., Greenberg, M., Bouffet, E., Laughlin, S., Taylor, M. D., Malkin, D., . . . Mabbott, D. (2015a). Visualization and segmentation of reciprocal cerebrocerebellar pathways in the healthy and injured brain. *Human Brain Mapping, 36*(7), 2615-2628. doi: 10.1002/hbm.22795

Law, N., Greenberg, M., Bouffet, E., Taylor, M. D., Laughlin, S., Strother, D., . . . Mabbott, D. J. (2012). Clinical and neuroanatomical predictors of cerebellar mutism syndrome. *Neuro-Oncology, 14*(10), 1294-1303. doi: 10.1093/neuonc/nos160

Law, N., Smith, M. L., Greenberg, M., Bouffet, E., Taylor, M. D., Laughlin, S., . . . Mabbott, D. (2015b). Executive function in paediatric medulloblastoma: The role of cerebrocerebellar connections. *J Neuropsychol*. doi:10.1111/jnp.12082

Levers-Landis, C. E., Burant, C. J., & Hazen, R. (2011). The concept of bootstrapping of structural equation models with smaller samples: An illustration using mealtime rituals in diabetes management. *Journal of Developmental and Behavioral Pediatrics*, *32*(8), 619-626.

Lezak, M. D., Howieson, D. B., Bigler, E., & Tranel, D. (2012) *Neuropsychological Assessment*, Fifth Edition. New York: Oxford University Press.

Luciano, M., Gow, A. J., Harris, S. E., Hayward, C., Allerhand, M., Starr, J. M., . . . Deary, I. J. (2009). Cognitive ability at age 11 and 70 years, information

processing speed, and APOE variation: the Lothian Birth Cohort 1936 study. *Psychol Aging, 24*(1), 129-138. doi:10.1037/a0014780

Madden DJ, Bennett IJ, Burzynska A, Potter GG, Chen NK, Song AW. (2012). Diffusion tensor imaging of cerebral white matter integrity in cognitive aging. *Biochim Biophys Acta, 1822,* 386 – 400.

Makris N, Kennedy DN, McInerney S, Sorensen AG, Wang R, Caviness Jr VS, Pandya DN (2005). Segmentation of subcomponents within the superior longitudinal fascicle in humans: a quantitative, in vivo, DT-MRI study. *Cereb Cortex 15,* 854–869.

Makris, N., Kennedy, D.N., McInerney, S., Sorensen, A.G., Wang, R., Caviness, Jr V.S., Pandya, D.N. (2005). Segmentation of subcomponents within the superior longitudinal fascicle in humans: a quantitative, in vivo, DT-MRI study. *Cereb Cortex 15,* 854–869.

Maldjian JA, Laurienti PJ, Kraft RA, Burdette JH. (2003). An automated method for neuroanatomic and cytoarchitectonic atlas-based interrogation of fMRI data sets. *NeuroImage, 19*, 1233-1239.

Mannarelli, D., Pauletti, C., Grippo, A., Amantini, A., Augugliaro, V., Curra, A., . . . Fattapposta, F. (2015). The Role of the Right Dorsolateral Prefrontal Cortex in Phasic Alertness: Evidence from a Contingent Negative Variation and Repetitive Transcranial Magnetic Stimulation Study. *Neural Plast, 2015*, 410785. doi:10.1155/2015/410785

Mapou, R.L., Spector, J., (1995). *Clinical Neuropsychological Assessment: A Cognitive Approach*. New York, NY: Springer Science.

Marvel, C. L., & Desmond, J. E. (2010). The contributions of cerebro-cerebellar circuitry to executive verbal working memory. *Cortex, 46*(7), 880-895. doi:10.1016/j.cortex.2009.08.017

Merchant, T. E., Hua, C. H., Shukla, H., Ying, X., Nill, S., & Oelfke, U. (2008). Proton versus photon radiotherapy for common pediatric brain tumors: Comparison of models of dose characteristics and their relationship to cognitive function. *Pediatric Blood & Cancer, 51*(1), 110-117. doi: 10.1002/pbc.21530

Mesulam MM. (1981). A cortical network for directed attention and unilateral neglect. *Ann Neurol, 10,* 309-325.

Middleton, F. A., & Strick, P. L. (2002). Basal-ganglia 'projections' to the prefrontal cortex of the primate. *Cereb Cortex, 12*(9), 926-935.

Milardi, D., Cacciola, A., Cutroneo, G., Marino, S., Irrera, M., … Quartarone, A. (2016). Red nucleus connectivity as revealed by constrained spherical deconvolution tractography. *Neuroscience Letters, 626*, 68-73. Miller, D. C. (2013). *Essentials of school neuropsychological assessment* (2nd ed.). Hoboken, NJ: John Wiley & Sons, Inc.

Miller, G. A. (1956). The magical number seven, plus or minus two: Some limits on our capacity for processing information. *Psychological Review, 63*(2), 81–97. doi:10.1037/h0043158. PMID 13310704.

Miller, K. M., Price, C. C., Okun, M. S., Montijo, H., & Bowers, D. (2009). Is the *N*-Back Task a Valid Neuropsychological Measure for Assessing Working Memory? *Archives of Clinical Neuropsychology*, *24*(7), 711–717. http://doi.org/10.1093/arclin/acp063

Mink, J. W., & Thach, W. T. (1991). Basal ganglia motor control. I. Nonexclusive relation of pallidal discharge to five movement modes. *J Neurophysiol, 65*(2), 273-300.

Monaco, M., Costa, A., Caltagirone, C., & Carlesimo, G. A. (2013). Forward and backward span for verbal and visuo-spatial data: standardization and normative data from an Italian adult population. *Neurol Sci, 34*(5), 749-754. doi:10.1007/s10072-012-1130-x

Moore, B. D., 3rd. (2005). Neurocognitive outcomes in survivors of childhood cancer. *J Pediatr Psychol, 30*(1), 51-63.

Morgan, S.F. and Wheelock, J. (1992). Digit Symbol and Symbol Digit Modalities Tests: Are they directly interchangeable? *Neuropsychology, 6*(4), 327-330.

Mori, S., & van Zijl, P. C. (2002). Fiber tracking: principles and strategies - a technical review. *NMR Biomed, 15*(7-8), 468-480. doi:10.1002/nbm.781

Morris, D. M., Embleton, K. V., & Parker, G. J. (2008). Probabilistic fibre tracking: differentiation of connections from chance events. *Neuroimage, 42*(4), 1329-1339. doi:10.1016/j.neuroimage.2008.06.012

Morris, E. B., Phillips, N. S., Laningham, F. H., Patay, Z., Gajjar, A., Wallace, D., . . . Ogg, R. J. (2009). Proximal dentatothalamocortical tract involvement in posterior fossa syndrome. *Brain: A journal of Neurology, 132*(Pt 11), 3087-3095. doi: 10.1093/brain/awp241

Mueller, S., & Chang, S. (2009). Pediatric brain tumors: current treatment strategies and future therapeutic approaches. *Neurotherapeutics: The journal of the American Society for Experimental NeuroTherapeutics, 6*(3), 570-586. doi: 10.1016/j.nurt.2009.04.006

Mukherjee, P., Berman, J. I., Chung, S. W., Hess, C. P., & Henry, R. G. (2008). Diffusion tensor MR imaging and fiber tractography: theoretic underpinnings. *AJNR Am J Neuroradiol, 29*(4), 632-641. doi:10.3174/ajnr.A1051

Mulhern, R. K., Merchant, T. E., Gajjar, A., Reddick, W. E., & Kun, L. E. (2004). Late neurocognitive sequelae in survivors of brain tumours in childhood. *The Lancet. Oncology, 5*(7), 399-408. doi: 10.1016/s1470-2045(04)01507-4

Mulhern, R. K., Palmer, S. L., Reddick, W. E., Glass, J. O., Kun, L. E., Taylor, J., . . . Gajjar, A. (2001). Risks of young age for selected neurocognitive deficits in medulloblastoma are associated with white matter loss. *J Clin Oncol, 19*(2), 472-479.

Mussen, A. T. (1927). Symposium on the cerebellum. *(4) Experimental Investigations on the cerebellum, 50*(3-4), 313-349. doi:10.1093/brain/50.3-4.313

Naidich, T.P., Duvernoy, H.M., Delman, B.N., Sorensen, A.G., Kollias, S.S., Haacke, E.M. (2009). *Duvernoy's atlas of the human brain stem and cerebellum high-field MRI: surface anatomy, internal structure, vascularization and 3D sectional anatomy*. Wien, Austria: Springer

Nejat, F., Khashab, M. E., & Rutka, J. T. (2008). Initial management of childhood brain tumors: Neurosurgical considerations. *Journal of Child Neurology, 23*(10), 1136-1148. doi: 10.1177/0883073808321768.

Ono, M., Kubik, S., and Abernathey, C.D. (1990). *Atlas of the cerebral sulci*. Thieme: New York.

Ostrom, Q. T., de Blank, P. M., Kruchko, C., Petersen, C. M., Liao, P., Finlay, J. L., . . . Barnholtz-Sloan, J. S. (2015). Alex's lemonade stand foundation infant and

childhood primary brain and central nervous system tumors diagnosed in the United States in 2007-2011. *Neuro-oncology, 16 Suppl 10*, x1-x36. doi: 10.1093/neuonc/nou327

Palmer, S. L. (2008). Neurodevelopmental impact on children treated for medulloblastoma: a review and proposed conceptual model. *Dev Disabil Res Rev, 14*(3), 203-210. doi:10.1002/ddrr.32

Palmer, S. L., Glass, J. O., Li, Y., Ogg, R., Qaddoumi, I., Armstrong, G. T., . . . Reddick, W. E. (2012). White matter integrity is associated with cognitive processing in patients treated for a posterior fossa brain tumor. *Neuro-oncology, 14*(9), 1185-1193. doi: 10.1093/neuonc/nos154

Palmer, S. L., Reddick, W. E., Glass, J. O., Gajjar, A., Goloubeva, O., & Mulhern, R. K. (2002). Decline in corpus callosum volume among pediatric patients with medulloblastoma: longitudinal MR imaging study. *AJNR Am J Neuroradiol, 23*(7), 1088-1094.

Parent, A. (1996). *Carpenter's Human Neuroanatomy.* Media, PA: Williams and Wilkins.

Patenaude, B., Smith, S.M., Kennedy, D., and Jenkinson M. (2011). A Bayesian Model of Shape and Appearance for Subcortical Brain. *NeuroImage, 56*(3), 907-922.

Paus T, Collins DL, Evans AC, Leonard G, Pike B, Zijdenbos A (2001). Maturation of white matter in the human brain: a review of magnetic resonance studies. *Brain Res Bull, 54*, 255–266. doi:10.1016/S0361-9230(00)00434-2

Peterson, L. R.; Peterson, M. J. (1959). Short-term retention of individual verbal items. *Journal of Experimental Psychology, 58*(3), 193–198. doi:10.1037/h0049234. PMID 14432252.

Petrides M, Pandya DN (2002). *Association pathways of the prefrontal cortex and functional observations.* In: Principles of frontal lobe function (Struss DT, Knight RT, eds), pp. 31--50. Oxford: Oxford University Press

Pfefferbaum, A., Mathalon, D. H., Sullivan, E. V., Rawles, J. M., Zipursky, R. B., & Lun, K. O. (1994). A quantitative magnetic resonance imaging study of changes in brain morphology from infancy to late adulthood. *Archives of Neurology, 51*, 874–887.

Philips, J. P. (2012). *Analysis of the factor structure of processing speed* (Unpublished doctoral dissertation). Denton, Texas.

Preacher, K. J., & Hayes, A. F. (2004). SPSS and SAS procedures for estimating indirect effects in simple mediation models. *Behavioral Research Methods, Instruments, & Computers, 36*, 717–731.

Preuss TM, Goldman-Rakic PS. (1989). Connections of the ventral granular frontal cortex of macaques with perisylvian premotor and somatosensory areas: anatomical evidence for somatic representation in primate frontal association cortex. *J Comp Neurol, 282,* 293—316

Price, C. J., Mummery, C. J., Moore, C. J., Frakowiak, R. S., & Friston, K. J. (1999). Delineating necessary and sufficient neural systems with functional imaging studies of neuropsychological patients. *J Cogn Neurosci, 11*(4), 371-382.

Puget, S., Boddaert, N., Viguier, D., Kieffer, V., Bulteau, C., Garnett, M., . . . Grill, J. (2009). Injuries to inferior vermis and dentate nuclei predict poor neurological and neuropsychological outcome in children with malignant posterior fossa tumors. *Cancer, 115*(6), 1338-1347. doi: 10.1002/cncr.24150

Qiu, D., Kwong, D. L. W., Chan, G. C. F., Leung, L. H. T., & Khong, P.L. (2007). Diffusion tensor magnetic resonance imaging finding of discrepant fractional anisotropy between the frontal and parietal lobes after whole-brain irradiation in childhood medulloblastoma survivors: Reflection of regional white matter radiosensitivity? *International Journal of Radiation Oncology • Biology • Physics, 69*(3), 846-851. doi:10.1016/j.ijrobp.2007.04.041

Ramnani, N., Behrens, T. E., Johansen-Berg, H., Richter, M. C., Pinsk, M. A., Andersson, J. L., . . . Matthews, P. M. (2006). The evolution of prefrontal inputs to the cortico-pontine system: diffusion imaging evidence from Macaque monkeys and humans. *Cereb Cortex, 16*(6), 811-818. doi:10.1093/cercor/bhj024

Rand, R. W. (1954). An anatomical and experimental study of the cerebellar nuclei and their efferent pathways in the monkey. *J Comp Neurol, 101*(1), 167-223.

Reddick WE, Russell JM, Glass JO, et al. (2000). Subtle white matter volume differences in children treated for medulloblastoma with conventional or reduced-dose cranial-spinal irradiation. *Magn Reson Imaging, 18*, 787–793.

Reddick, W. E., Glass, J. O., Palmer, S. L., Wu, S., Gajjar, A., Langston, J. W., . . . Mulhern, R. K. (2005). Atypical white matter volume development in children following craniospinal irradiation. *Neuro-oncology, 7*(1), 12-19. doi: 10.1215/S1152851704000079

Rehme, A. K., & Grefkes, C. (2013). Cerebral network disorders after stroke: evidence from imaging-based connectivity analyses of active and resting brain states in humans. *J Physiol, 591*(1), 17-31. doi:10.1113/jphysiol.2012.243469

Reinhold, H. S., Calvo, W., Hopewell, J.W., & Van Den Breg, A. P. (1990). Development of blood vessel-related radiation damage in the fimbria of the central nervous system. *International Journal of Radiation Oncology Biology Physics, 18*, 37–42.

Ridgway G. (2007) get_totals.m. [Computer software]. Retrieved August, 1. 2014, from http://www.cs.ucl.ac.uk/staff/G.Ridgway/vbm/

Riggs, L., Bouffet, E., Laughlin, S., Laperriere, N., Liu, F., Skocic, J., . . . Mabbott, D. J. (2014). Changes to memory structures in children treated for posterior fossa tumors. *Journal of the International Neuropsychological Society, 20*(2), 168-180. doi: 10.1017/s135561771300129x

Ripollés, P., Marco-Pallares, J., de Diego-Balaguer, R., Miro, J., Falip, M., Juncadella, M., . . . Rodriguez-Fornells, A. (2012). Analysis of automated methods for spatial normalization of lesioned brains. *NeuroImage, 60*(2), 1296-1306. doi: 10.1016/j.neuroimage.2012.01.094

Roberts, S. (2016). Structural connectivity of the inferior frontal gyrus, thalamus, and basal ganglia in healthy young adults. (Unpublished master's thesis). Georgia State University, Atlanta, GA.

Rohkamm, R. (1977). *Degeneration and regeneration in neurons of the cerebellum.* New York: Springer-Verlag.

Rorden, C., Karnath, H.-O., & Bonilha, L. (2007). Improving Lesion-Symptom Mapping. *Journal of Cognitive Neuroscience, 19*(7), 1081-1088. doi: 10.1162/jocn.2007.19.7.1081

Rueckriegel, S. M., Bruhn, H., Thomale, U. W., & Hernaiz Driever, P. (2015). Cerebral white matter fractional anisotropy and tract volume as measured by MR imaging

are associated with impaired cognitive and motor function in pediatric posterior fossa tumor survivors. *Pediatric Blood & Cancer, 62*(7), 1252-1258. doi: 10.1002/pbc.25485

Salmi, J., Pallesen, K. J., Neuvonen, T., Brattico, E., Korvenoja, A., Salonen, O., & Carlson, S. (2010). Cognitive and motor loops of the human cerebro-cerebellar system. *J Cogn Neurosci, 22*(11), 2663-2676. doi:10.1162/jocn.2009.21382

Salmi, J., Rinne, T., Koistinen, S., Salonen, O., & Alho, K. (2009). Brain networks of bottom-up triggered and top-down controlled shifting of auditory attention. *Brain Res, 1286*, 155-164. doi:10.1016/j.brainres.2009.06.083

Sanfilipo, M.P., Benedict, R.H., Zivadinov, R., & Bakshi, R. (2007). Correction for intracranial volume in analysis of whole brain atrophy in multiple sclerosis: The proportion vs. residual method. *Neuroimage, 22*(4), 1732–1743.

Shan, Z. Y., Liu, J. Z., Glass, J. O., Gajjar, A., Li, C. S., & Reddick, W. E. (2006). Quantitative morphologic evaluation of white matter in survivors of childhood medulloblastoma. *Magnetic Resonance Imaging, 24*(8), 1015-1022. doi: 10.1016/j.mri.2006.04.015

Shiffrin, R. M., & Nosofsky, R. M. (1994). Seven plus or minus two: A commentary on capacity limitations. *Psychological Review, 101*, 357-361.

Shucard, J. L., Hamlin, A. S., & Shucard, D. W. (2011). The Relationship Between Processing Speed and Working Memory Demand in Systemic Lupus Erythematosus: Evidence from a Visual N-Back Task. *Neuropsychology*, *25*(1), 45–52. http://doi.org/10.1037/a0021218

Skudlarski, P., Jagannathan, K., Calhoun, V. D., Hampson, M., Skudlarska, B. A., & Pearlson, G. (2008). Measuring brain connectivity: diffusion tensor imaging validates resting state temporal correlations. *Neuroimage, 43*(3), 554-561. doi:10.1016/j.neuroimage.2008.07.063

Smith A. (1982). *Symbol Digit Modality Test.* Western Psychological Services, Los Angeles, CA.

Smith S.M., Jenkinson M., Woolrich W.M., Beckmann C.F., Behrens T.E.J., Johansen-Berg H., Bannister P.R., De Luca M., Drobnjak I., Flitney D.E., Niazy R., Saunders J., Vickers J., Zhang Y., De Stefano N., Brady J.M., and Matthews P.M. (2004). Advances in functional and structural MR image analysis and implementation as FSL. *NeuroImage, 23*(S1):208-19

Smith, K. M., King, T. Z., Jayakar, R., & Morris, R. D. (2014). Reading skill in adult survivors of childhood brain tumor: A theory-based neurocognitive model. *Neuropsychology, 28*(3), 448-458. doi: 10.1037/neu0000056

Smith, K.M. (2016). *Corpus callosum and word reading in adult survivors of childhood posterior fossa tumors*. (Unpublished doctoral dissertation). Georgia State University, Atlanta, GA.

Soelva, V., Hernaiz Driever, P., Abbushi, A., Rueckriegel, S., Bruhn, H., Eisner, W., & Thomale, U. W. (2013). Fronto-cerebellar fiber tractography in pediatric patients following posterior fossa tumor surgery. *Child's Nervous System: Official journal of the International Society for Pediatric Neurosurgery, 29*(4), 597-607. doi: 10.1007/s00381-012-1973-8

Song SK, Yoshino J, Le TQ, Lin SJ, Sun SW, Cross AH, et al. (2005). Demyelination increases radial diffusivity in corpus callosum of mouse brain. *Neuroimage, 26*, 132–140.

Spanos, G.K., Wilde, E.A., Bigler, E.D., Cleavinger, H.B., Fearing, M.A., Levin, H.S., … Hunter, J.V. (2007). Cerebellar atrophy after moderate-to-severe pediatric traumatic brain injury. *American Journal of Neuroradiology, 28*, 537-42.

Spreen, O. and Strauss, E. (1998). *A Compendium of neuropsychological tests: Administration, norms, and commentary*. (2nd ed.). New York, NY: Oxford University Press.

Stevens, M. C., Skudlarski, P., Pearlson, G. D., & Calhoun, V. D. (2009). Age-related cognitive gains are mediated by the effects of white matter development on brain network integration. *Neuroimage, 48*(4), 738-746. doi: 10.1016/j.neuroimage.2009.06.065

Stoodley, C. J., & Schmahmann, J. D. (2009). Functional topography in the human cerebellum: a meta-analysis of neuroimaging studies. *Neuroimage, 44*(2), 489-501. doi:10.1016/j.neuroimage.2008.08.039

Strauss, E., Sherman, E. M., Spreen, O., & Spreen, O. (2006). *A compendium of neuropsychological tests: administration, norms, and commentary*. Oxford: Oxford University Press.

Stuss, D., Stethem, L., & Pelchat, G. (1988). Three tests of attention and rapid information processing: An extension. *Clinical Neuropsychologist 2*(3), 246–250.

Szathmari, A., Thiesse, P., Galand-desmé, S., et al. (2010). Correlation between pre- or postoperative MRI findings and cerebellar sequelae in patients with medulloblastomas. *Pediatr Blood Cancer, 55*(7), 1310-6.

Szathmari, A., Thiesse, P., Galand-desme, S., Mottolese, C., Bret, P., Jouanneau, E., . . . Frappaz, D. (2010). Correlation between pre- or postoperative MRI findings and cerebellar sequelae in patients with medulloblastomas. *Pediatr Blood Cancer, 55*(7), 1310-1316. doi:10.1002/pbc.22802

Taiwo, Z., Na, S., & King, TZ. (2017). The Neurological Predictor Scale: A predictive tool for neurocognitive late effects in survivors of childhood brain tumors. *Pediatric Blood and Cancer, 64*(1), 172-179. DOI: 10.1002/pbc.26203

Taylor, H., & Alden, J. (1997). Age-related differences in outcomes following childhood brain insults: an introduction and overview. *Journal of the International Neuropsychological Society*, *3*(6), 555-567.

Thiebaut de Schotten M, Urbanski M, Duffau H, Volle E, Levy R, Dubois B, and Bartolomeo P. (2005). Direct evidence for a parietal–frontal pathway subserving spatial awareness in humans. *Science, 309,* 2226–2228.

Thiebaut de Schotten, M., Dell'Acqua, F., Forkel, S. J., Simmons, A., Vergani, F., Murphy, D. G., & Catani, M. (2011). A lateralized brain network for visuospatial attention. *Nat Neurosci, 14*(10), 1245-1246. doi:10.1038/nn.2905

Tournier, J. D., Mori, S., & Leemans, A. (2011). Diffusion tensor imaging and beyond. *Magn Reson Med, 65*(6), 1532-1556. doi: 10.1002/mrm.22924

Turken, A. U., & Dronkers, N. F. (2011). The neural architecture of the language comprehension network: converging evidence from lesion and connectivity analyses. *Front Syst Neurosci, 5*, 1. doi:10.3389/fnsys.2011.00001

Urbanski M, Thiebaut de Schotten M, Rodrigo S, Catani M, Oppenheim C, Touze E, Chokron S, Meder J-F, Levy R, Dubois B, and Bartolomeo P. (2008). Brain networks of spatial awareness: evidence from diffusion tensor imaging tractography. *Journal of Neurology, Neurosurgery and Psychiatry, 79,* 598–601.

Viallon, M., Cuvinciuc, V., Delattre, B., Merlini, L., Barnaure-Nachbar, I., Toso-Patel, S., . . . Haller, S. (2015). State-of-the-art MRI techniques in neuroradiology: Principles, pitfalls, and clinical applications. *Neuroradiology, 57*(5), 441-467. doi:10.1007/s00234-015-1500-1

von Monakow C. (1914). *Die Localization im Grosshirn und der Abbau der Funktion durch korticale Herde.* Wiesbaden, Germany: JF Bergmann.

Voogd, l (1964). *The cerebellum of the cat. Structure and fibre connexions*. Assen, Netherlands: Van Gorcum & Co.

Wakana S, Jiang H, Nagae-Poetscher LM, van Zijl PC, Mori S. (2004). Fiber tract—based atlas of human white matter anatomy. *Radiology, 230*, 77—87.

Waxman, S. G. (2009). *Clinical neuroanatomy*. New York: McGraw-Hill Education.

Wechsler, D. (1987). *Manual for the Wechsler Memory Scale-Revised*. The Psychological Corporation, San Antonio, TX.

Wechsler, D. (1997). *Wechsler Memory Scale - Third Edition. Manual*. San Antonio, TX: The Psychological Corporation.

Wechsler, D. (1999). *WASI Manual.* San Antonio: Psychological Corporation.

Weinberg, J., Diller, L., Gerstman, L., & Schulman, P. (1972). Digit span in right and left hemiplegics. *J Clin Psychol, 28*(3), 361.

Westlye, L. T., Walhovd, K. B., Dale, A. M., Bjornerud, A., Due-Tonnessen, P., Engvig, A., . . . Fjell, A. M. (2010). Life-span changes of the human brain white matter: diffusion tensor imaging (DTI) and volumetry. *Cereb Cortex, 20*(9), 2055-2068. doi:10.1093/cercor/bhp280

Wheeler-Kingshott, C. A., & Cercignani, M. (2009). About "axial" and "radial" diffusivities. Magn Reson Med, 61(5), 1255-1260. doi: 10.1002/mrm.21965

Whiting, B. A., & Barton, R. A. (2003). The evolution of the cortico-cerebellar complex in primates: anatomical connections predict patterns of correlated evolution. *Journal of human evolution, 44*(1), 3-10.

Willing, J. and Juraska, J.M. (2015). The timing of neuronal loss across adolescence in the medial prefrontal cortex of male and female rats. *Neuroscience, 301,* 268–275.Wolfe, K. R., Madan-Swain, A., & Kana, R. K. (2012). Executive dysfunction in pediatric posterior fossa tumor survivors: a systematic literature review of neurocognitive deficits and interventions. *Developmental Neuropsychology, 37*(2), 153-175. doi:10.1080/87565641.2011.632462

Woods RP, Grafton ST, Holmes CJ, Cherry SR, Mazziotta JC. (1998). Automated image registration: I. General methods and intrasubject, intramodality validation. *Journal of Computer Assisted Tomography, 22*, 139-152.

Yo, T. S., Anwander, A., Descoteaux, M., Fillard, P., Poupon, C., & Knosche, T. R. (2009). Quantifying brain connectivity: a comparative tractography study. *Med Image Comput Comput Assist Interv, 12*(Pt 1), 886-893.

Zhang, J. X., Leung, H. C., & Johnson, M. K. (2003). Frontal activations associated with accessing and evaluating information in working memory: An fMRI study. *Neuroimage, 20*(3), 1531-1539.

Zhang, Y., Zou, P., Mulhern, R. K., Butler, R. W., Laningham, F. H., & Ogg, R. J. (2008). Brain structural abnormalities in survivors of pediatric posterior fossa brain tumors: A voxel-based morphometry study using free-form deformation. *NeuroImage, 42*(1), 218-229. doi: 10.1016/j.neuroimage.2008.04.181

Ziemus, B., Baumann, O., Luerding, R., Schlosser, R., Schuierer, G., Bogdahn, U., & Greenlee, M. W. (2007). Impaired working-memory after cerebellar infarcts paralleled by changes in BOLD signal of a cortico-cerebellar circuit. *Neuropsychologia, 45*(9), 2016-2024. doi:10.1016/j.neuropsychologia.2007.02.012